# BMR JOURNAL
## OF AUSTRALIAN GEOLOGY & GEOPHYSICS

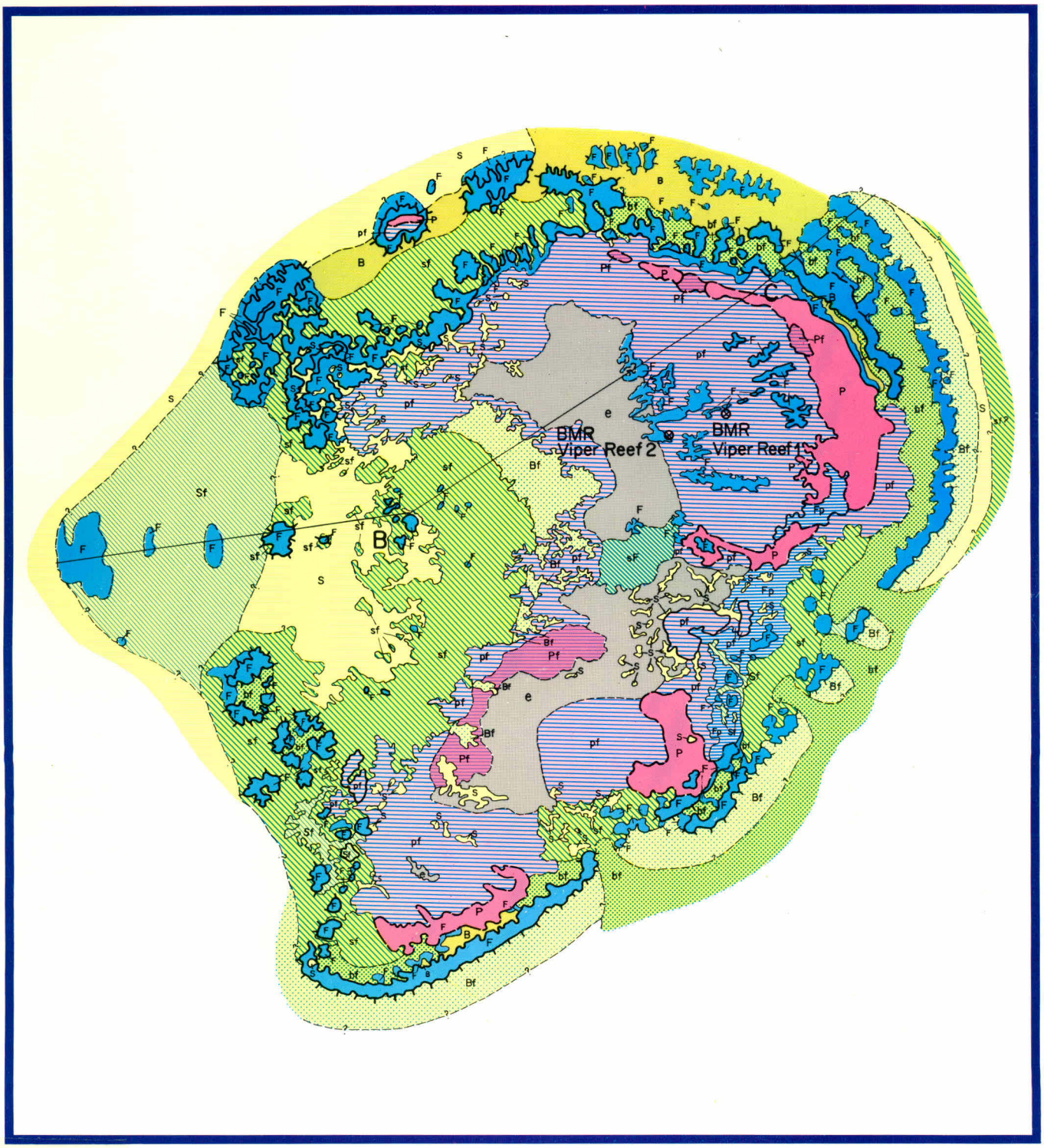




VOLUME 8 NUMBER 4 DECEMBER 1983

# BMR JOURNAL
## OF AUSTRALIAN GEOLOGY & GEOPHYSICS

VOLUME 8 NUMBER 4 DECEMBER 1983

CONTENTS



Front cover: Viper Reef—part of a map published by BMR, showing surficial facies of part of the central Great Barrier Reef, mapped using the concept of entropy ratio. A paper by B. M. Radke in this issue explains the concept and describes its application.

AUSTRALIAN GOVERNMENT PUBLISHING SERVICE CANBERRA 1983

**Department of Resources and Energy**

Minister: Senator the Hon. Peter Walsh

Secretary: A. J. Woods

**Bureau of Mineral Resources, Geology and Geophysics**

Director: R. W. R. Rutland

Editor, BMR Journal: I. M. Hodgson

The BMR Journal of Australian Geology & Geophysics is a quarterly journal of research and related activities. Contributions are from officers of the BMR, from BMR officers working in collaboration with others, or requested work sponsored by the BMR. In addition to articles, the Journal may include shorter notes and discussion of papers published in it. Discussion of papers is invited from anyone.

Annual subscription to the Journal is $27 (Australian). Individual numbers, if available, cost $8.60. Subscriptions, etc., made payable to the Receiver of Public Moneys, in Australian dollars, should be sent to the Director, Bureau of Mineral Resources, Geology and Geophysics, GPO Box 378, Canberra, A.C.T. 2601, Australia.

Others matters concerning the Journal should be sent to the Director, marked for the attention of the Editor, BMR Journal.

The text figures in this issue were drafted by R. Bates, P. Griffiths, P. Jorritsma, B. Pashley, & M. Steele.



ISSN 0312-9608

Printed by Graphic Services Pty. Ltd. 516-518 Grand Junction Road, Northfield, S.A. 5085

BMR Journal of Australian Geology & Geophysics, 8, 293–305 

# THE SEARCH FOR A MORE REALISTIC METALLOGENIC MAP FORMAT, WITH REFERENCE TO THE PINE CREEK GEOSYNCLINE

Peter Laznicka*

The format of most existing metallogenic maps is not adequate for scales of 1:500 000 or less. The major problem is the colourful out-of-scale locality symbols, which mask the map detail in the most important areas, the immediate vicinity of the ore occurrences. The design of the symbols is also a problem, most being influenced considerably by genetic interpretations that are subjective and change with time; they are incapable of expressing transitionality, correlation of metallogenetic and lithogenetic events, and they cannot accommodate incomplete information. A substantially different philosophy of metallogenic mapping has been tested using the Pine Creek Geosyncline as an example. Ideally, the product would be a set of three matching maps. Map 1 would be a base map, a modified geological map that consistently shows the age of units by colour and the lithology of units by pattern, regardless of genesis and the level of emplacement. Mineralised occurrences would be identified in the simplest way possible, so as not to obscure the background information. Map 2 would be a gitological map, or map of mineral deposits, providing information on the geological properties of occurrences. The symbols suggested are based on simplified geological cross-sections, and are colour and pattern coordinated with the base map, to give the reader an immediate impression about the contemporaneity of rock-and ore-forming events and of the hosts to the ore. Within the symbol framework for a given 'mineralisation style', a wide range of properties of individual occurrences can be shown, and unknown information can be truthfully expressed as a blank component of the symbol. Map 3 would be a commodity map, showing the ore metals, their individual and total accumulations, and the concentration of the major metal.

## Introduction

Metallogenic, metallogenetic, or metallotectonic maps show the nature and distribution of mineral deposits in a geological or tectonic framework (e.g. Lang, 1961; Shatalov & others, 1966). Despite their almost 80-year history of development (de Launay, 1907, 1913), of which the last twenty years have been a period of accelerated development, metallogenic maps have not yet acquired a universally accepted style, as have geological maps. And despite the existence of the International Subcommission for the Metallogenic Map of the World and its efforts to produce a uniform global map, national institutions such as geological surveys continue, independently, to prepare metallogenic maps of their countries or continents, consistent with their local experience, needs, and traditions. The new Metallogenic Map of North America at 1:5 million (Guild & others, 1980) is an example. Here, 'the compilers of this map have departed from conventional practice and devised a legend which requires a little study to comprehend'.

The Bureau of Mineral Resources produced a Metallogenetic Map of Australia and Papua New Guinea at a scale of 1:5 million (Warren, 1972), and, although this project was aimed at producing a map modelled on the Metallogenic Map of Europe (Comité de la Carte Métallogenique de l'Europe, 1968–1973), the final map was considerably modified to suit the local conditions — for example, it incorporates the distinct Australian tectonic divisions and their unique cartographic expression.

Among the Australian states, only New South Wales has under way an ambitious program of metallogenic map production on the scale of 1:250 000 (1:50 000 for the Broken Hill area), and the Lachlan Fold Belt has now been completely covered. Mapping continues in the New England Belt, and production of metallogenic maps of large regions and orogenic belts is planned (Suppel, personal communication, 1981). Bowman & Stevens (1978) comprehensively summarised the objectives and achievements of the New South Wales metallogenic mapping program, and discussed in detail the philosophical problems of metallogenic mapping.

There is a considerable variety of metallogenic maps, and Bowman & Stevens (1978) provided a good review of eleven of them. To these should be added the recently released Metallogenic Map of North Americal (Guild & others, 1982) and the Metallogenic Map of the U.S.S.R. (Grushevoi & others, 1971).

Despite differences in detail these maps have many common features: all use a tectonic or geologic map base reduced in detail; all have over-sized, out-of-scale symbols of mineral occurrences, many of variable size to indicate the importance of the locality; and all use colour of the locality symbol to show the commodity. The maps are colourful and give a very forceful, instant picture of the regional commodity distribution in a broad tectonic or geologic framework.

Most existing metallogenic maps are compilations of national territories (e.g. Finland, Japan, Iran, Brazil), continents (Europe, North America) or both (Australia), and are one-of-a-kind maps. They have been prepared not only for geologists, but for the general public as well. All are overview maps, showing only a fraction of the existing localities.

A minority of metallogenic maps are based on topographic map sheets of more detailed scale and have been issued as one-of-a-kind (e.g. Rouyn-Noranda area, Canada; Sharpe, 1968) or as part of a series (e.g. the Carte des Gites Mineraux de la France, 1:320 000; Metallogenetic Map of New South Wales 1:250 000). These maps are designed more exclusively for geologists. One would expect such maps to show all mineralised localities and aim at the most faithful representation of the relationship of mineralisation to geology. Yet they use the same techniques and symbols as the national and continental overview maps: the French maps are striking and lavish, the New South Wales maps more subdued. A first size category ore deposit on the French map, for example the Romanéche Mn vein on the Lyon sheet (Permingeat, 1963), is a small deposit by Australian standards (408 330 t ore; Lougnon, 1956). Yet its 14-mm diameter symbol solidly covers about 30 km$^2$ of the map. The actual outcrop area of Romanéche veins does not exceed 0.1 km$^2$, so the symbol is at least 300 times exaggerated. Because the centre of the symbol corresponds to the precise geographic location, the geological information in the background map is obscured in the most important area. As a consequence, the enclosing rocks have had to be shown by additional graphic symbols, which are inconspicuous, poorly legible, and difficult to locate in crowded areas. Such maps have a reduced usefulness in mining exploration.

*Department of Earth Sciences, University of Manitoba, Winnipeg, Manitoba, Canada, R3T 2N2

In this paper I am proposing a new approach to the compilation of metallogenic maps, drawing on my experience in preparing a manuscript metallogenic map of Australia and illustrating it by reference to the metallogenesis of the Pine Creek Geosyncline.

## A manuscript metallogenic map of Australia

In 1973, compilation was completed of a manuscript metallogenic map of Australia. This map was the product of experimentation on the compilation of global and continental metallogenic maps, using a computerised data base of metallic deposits of the world, MANIFILE (Laznicka, 1975). Australia was selected as a pilot project because of the unique availability of up-to-date published information on its mineral deposits (Edwards & others, 1953; McAndrew & others, 1965; McLeod, 1965; Knight & others, 1975) and the geographic, political, and economic unity of such a large territory. MANIFILE 2, used for the Australian project, included over 800 Australian deposits, compiled from the literature, with about 20 per cent of the localities checked in the field. The map, at a scale of 1:5 million, includes numerous improvements and modifications, departing from the pattern of existing metallogenic maps available in the early 1970s (Fig. 1). The changes were designed to improve map readability, and to make it more realistic, factual, and as independent as possible from the rapidly changing genetic and geotectonic models. Particular emphasis was directed towards colour coordination, which is used exclusively to show geological age: age of rock generation, rock deformation, and ore deposit formation. Other information, some highly quantitative and based on computer plots, is expressed by a variety of symbol shapes and patterns.

### Base map

The base map is essentially a stratigraphic-facies map compiled from published sources, rather than a tectonic map, as used on most conventional maps. This was chosen to remove an important aspect of conceptual impermanency and subjectivity, so common with tectonic divisions. The colour of a unit indicates the geological age of its orginal lithogenesis, i.e. its 'first formation', and is the same for supracrustal (sedimentary and volcanic) and subcrustal (intrusive) rocks. The relative abundance, by 1970, of isotopic ages of most intrusive and metamorphic units made the traditional legends of geologic maps, which colour supracrustals by their stratigraphic age (e.g. Devonian, Lower Proterozoic) and intracrustals by their lithology (e.g. granite, gabbro), obsolete. The new design makes the relationship of contemporary rocks, although of different geneses and emplacement levels, immediately obvious. This is necessary for showing the background to metallogeny, because mineralisation is usually a product of lithogene interactions at different depths.

Geological units with complex history (mainly the 'geosynclinal' and 'basement' units) are shown in solid colour, representing their depositional age, over which are superimposed: patterns indicating post-depositional modification (deformation, metamorphism, granitisation), drawn in a colour corresponding to the age of such a process; patterns indicating lithologic association/facies (e.g. continental epiclastic coarse sediments, shallow marine carbonates, mafic submarine-volcanic-sedimentary associations, etc. ), drawn in a neutral colour.

'Unmodified' (i.e. undeformed, unmetamorphosed) rock units, such as the late or terminal products of local lithogenesis (e.g. post-kinematic 'granite' intrusions, platformic sediments, etc.), are shown by a lithologic pattern, colour corresponding to the formational age, over a white background. Both the lithologic and modification (e.g. intensity of metamorphism) patterns are arranged in the geologically true trend.

### Locality symbols

The out-of-scale symbols are superimposed on the base map, and consist of:

(1) a geographic location point, which may be obscured by the metal ratio rosettes, in which case it is their centre.

(2) Genetic/orebody shape/ore substance distribution/mineralisation symbol, located in the central part of the composite symbol. This is similar to symbols used on conventional metallogenic maps. Its geometry indicates orebody shape/mineralisation type; its orientation corresponds to the actual orientation of elongated orebodies; and the inside of the symbol may show the type of ore distribution (e.g. disseminated, banded, massive) by a black pattern. The colour of the inner symbol represents the age of mineralisation, and is a darker shade of that indicating the geological age of the rock unit on the base map. This immediately indicates the genetic relationship of the ores with the phase of development of the host rocks. Three relationships are common: (a) colour of the ore symbol corresponds to the 'depositional' age of the host unit, representing contemporaneity of rock and ore deposition (e.g. as in stratiform deposits); (b) colour of the ore symbol corresponds to the age of deformation or adjacent intrusions, representing magmatic or postmagmatic mineralisation, tectonometamorphic mobilisation, etc; (c) colour of an ore symbol located in a 'basement unit' corresponds to the colour of a nearby undeformed 'cover unit', representing mineralisation resulting from basement reworking by young near-surface agents, e.g. placers or mineralised laterites (The size of the inner symbols is uniform, regardless of the economic importance of the locality).

(3) Magnitude of mineralisation/grade category/metals information occupies the perimeter of the genetic symbol, and is significantly different from that on existing maps, both in the type of units used and the method of expression. The unit of magnitude of metal accumulation (ore deposits's 'size') is a 'ton-accumulation index' (Laznicka, 1970; see Fig. 1 for explanation) based on the mean crustal content of metals as a standard. This is an abstract unit that involves considerable calculation, and is, therefore, most conveniently derived from computerised data bases. Its initial disadvantage is that the user must become familiar with its derivation before using the map, but this is far outweighed by the unit's relative permanency (it changes only with revision of clarke values, and is insensitive to change of economic indicators, such as fluctuating metal price), and a rational logic in expressing cumulative magnitudes of polymetallic deposits. The tonnages of contained metal, or dollar values, are read directly from a set of graphs.

The anatomy and derivation of the metal/magnitude portion of the map symbol follows from Figure 1. Every metal is assigned an azimuth and shown by a spike in the map symbol. Twelve can be clearly accommodated in a single set, and membership in sets is distinguished by different patterns of spike; for example, a spike pointing 60° (ENE) represents tungsten if drawn as a solid line, and cobalt if dashed. The length of spike represents a 'ton-accumulation index' (quantity) of each metal in the ore deposit, and its magnitude can be obtained from a continuous, logarithmic scale. The outer ring represents the composite magnitude of an ore deposit, and is the sum of ton-accumulation indexes of constituent metals, based on the continuous log scale. The magnitude of metal concentration (ore grade) of the major metal is expressed by the pattern of the inner circle.

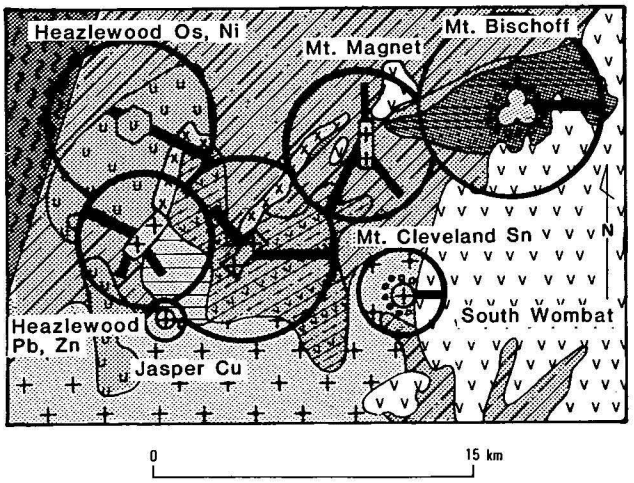


MINERALISATION STYLE

- *Magmatogene (segregation, etc.)*
- *Fissure vein (strike indicated)*
- *Replacement lode*
- *Irregular replacement mass*
- *Disseminations*
- *Placer*

Colour/pattern of a symbol indicates stratigraphic or lithologic affiliation of ore to a rock unit.

STRATIGRAPHY

- Tertiary
- Silurian, Devonian
- Cambrian
- Proterozoic

METAL COMMODITY

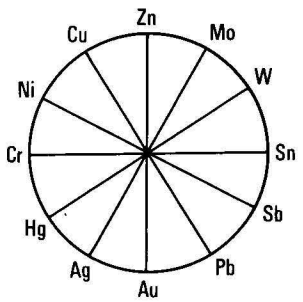


LITHOLOGIC ASSOCIATION

- *Continental olivine basalt flows*
- *Slate-quartzite*
- *Marine shale*
- *Quartz monzonite-granite*
- *Marine litharenite-shale (turbidite)*
- *Ultramafics-gabbro*
- *Marine argillite-quartzite*
- *Gabbro*
- *Marine basic/intermediate volcanics; shale, litharenite*

MAGNITUDE OF METAL ACCUMULATION

Shown as TON-ACCUMULATION INDEX $= \frac{\text{economic metal tonnage in a deposit} \times 10^6}{\text{metal clarke, ppm}}$

The symbol dimension is based on a continuous log scale

TON-ACCUMULATION INDEX

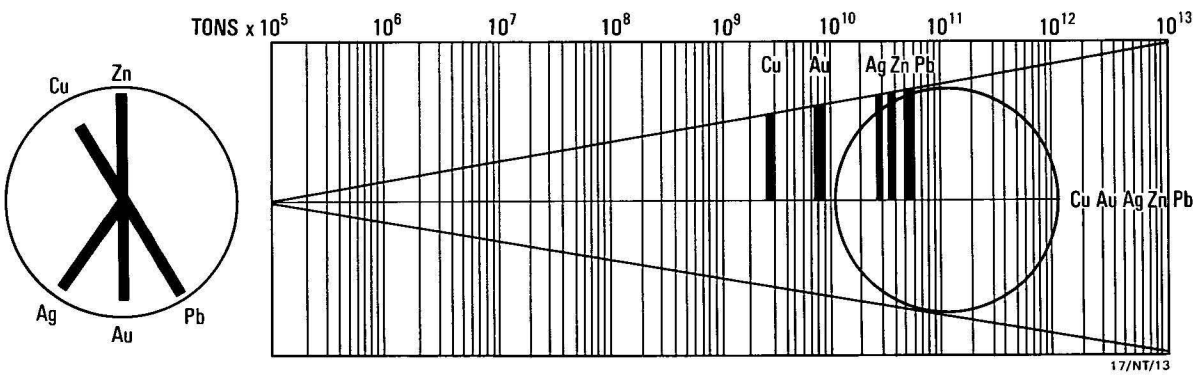


**Figure 1. Manuscript metallogenic map of Australia, 1973. An inset showing the Waratah-Luina area, N.W. Tasmania, and its legend.**

The manuscript metallogenic map of Australia has been demonstrated to a limited number of potential users, most of them practicing exploration geologists. Their reaction has been favourable. The colour of mineralisation age, matching the colours of lithogenesis, metamorphism, etc. in the base map, has been found to be extremely helpful for exploration and metallogenic assessments, and superior to the colour application on previously existing metallogenic maps. However, some short-comings have been noted. The metal magnitude and ratio symbols do not stand out sufficiently against the geological background, and their black colour interferes with fault lines as well as with geographic information. The symbols are particularly difficult to read in crowded areas, but this is a problem with all kinds of metallogenic maps, and not yet sufficiently solved. The manuscript metallogenic map of Australia also does not show localities of nonmetallics and fuels. Over all, experience with the map showed the need for further experimentation and this, in turn, showed that the amount of information incorporated in an ore deposit symbol had long since reached its limit. Suggestions for the future favour a series of metallogenic maps, illustrating particular aspects of ore deposits, plotted over either a uniform map base or, alternatively, several base maps giving different geological or geochemical backgrounds.

## Metallogenic maps with geologically more realistic symbolism

If the style and symbolism of existing metallogenic maps is ignored and a search started for the most realistic graphic representation of an ore occurrence on a metallogenic map, a geological section of such occurrence comes as an obvious solution. A locality section that is coordinated by colour and pattern with its geological base map can present the most faithful image of the spatial and temporal relationship of the ore with its surroundings, almost free of the compiler's subjective input. To show the necessary detail, however, most sections have to be prepared on a more detailed scale than that of the base map. However, there are two formidable groups of obstacles to this: (1) incompleteness of data; and (2) limitations in cartographic expression.

### Incompleteness of data

In an area such as the Pine Creek Geosyncline, three categories of ore occurrence, arranged by decreasing completeness and reliability of information, can usually be recognised: (1) well-studied and recently described localities, most of which are operating mines or economic deposits ready for production (e.g. Ranger, Jabiluka, Koongarra, and Nabarlek deposits in the Alligator Rivers district); (2) partially studied and described localities, most of which are small former producers (e.g. Mt. Bundey — Fe; Cosmopolitan Howley — Au), and localities that are part of clusters of ore occurrences of similar type, but different in detail (e.g. localities in the Maranboy Tinfield, Pine Creek — Union Reefs Goldfield, etc.); and (3) small occurrences, inaccessible mines, and recent confidential discoveries, on which very little reliable data are available (e.g. the numerous numbered Ranger prospects in the Jabiru area).

Only localities in category (1) and a few localities in category (2), about 40 out of the total of approximately 520 on the Pine Creek Geosyncline map sheet, would provide sufficiently accurate individual geological sections that could be directly incorporated onto the map. Of the rest, about 65 to 75 per cent are understood to the extent that simple category symbols showing mineralisation style, host rocks, and age of mineralisation could be prepared. The precise dimension, orientation, and characteristics of mineralisation are not known well enough to be shown. The meagre information available for the remainder of occurrences makes it possible to plot only their geographic location together with name and commodity symbol. As a result, a metallogenic map based on the above philosophy would have three categories of symbols by completeness, a solution that preserves the highest possible degree of realism, but also one likely to be criticised by advocates of metallogenic map uniformity.

### Uniform map symbols

Uniform symbols for mineralised occurrences based on the above data and principles can be obtained only if: (1) only the information available for all ore occurrences is included; (2) missing pieces of information are replaced by assumption; or (3) only information-rich localities are shown, and others excluded.

'Minerals Maps', such as the U.S. Mineral Investigations Resource Maps (e.g. Koschmann & Bergendahl, 1962) correspond to category (1) and show occurrences as location plots broadly graded by tonnage and an index number and/or name of locality. Most existing metallogenic maps are a combination of categories (2) and (3).

In detailed metallogenic maps of areas such as the Pine Creek Geosyncline, it is required that all localities be shown. On the other hand, the variety of mineralisation is considerably less than on metallogenic maps of entire continents, and most localities, although not necessarily described in detail in the literature, can, nevertheless, be assigned to a certain local mineralisation style be and given a symbol on the metallogenic map.

The concept of ore (mineralisation) types has recently been reviewed (Laznicka, 1981) with the conclusion that, despite a degree of inaccuracy, ore types are useful in regional metallogenic studies, if they are adequately defined and only similar size categories are considered together. Mineralisation styles are looser groupings of occurrences that, despite many similarities, are too heterogenous to enable a single representative locality to be selected.

**Table 1. Characteristics of mineralisation styles, Pine Creek Geosyncline.**

| *Code* | *Metals* | *Characteristics* | *Example localities* |
|---|---|---|---|
| S | Pb,Zn,Cu (Au,Ag) | Pyrite, pyrrhotite, sphalerite, galena, chalcopyrite, disseminated to massive banded, form stratiform lenses in carbonaceous (black), dolomitic or siliceous, marine volcanogenic low-grade Lower Proterozoic metasediments. | Iron Blow<br>Mount Bonnie<br>Rum Jungle-Embayment |
| | Au (Ag,As) | Gold-bearing pyrite, arsenopyrite and minor base metal sulphides disseminated in stratiform lenses, in the same association as above. | Golden Dyke |
| M | Pb,Zn,Cu (Au,Ag) | Sphalerite, galena, chalcopyrite, pyrite etc., in dolomite, quartz, etc. gangue form transgressive veins in the same association as the S style, from which they may have developed by remobilisation. | Woodcutters |
| | Au (Ag,As) | Quartz, pyrite, arsenopyrite, gold and minor base-metal sulphides, transgressive veins occuring in the same association as Fleur de Lys the S style, from which they may have developed by remobilisation. | Cosmopolitan Howley<br>Fleur de Lys |

| | | | |
|---|---|---|---|
| $G_1$ | Sn,W (Ta,Nb) | Scattered and disseminated cassiterite + wolframite in metasomatic pegmatites, often grading to greisens, in or near to granitic plutons. Locally abundant tantalite and lithium silicates. | Mountain View (W) Mt Finniss Mt Tolmer |
| $G_2$ $G_3$ | Sn(W) | Disseminations ($G_2$) and stockworks of veinlets, of cassiterite + wolframite in altered granite. Transitional to $G_2$, $G_4$ and $G_5$. | Yeuralba (partly) |
| $G_4$ | Sn,W | Scattered cassiterite and/or wolframite, arsenopyrite, chalcopyrite, etc. in quartz-mica 'katathermal' veins within granite. | Yeuralba (partly) |
| | W,Mo | Wolframite and molybdenite scattered in quartz veins within altered aplite dykes intruding a granite stock | Yenberrie |
| $G_4$ | U | Torbernite, autunite, hematite + apatite disseminations and small quartz veins in silicified shears and fractures in granite. | Fergusson R Edith R. |
| $G_5$ $G_6$ | Sn,W (Cu) | Quartz, cassiterite + chalcopyrite, arsenopyrite, etc. fissure 'katathermal' veins proximal to granite plutons. | Mt Wells Maranboy Yeuralba |
| $G_7$ | | Hydrothermal ('mesothermal') fissure veins and mineralized tectonic breccias, occurring in the thermal aureole of granitic plutons, with which they appear to be coeval. Transitional to 'M' style. | |
| | Pb,Zn(Cu) | Quartz-galena, sphalerite (primary), abundant secondary cerussite, smithsonite, hydrozincite, etc. | Mary River Coronet Hill, Minglo, etc. |
| | Cu | Quartz, chalcopyrite, pyrite (primary) abundant secondary malachite, azurite, chrysocolla, cuprite, chalcocite, etc. | Mt Diamond, Mt Ellison, Daly River |
| | Au(Ag,As) | Quartz, pyrite, arsenopyrite, minor base metal sulphides | Northern Hercules |
| | U (Cu) | Quartz, pitchblende + pyrite, chalcopyrite secondary torbernite, autunite | Adelaide R. George Creek |
| $G_8$ | Pb,Zn,(Cu) | Replacement bodies in carbonates, in same setting and transitional into $G_7$. | Evelyn |
| $G_9$ | Au | Quartz, pyrite, arsenopyrite, gold, shear, cleavage, and fissure-controlled open space filling and replacement veins, in tightly folded slates and greywackes in embayments near granite massifs | Pine Creek-Union Reefs |
| U | U(Au,Cu) | Dispersed, disseminated, fracture coatings, veinlets, veins of pitchblende, and a variety of secondary U minerals, in places with Pb, Zn, Cu, Ni, Co sulphides and arsenides and with gold. Form shallow, tabular to irregular orebodies preferentially in retrogressively metamorphosed, sheared, and brecciated schists and associated carbonates, chlorite and hematite altered, close to unconformities and basement massifs. | |
| $U_1$ | U(Au) | In metasediments, close to unconformity. | Ranger I Jabiluka |
| $U_2$ | U | In metasediments, under unconformable cover of Carpentarian sediments. | |
| $U_3$ | U | In metasediments, under cover of Cretaceous sediments. | Ranger 68 |
| $U_4$ | U | In erosional basement window, narrow tabular orebodies, high grade host metamorphism obscures Archean basement relationships. | Nabarlek |
| $U_5$ | U(Co,Ni Cu,Pb,Zn) | In metasediments, relationship to unconformable cover rocks weaker. | Rum Jungle |
| $U_6$ | U(Au) | In Carpentarian cover rocks. | partly El Sherana, etc. |
| R | | Residual mineralisation developed at paleosurface. | |
| $R_1$ | Fe | Massive to porous hematite and minor limonite overlying ferruginous and pyritic slates and schists. | Frances Creek Mt Bundey |
| $R_2$ | Mn | Porous Mn oxides overlying siltstone regolith. | Green Ant Cr. |
| $D_1$ | Sn(W) | Cassiterite in alluvial placers usually close to the bedrock source. | Mt Wells Myra Falls |
| | Au | Gold in proximal alluvial placers. | Pine Creek |
| $D_2$ | Ti,Zr,Fe | Distal beach placers of heavy minerals (magnetite, ilmenite, rutile, zircon). | Point Blaze |
| $D_3$ | | Paleoplacers — detrital heavy minerals in consolidated sediments. | |
| | Th,REE | Thorianite, monazite in Proterozoic sandstones. | Crater, Crusader |
| | Fe,Ti | Ilmenite, titanomagnetite in Proterozoic sandstone and siltstone. | Kapalga |

Compiled from data in Crohn (1968), Needham & Roarty (1980) and Needham (1981 — unpublished thesis).

Table 1 lists a suggested selection of mineralisation styles distinguished in the Pine Creek Geosyncline, and Figure 2 shows the corresponding geological section symbolisation. In contrast to the classification of mineral deposits in the Pine Creek Geosyncline proposed by Needham & Roarty (1980), no stratigraphic position is emphasised here, because it is variable and apparent from each individual map symbol.

Because of the considerable degree of subjectivity in introducing the mineralisation styles, it is preferable that their scope be broad rather than narrow, and that boundaries of mineralisation styles be based on distinct natural breaks, if at all possible, rather than on an accessory variation within a broad, transitional series of deposits.

Figure 3 compares the mineralisation-style symbols with the actual geological sections of twelve uranium deposits, members of the U category in Figure 2. Considerable variation in shape and position of individual ore bodies, local tectonic structures, immediate host rocks, size, etc. is obvious. It is, however, also clear that the variations are transitional and that only a few features are sufficiently strong or individual to justify a sensible subdivision of this mineralisation style into several sub-styles. Some localities appear to be the result of mixing of two or more mineralisation styles, for example, the Embayment mineralised zone at Rum Jungle (Dyson's and White's ore bodies; Fig. 3), where the U and S styles overlap. Elsewhere, two distinct mineralisation styles contribute to production or reserves at a single locality (e.g. tin-bearing veins and placers, as at Mt. Wells).

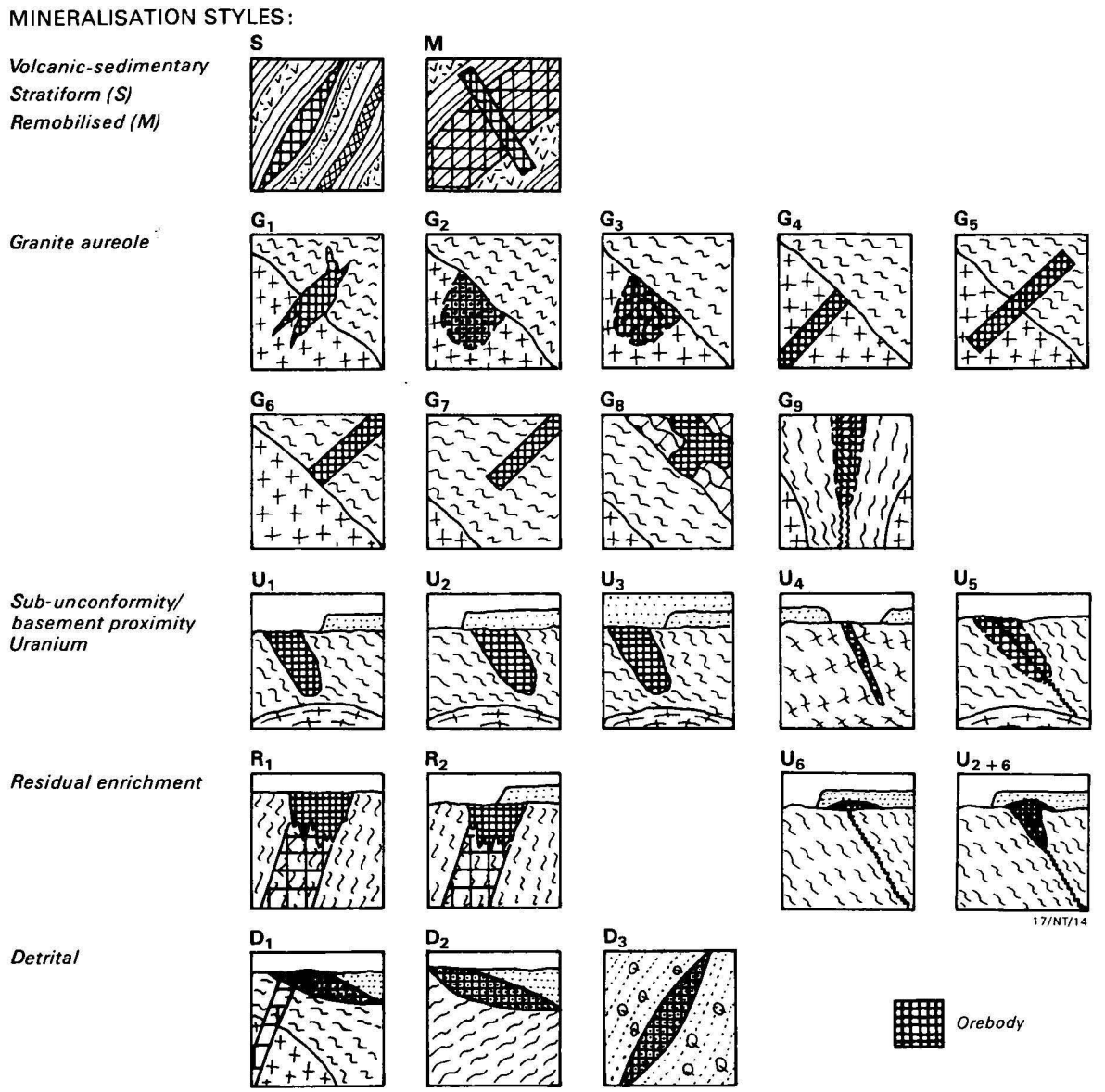


**Figure 2. Suggested symbols for mineralisation styles, Pine Creek Geosyncline map.**
(See Table 1 for the description of coded styles).

It is important to note that the geological section symbols do not indicate genesis. Vein deposits located in a 'granite' aureole (Fig. 2, category G) are distinguished by their position relative to the 'granite' contact and their approximately coeval relationship with the 'granite' is shown by the same 'age' colour. The reader is, however, not being pressed into accepting that the veins have been filled from below, from above, or laterally, or that the ore substance has been supplied by the 'granite' or from elsewhere. This gives him the freedom to decide according to his own belief and the latest genetic model in force. Elimination of the genetic aspects from locality symbols makes metallogenic maps more durable, credible and almost immune to the continuous change of genetic ideas.

Section-style locality symbols are especially convenient for multistage and genetically complex ore occurrences, which, on conventional maps, are displayed only as products of the very last generation or regeneration process. For example, the symbol for proximal detrital deposits (Fig. 2, category $D_1$) of gold and cassiterite shows the detrital orebody (placer gravel lens or sheet) as well as its primary bedrock source.

The section-style symbols have another advantage: they enable the expresssion of incomplete information and remove the need to complete it with guesses. If a locality is a vein located in a 'granite' aureole, but there is no proof that the vein and 'granite' are coeval, then the vein symbol will appear in the correct position, but its age colour will be white, that is, unknown. If the locality is an ore placer and its bedrock is unknown, only the placer part is shown in colour and pattern, whereas its bedrock remains blank.

## Limitations of cartographic expression

Because of the close connection between the base map and mineralisation symbol, colour, and pattern, it is paramount that the most critical area, the immediate surroundings of the locality on the base map, is not masked by the locality symbol. This presents a formidable problem to the method of cartographic expression.

The ideal solution would be a three-dimensional map, prepared, for example, from a base map with locality symbols pinned into it (Fig. 4). A variety of arrangements for such a map would possible, but all would be cumbersome to handle and impossible to print. To achieve the objective outlined above using conventional map techniques, a set of maps is needed, and their characteristics appear in the suggestions that follow.

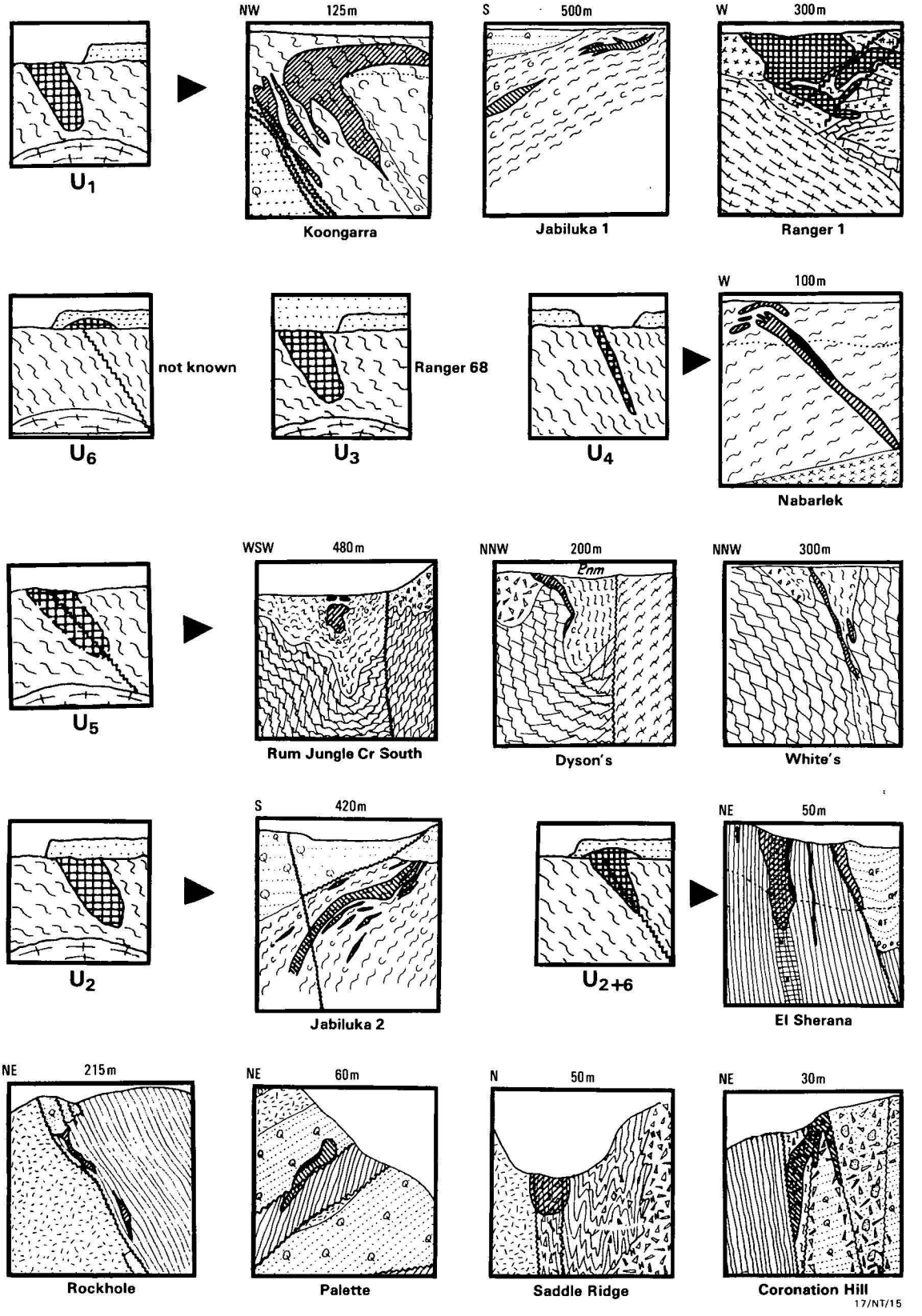


**Figure 3. Comparison of mineralisation-style symbols (marked U) with the actual geological sections of twelve uranium deposits in the East Alligator River, South Alligator River, and Rum Jungle districts.**

Based on data in Crohn (1968), Hegge & Rowntree (1978), Crick & others (1980), Fraser (1980), Hegge & others (1980), Stuart-Smith, personal communication (1981), and author's visits (1981).

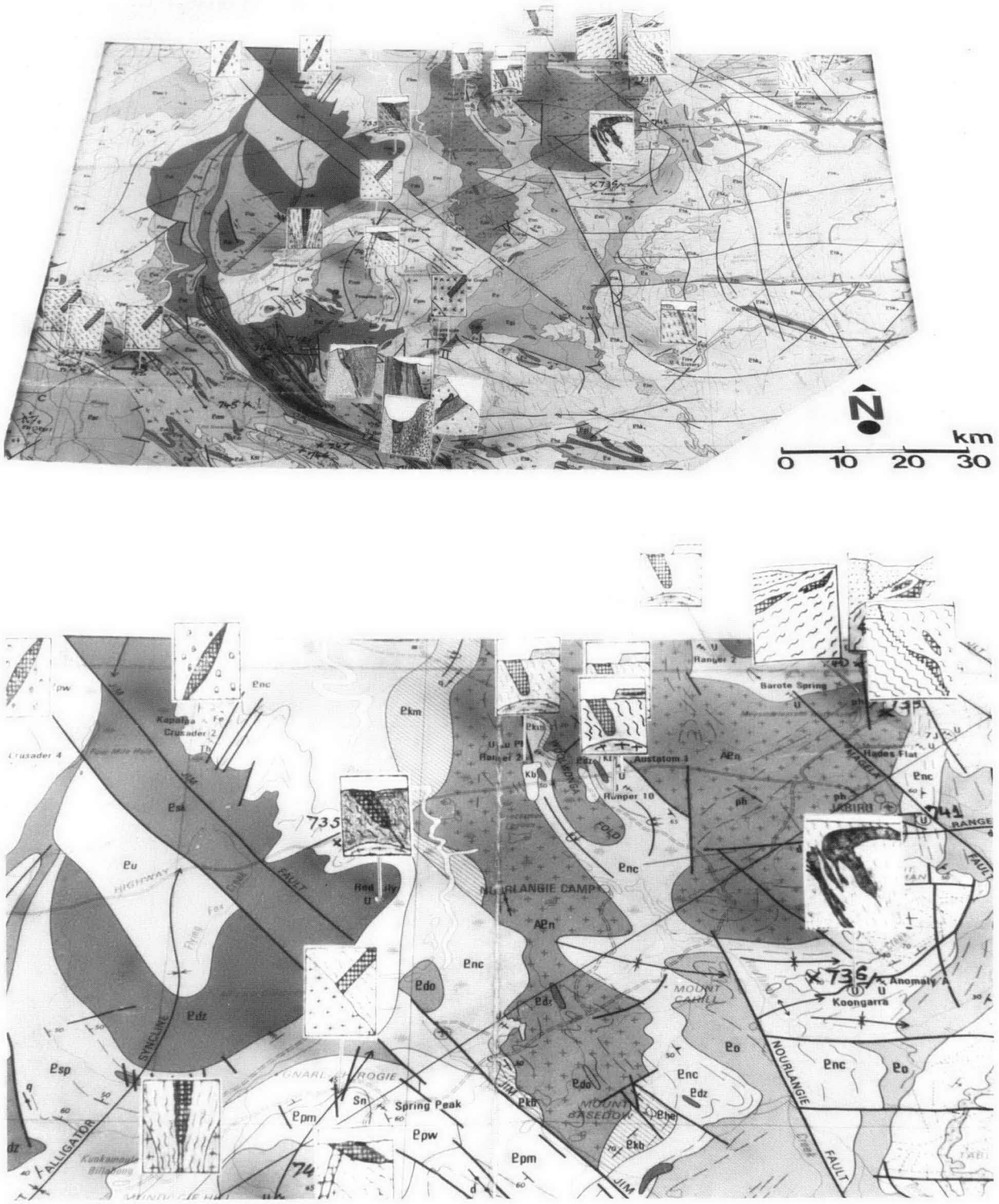


**Figure 4. Three-dimensional gitological map of a portion of the Pine Creek Geosyncline, showing section-style symbols of mineralised occurrences pinned in vertical position onto the base map.**

## A realistic metallogenic map, illustrated by the Pine Creek Geosyncline

The regional geology and mineralisation in the Pine Creek Geosyncline have been summarised by Walpole & Crohn (1968), Crohn (1975), Needham & others (1980), and Needham & Roarty (1980), and a coloured 1:500 000 geological map has been produced (Needham, 1979). A matching map of mineral occurrences and mineral districts accompanied by a very comprehensive data list forms part of Needham's M.Sc. thesis.

Abundant literature describes the geology of local areas, mineral deposits and occurrences in the region, and the history of ore discoveries, from the relatively small gold, tin, and lead-silver occurrences (Noakes, 1949; Sullivan, 1953), to the uranium and base metal finds in the Rum Jungle area (e.g. Roberts, 1960; Berkman, 1968), and the large uranium

discoveries in the East Alligator River district (e.g. Eupene & others, 1975; Rowntree & Mosher, 1976; Anthony, 1976). The symposium volume, Uranium in the Pine Creek Geosyncline (Ferguson & Goleby, 1980), provides the most comprehensive summary and reinterpretation to date of the Pine Creek Geosyncline metallogeny, not only of uranium.

The metallic mineralisation is widely, but very unevenly, distributed, and densely mineralised fields alternate with areas devoid of mineralisation. Needham & Roarty (1980) rated the mineralisation in the Pine Creek Geosyncline by value, and concluded that almost 97 per cent of the total value is due to uranium. Significant uranium mineralisation, however, is confined to three areas only, and the East Alligator Rivers field alone accounts for over 95 per cent of the total.

Needham & Roarty (1980) subdivided the mineral occurrences in the region into five categories by type and stratigraphic association:
(1) stratabound U and U-Au deposits in the Masson and Cahill Formations close to the Archaean basement; (2) stratiform and stratabound Ag, Pb, Zn, and Cu deposits, also in the Masson and Cahill Formations, throughout the former basin; (3) stratiform Au, U-Au, Pb, Zn, and Cu deposits in the Koolpin, Gerowie, and Kapalga Formations; (4) vein-type Au, Sn, Ag-Pb, W, Ta, Cu, Bi, etc. deposits, associated mainly with the early Carpentarian granites; (5) supergene Fe and Fe- Au deposits, located mainly in the Wildman Siltstone.

Genetically, the ore occurrences form a broad sequence from single stage to multistage mineralisation. Single-stage mineralisation resulted from an almost continuous process of concentration and accumulation of one or more ore metals, initiated against an almost geochemically neutral background by, for example, the process of igneous and sedimentogenic differentiation. The tin-tungsten veins in granite aureoles, an indisputable final product of granite differentiation, represent the most obvious example, although it can be argued that the granites themselves inherited their tin specialisation from their precursors. Single-stage ores show the most obvious and intimate relation to their parent units and their development history, and easily fit into conventional metallogenic classifications (including metallogenic map symbols).

Multistage mineralisation demonstrably forms by a series of steps, where, typically, each step increases the local accumulation of ore metals, mostly by confining the former broader metal reservoir into a progressively restricted volume of host rock or a mineralised structure. A generally accepted chain of events leading to the formation of uranium deposits in the Alligator Rivers and Rum Jungle ore fields that has emerged in the past ten years (e.g. Dodson & others 1974; Needham & Stuart-Smith, 1980), has three major steps: (1) local metamorphogenic and igneous-metasomatic enrichment of uranium in the Archaean basement complexes; (2) redeposition of detritus and uranium from (1), and additional uranium enrichment in certain lithologically favourable Lower Proterozoic units, e.g. in the Masson and Cahill carbonaceous shales; and (3) economic accumulation of uranium during localised, endogenous or exogenous, retrogressive reconstitution of (2) at shallow crustal levels.

Multistage mineralisation is exceedingly difficult to accommodate in conventional metallogenic models, because each enrichment step has to be considered separately and certain steps, often the final ones, coincide with lithogenically obscure and regionally unimportant events, such as the 1700–500 Ma events that finalised the uranium deposition in the Alligator Rivers district (Dodson & others, 1974; Hills & Richards, 1976).

Much mineralisation in the region falls, by its complexity, between the single-stage veins and the multistage unconformity uranium deposit; for example, the gold ores at the Cosmopolitan Howley mine (Sullivan, 1953) appear to have an identifiable two-stage genesis, having resulted from a tectonometamorphic remobilisation of a volcanic-sedimentary metal-enriched stratiform horizon (Needham & Roarty, 1980). Many Pb, Zn, Cu, Au, and Ag occurrences in the area appear to have a similar origin, and the proportion of the first-stage (stratiform) and second-stage (remobilised in veins or breccia) ores varies widely at different localities. No doubt, the most difficult task is the categorisation of epigenetic Pb-Zn(Cu) deposits hosted by contact-modified Lower Proterozoic supracrustals, in the aureole of the late orogenic granites (e.g. the Mary River, Namoona prospects): are they multistage products of remobilisation of stratiform metals in the host sequence or single-stage products of magmatic differentiation, independently supplied by the granite, without much contribution from the supracrustals? Problems like this fit into Krauskopf's (1968) category of 'unsolvables', problems that remain, no matter how much research is put into the attempted solution. Obviously, there is no sharp boundary between the above categories because of the widespread convergence, and there does not appear to be a practical pressing need for a solution, except, perhaps, one. This is the categorisation of genetic types of mineralisation, which, in turn, is needed for symbol construction on conventional metallogenic maps.

I believe that metallogeny of areas such as the Pine Creek Geosyncline can best be cartographically represented by a set of three maps: (1) a modified geological base map; (2) a gitological (= mineral deposits) map; and (3) a metallic map. This, however, does not take into account the practical requirements of production cost, and various modifications of the suggested format are certainly possible. One solution, suggested by the critical readers, was to place part of the information on the map margin, thus reducing the number of maps in the set.

(1) The base map is of utmost importance, and the compilers should take into account the requirements, outlined earlier, necessary for its coordination with the map bearing the locality symbols. For the Pine Creek Geosyncline, 1:500 000 would be the most suitable scale for the base map.

(2) The map showing geological properties of ore occurrences (gitological map, Fig. 5A, B) has out-of-scale symbols, placed in a uniform position in respect to the topographic location point (e.g. the point will be in the left- hand corner of the symbol, in the centre of the symbol, or offset in crowded areas, and indicated by an arrow). There is a wide selection of possible symbols, and it is thought that the mineralisation-style symbols described earlier are the most suitable for this map. The characteristics of the mineralisation styles and their limitations, however, will have to be thoroughly described on the map margin or in a companion report.

(3) The metallic (metal, commodity) map (Fig. 5C, D) shows the economically accumulated metals, their ratios, individual and composite magnitudes of accumulation, and intensity of concentration. It is suggested that the quantitative system of expression developed for the manuscript metallogenic map of Australia (Fig. 1) be used, possibly improved by the use of colour. Additional means of expression will have to be devised to show metals listed as commodities of small occurrences, where the lack of data prevents the use of the quantitative symbols. Uniform size colour dots have been used in Figure 5C, D. The background map is the same as the background of the gitological sheet.

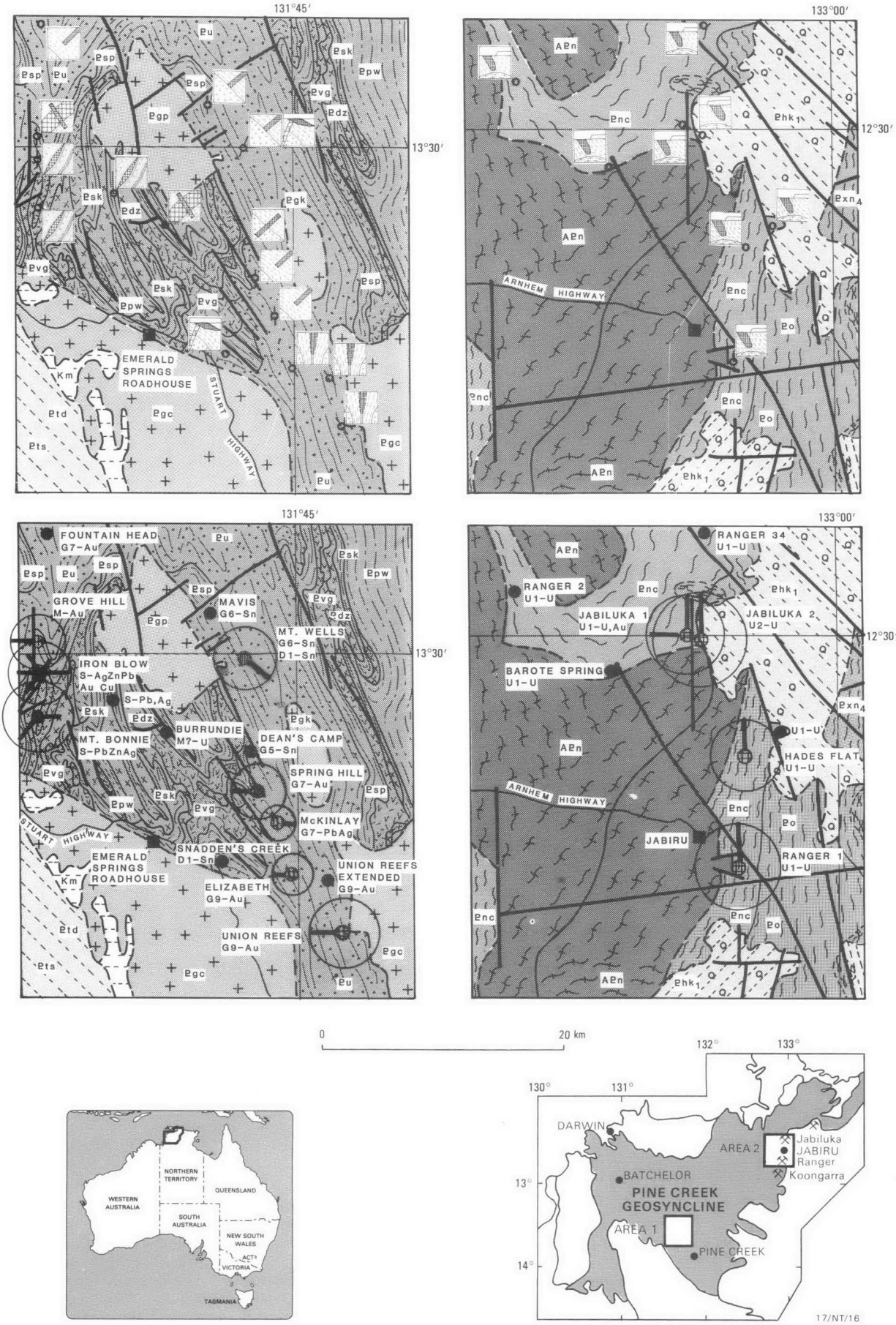


**Figure 5. Two areas (Margaret Syncline — Mt Wells — Union Reefs, and Jabiru area, East Alligator River Uranium Field) of the Pine Creek Geosyncline, 1:500 000, illustrating the proposed gitologic (top) and metallic (bottom) maps, and their references.**

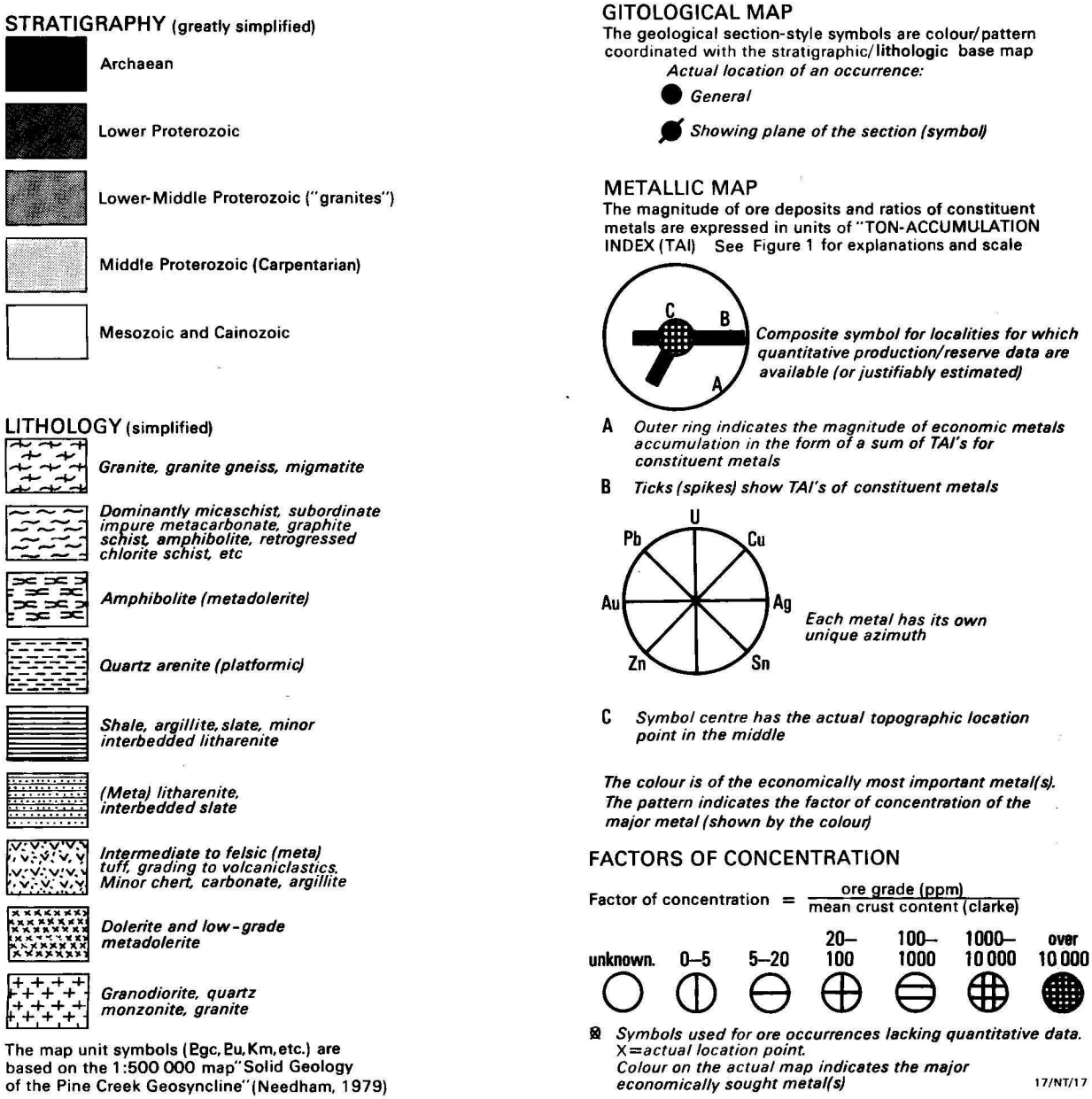


In contrast to many existing metallogenic maps, such as the Metallogenic Map of Australia (Warren, 1972) or Europe (Comité de la Carte Métallogenique de l'Europe, 1968–1973), metallogenic contouring or hatching to show outlines of metallogenic belts and provinces is not recommended here. Given the uncertain status of the regional metallogenic divisions (e.g. Turneaure, 1955; Petrascheck, 1965; Routhier, 1980) and a multitude of factors that control them — each factor having its individual outline, contouring appears justified only on large-scale maps, where it compensates for the impossibility of plotting all (or at least most) mineral occurrences.

Other than for showing the extent of mineral deposits distributed over large areas, such as coal, bedded iron ores, bauxite, etc., metallogenic contouring does not seem justified in detailed local maps such as the Pine Creek Geosyncline. Here, the established geological controls of mineralisation follow from the geological base map: the batholiths and their aureoles, the belts or units with favourable lithology likely to contain stratabound deposits, the traces of unconformities, the Archaean basement complexes. Controls not shown by the geological map are usually hypothetical and their inclusion could mislead the reader more than help him. How, for example, would the 'Uranium metallogenic province of the Alligator Rivers' be outlined?

The value of any geological report or compilation can be further enhanced by the availability of representative rock and mineral suites for public perusal. Particularly suitable for the representation of lithology and mineralogy of a metallogenic map area such as the Pine Creek 'Geosyncline', would be the portable documentation system 'LITHOTHEQUE' (Laznicka, 1974). This is a 'library' of rock and mineral specimens arranged cemented to aluminium plates, equipped by description/legend sheets and stored in a book-like manner.

## Acknowledgements

I am grateful to the Bureau of Mineral Resources, and particularly to Drs. J.N. Casey, K.R. Walker, and R.G. Dodson, for the hospitality and friendly assistance received during my short sabbatical stay in Canberra. Thanks are due to R.S. Needham for proposing the project and introducing me to the Pine Creek geology and for providing me with unpublished material from his Master's thesis, and to P.G. Stuart-Smith for

arranging and accompanying me on a highly informative tour of the Alligator Rivers region and its mines. Professors H.D.B. Wilson and W.C. Brisbin in Winnipeg, and Drs R.G. Dodson, J. Ferguson, K.R. Walker, and R.S. Needham and P.G. Stuart-Smith in Canberra are thanked for reading the manuscript.

## References

Anthony, P.J., 1975 — The Nabarlek uranium deposit. *In* Knight, C.L. (editor), Economic geology of Australia and Papua New Guinea. Volume 1 — Metals. *Australasian Institute of Mining and Metallurgy, Monograph* 5, 304–308.

Berkman, D.A., 1968 — The geology of the Rum Jungle uranium deposits. *In* Uranium in Australia Symposium. *Australasian Institute of Mining and Metallurgy, Melbourne*, 12–31.

Bowman, H.N., & Stevens, B.P.J., 1978 — The philosophy, design and application of the New South Wales Geological Survey's metallogenic mapping programs. *Journal of the Geological Society of Australia*, 25(3) 121–140.

Comite de la Carte Metallogenique de l'Europe 1968–1973 — Carte Metallogenique de l'Europe, echelle 1:2 500 000. *Bureau de Recherche Geologique et Miniere and UNESCO, Paris.*

Crick, I.H., Muir, M.D., Needham, R.S., & Roarty, M.J., 1980 — The geology and mineralisation of the South Alligator Valley Uranium Field. *In* Ferguson, J., & Goleby, A.B. (editors), Uranium in the Pine Creek Geosyncline. *Proceedings of the International Uranium Symposium on the Pine Creek Geosyncline, Australia 1979*, 273–285.

Crohn, P.W., 1968 — The mines and mineral deposits of the Katherine — Darwin region. *Bureau of Mineral Resources, Australia, Bulletin* 82, 171–304.

Dodson, R.G., Needham, R.S., Wilkes, P.G., Page, R.W., Smart, P.G., & Watchman, A.L., 1974 — Uranium mineralization in the Rum Jungle-Alligator River province, Northern Territory, *Bureau of Mineral Resources, Australia, Record* 1974/37.

Edwards, A.B. (editor), 1953 — The geology of Australian ore deposits. *5th Empire Mining and Metallurgical Congress Publications*, Volume 1.

Eupene, G.S., Fee, P.H., & Colville, R.G., 1975 — Ranger One uranium deposits. *In* Knight, C.L. (editor), Economic geology of Australia and Papua New Guinea. Volume 1 — Metals. *Australasian Institute of Mining and Metallurgy, Monograph* 5, 308–317.

Ferguson, J., Ewers, G.R., & Donnelly, T.H., 1980 — Model for the development of economic uranium mineralization in the Alligator Rivers Uranium Field. *In* Ferguson, J., & Goleby, A.B. (editors), Uranium in the Pine Creek Geosyncline. *Proceedings of the International Uranium Symposium on the Pine Creek Geosyncline, Australia, 1979*, 563–574.

Ferguson, J., & Goleby, A.B. (editors), 1980 — Uranium in the Pine Creek Geosyncline. Proceedings of the International Uranium Symposium on the Pine Creek Geosyncline, Australia, 1979. *International Atomic Energy Agency Vienna.*

Fraser, W.J., 1980 — Geology and exploration of the Rum Jungle Uranium Field. *In* Ferguson, J., & Goleby, A.B. (editors), Uranium in the Pine Creek Geosyncline. *Proceedings of the International Uranium Symposium on the Pine Creek Geosyncline, Australia, 1979*, 287–297.

Goulevitch, J., 1980 — Stratigraphy of the Kapalga Formation in the Pine Creek area and its relationship to base metal mineralization. *In* Ferguson, J., & Goleby, A.B. (editors), Uranium in the Pine Creek Geosyncline. *Proceedings of the International Uranium Symposium on the Pine Creek Geosyncline, Australia, 1979*, 307–318.

Grushevoi, V.G., & others, 1971 — Metallogenicheskaya karta S.S.S.R. mashtaba 1:2 500 000. 16 sheets. *Leningrad.*

Guild, P.W., & others, 1982 — Preliminary metallogenic map of North America, 1:5 000 000. *U.S. Geological Survey, Washington.*

Hegge, M.R., Mosher, D.V., Eupene, G.S., & Anthony, P.J., 1980 — Geologic setting of the East Alligator uranium deposits and prospects. *In* Ferguson, J., & Goleby, A.B. (editors), Uranium in the Pine Creek Geosyncline. *Proceedings of the International Uranium Symposium on the Pine Creek Geosyncline, Australia, 1979*, 259–272.

Hegge, M.R., & Rowntree, J.C., 1978 — Geologic setting and concepts on the origin or uranium deposits in the East Alligator River region, Northern Territory, Australia. *Economic Geology*, 73, 1420–1429.

Hills, J.H., & Richards, J.R., 1976 — Pitchblende and galena ores in the Alligator Rivers region, Northern Territory, Australia. *Mineralium Deposita*, 11, 133–154.

Knight, C.L., (editor) 1975 — Economic geology of Australia and Papua New Guinea. Volume 1 — Metals. *Australasian Institute of Mining and Metallurgy, Monograph* 5.

Koschmann, A.H., & Bergendahl, M.H., 1962 — Gold in the United States. *U.S. Geological Survey, Mineral Investigation Resources*, Map MR 24.

Krauskopf, K.B., 1968 — A tale of ten plutons. *Geological Society of America, Bulletin* 79, 1–17.

Lang, A.H., 1961 — A preliminary study of Canadian metallogenic provinces. *Geological Survey of Canada, Paper* 60–33.

Launay, de, L., 1907 — Le metallogenie de l'Italie et des regions avoisinantes. *10th International Geological Congress*, 1, 555–694.

Launay, de, L., 1913. Traite de metallogenie. Gites mineraux et metalliferes. *Beranger, Paris.*

Laznicka, P., 1970 — Quantitative aspects in the distribution of base and precious metal deposits of the world. *Ph.D. Thesis, University of Manitoba, Winnipeg.*

Laznicka, P., 1974 — LITHOTHEQUE — a system of rock and mineral specimens arrangement in geological education, documentation and exploration. *Centre for Precambrian Studies, University of Manitoba, Publication* 5.

Laznicka, P., 1975 — MANIFILE — the University of Manitoba computer-based file of world's nonferrous metallic deposits. *Geological Survey of Canada, Paper* 75–20.

Laznicka, P., 1981 — The concept of ore types — summary, suggestions and a practical test. *In* Wolf, K.H. (editor), Handbook of strata-bound and stratiform ore deposits. Volume 8 — General studies. *Elsevier, Amsterdam*, 499–511.

Lougnon, J., 1956 — Rapport général sur les gisements de manganese en France. *In* Reyna, J.G. (editor) Symposium sobre yacimientos de manganeso. 5, 63–171. *20th International Geological Congress, Mexico.*

McAndrew, J. (editor), 1965 — The geology of Australian ore deposits. *8th Commonwealth Mining and Metallurgical Congress, Publications*, Volume 1.

McLeod, I.R. (editor), 1965 — Australian mineral industry — the mineral deposits. *Bureau of Mineral Resources, Australia, Bulletin* 72.

Needham, R.S., 1979 — Solid geology of the Pine Creek Geosyncline, Northern Territory, geological map, 1 500 000. *Bureau of Mineral Resources, Australia.*

Needham, R.S., Crick, I.H., & Stuart-Smith, P.G., 1980 — Regional geology of the Pine Creek Geosyncline. *In* Ferguson, J., & Goleby, A.B. (editors) Uranium in the Pine Creek Geosyncline. *Proceedings of the International Uranium Symposium on the Pine Creek Geosyncline, Australia, 1979*, 1–22.

Needham, R.S., & Roarty, M.J., 1980 — An overview of metallic mineralization in the Pine Creek Geosyncline. *In* Ferguson, J., & Goleby, A.B. (editors), Uranium in the Pine Creek Geosyncline. *Proceedings of the International Uranium Symposium on the Pine Creek Geosyncline, Australia, 1979*, 157–173.

Needham, R.S., & Stuart-Smith, P.G., 1980 — Geology of the Alligator Rivers Uranium Field. *In* Ferguson, J., & Goleby, A.B. (editors), Uranium in the Pine Creek Geosyncline. *Proceedings of the International Uranium Symposium on the Pine Creek Geosyncline, Australia, 1979*, 233–257.

Noakes, L.C., 1949 — A geological reconnaisance of the Katherine-Darwin region, Northern Territory, with notes on the mineral deposits. *Bureau of Mineral Resources, Australia, Bulletin*, 16.

Page, R.W., Compston, B.W., & Needham, R.S., 1980 — Geochronology and evolution of the late-Archaean basement and Proterozoic rocks in the Alligator Rivers Uranium Field, Northern Territory, Australia. *In* Ferguson, J., & Goleby, A.B. (editors), Uranium in the Pine Creek Geosyncline. *Proceedings of the International Uranium Symposium on the Pine Creek Geosyncline, Australia, 1979* 39–68.

Permingeat, F., 1963 — Carte de gites mineraux de la France au 1 320 000, Lyon. *Bureau de Recherche Géologiques et Minières, Orleans.*

Petrascheck, W.E., 1965 — Typical features of metallogenic provinces. *Economic Geology*, 60, 1620–1634.

Roberts, W.M.B., 1960 — Mineralogy and genesis of Whites's orebody, Rum Jungle uranium field, Australia. *Neues Jahrbuch fur Mineralogie, Abhandlungen*, 94, 868–889.

Routhier, P., 1980 — Ou sont les metaux pour l'avenir? *Mémoires du Bureau de Recherche Géologiques et Minières* 105.

Rowntree, J.C. & Mosher, D.V., 1976 — Case history of the discovery of the Jabiluka uranium deposits, East Alligator River region, Northern Territory of Australia. *In* Exploration for uranium ore deposits. *International Atomic Energy Agency, Vienna*, 551–573.

Sharpe, J.I., 1968 — Mineral deposits map of Rouyn-Noranda area, scale 1:63 60 *Mineral Deposits Service, Quebec.*

Shatalov, Ye. T., & others, 1966 — Printsipy i metodika sostavleniya metallogenicheskikh i prognoznykh kart. *Nedra, Moscow.*

Stevens, B.P.J., 1972 — Metallogenic map sheet SI 55 — 8, Bathurst, 1:250 000. *New South Wales Department of Mines, Sydney.*

Sullivan, C.J., 1953 — The Katherine — Darwin metalliferous province. *In* Edwards, A.B., (editor), The geology of Australian ore deposits. *5th Empire Mining and Metallurgical Congress, Publication*, 1, 297–304.

Turneaure, F.S., 1955 — Metallogenetic provinces and epochs. *Economic Geology*, 50th Anniversary Volume 1905 — 1955, Part. 1, 38–98.

Walpole, B.P., Dunn, P.R., Randal, M.A., Skwarko, S.K., & Hays, J., 1968 — Geology of the Katherine — Darwin region, Northern Territory. *Bureau of Mineral Resources, Australia, Bulletin* 82, 1–170.

Warren, R.G., 1972 — A commentary on the metallogenic map of Australia and Papua New Guinea. *Bureau of Mineral Resources, Australia, Bulletin* 145.

BMR Journal of Australian Geology & Geophysics, 8, 307–311


# APPLICATION OF ENTROPY-RATIO MAPS TO SURFICIAL REEF FACIES, GREAT BARRIER REEF

B.M. Radke

Entropy-ratio maps enable mapping of surficial facies of coral reefs at any chosen resolution. A ternary classification uses detritus, framework encrustation, and pavement as end-members, and is subdivided on the degree of mixing of these. The classification is sensitive to all reef environments, particularly to zonation across reef flats. It can also be superimposed on other classifications. An example is given of its use in the Great Barrier Reef.

## Introduction

This paper describes an entropy-ratio classification of surficial facies and demonstrates its application to the mapping of coral reefs. Field procedures and techniques are outlined.

In reef studies there is a diversity of disciplinary interests, each with its own concepts and information to be presented in maps. Within each discipline there is a range of possible classifications that can be used to categorise data, from purely descriptive to totally genetic, and qualitative or quantitative in approach. Any one classification, however, is likely to be too specific to be extendable to other disciplines or to describe interdisciplinary relationships. One way of overcoming this problem is to superimpose the different classifications. Classifications may be general or specific, but if they have a well-defined quantitative basis they will be of much more value. There is also a need, particularly in reef studies, to standardise data- categorising procedures within disciplines, to ensure comparability of data and, thereby, the identification of reef variation both on local and regional scales (Stoddart, 1969). Entropy-ratio classification provides just such a standardised quantitative basis and entropy-ratio maps are ideally suited for interdisciplinary studies.

An entropy-ratio map is a facies map based on the degree of mixing of three end members of a given stratigraphic unit and that indicates by map pattern the nature of the lithologic 'mixture' through which a given end member is approached (Bates & Jackson, 1980; Forgotson, 1960).

In a Bureau of Mineral Resources' (BMR) reconnaissance study, an entropy-ratio classification has been developed for comparison of surficial reef cover, and used to produce maps of Wheeler, Viper, and East Stanley Reefs in the Great Barrier Reef (BMR, 1982). Geologically, the nature and distribution of surface facies of reefs can be extrapolated for interpretation of the subsurface, using Walther's law (Friedman & Sanders, 1978), and the entropy-facies classification can be modified for use on the subsurface sequence. However, the classification and maps discussed here refer only to the surficial sediments (uppermost 5 cm, approximately).

## Concept and method

Surficial facies are defined in a ternary system using framework encrustation, pavement, and detritus as end members (Fig.1).

**Framework encrustation (F)** encompasses all the substrate-bound hard skeletons of sessile organisms that construct open interlocking frameworks. The skeletal material itself, therefore, controls the morphology of the surface. The most significant organisms on present-day coral reefs are corals and coralline algae (Fig. 2a), and, to a lesser extent, substrate-bound pelecypods.

**Pavement (P)** is a cemented or bound surface with no active framework encrustation (Fig. 2b) and, arbitrarily, less than 5 cm of detrital cover. It is commonly a relatively flat eroded

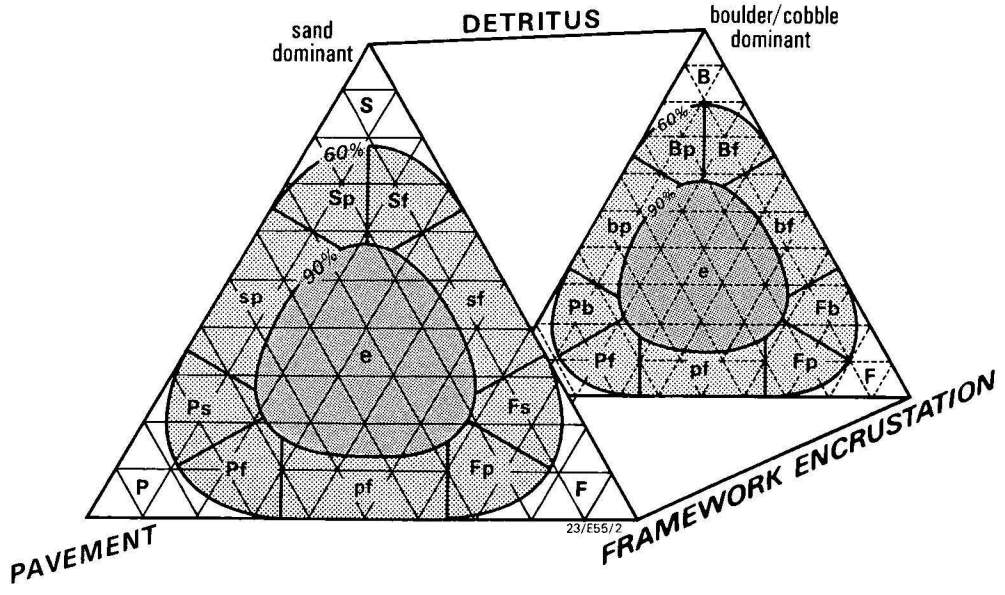


**Figure 1. Classification of surficial cover facies.**

a

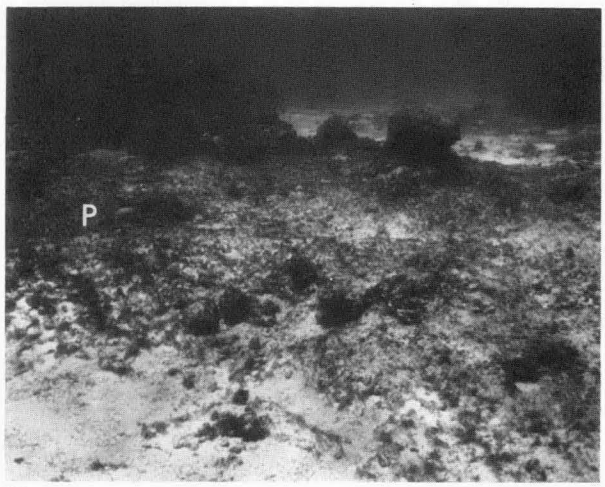


b

c

**Figure 2.**
A–Total framework encrustation of the windward reef crest at the change of slope from vertical wall to shallow subtidal ramp. There is extensive cover of overlapping platy and branching forms of *Acropora* at moderate depth, and more compact coral forms at the shallowest subtidal level. Viper Reef, (2 m at low water). B–Slightly raised pavement (P) interspersed with areas of detritus (light tones in foreground and background). Small bombies of framework encrustation rise off the pavement, which has low, scattered soft algal tufts. Viper Reef (1.5 m at low water). C–Profusely bioturbated sands with mounds of callianassid origin. Scattered patches of filamentous algae cover older sediment surfaces between mounds. Viper Reef (15 m at low water).

surface exposing indurated sediment and relict reef framework. It may also be hummocky and smooth, pitted, or potholed. Exposed pavement is commonly colonised by endolithic and epilithic soft algae, which give it a dark grey-green to brown-green appearance. Lighter-toned areas probably indicate grazing of the algae or abrasion by sediment.

**Detritus** is unconsolidated sediment (Fig. 2c), on most reefs almost exclusively calcium carbonate. It comprises reworked debris of disarticulated skeletons, whole tests of foraminifera, and material eroded from framework encrustation, pavement, or existing detritus. Detritus is subdivided on the relative abundance of fine and coarse components into sand-dominant (S) and boulder/cobble-dominant (B) categories, giving two parallel ternary systems. The sand-dominant group has a predominance of particles less than 1 ø *f*2 mm diameter), compared to the boulder/cobble-dominant field with particles predominantly above –6 ø (64 mm diameter).

The three substrate types, framework encrustation, pavement, and detritus, are invariably intermixed in most reef environments and, depending on the mapping scale used, cannot always be separated. The ternary fields are, therefore, subdivided into levels of relative entropy, which express the degree of mixing of the substrate types. (Relative entropy as defined by Pelto (1954) is the ratio of actual entropy to the maximum entropy which could be obtained with the same set of components.) With a limit of 60 per cent relative entropy, three fields are defined adjoining end members at the apices of the ternary system (Fig. 1). A field of maximum relative entropy is defined within the 90 per cent contour. Between the 60 per cent and 90 per cent contours of relative entropy, an intermediate zone is subdivided into 9 fields that are most easily distinguished from reconnaissance observations. With the subdivision of detritus into sand-dominant and boulder/cobble-dominant categories, parallel ternary classifications are produced. The maximum-entropy zones of the two classifications are undivided, and the total number of facies is 20 (Fig. 1).

In some circumstances, this degree of subdivision may be cumbersome for communication or comprehension. In these cases the number of classes in the 60–90 per cent relative entropy field can be reduced from 9 to 3 in each ternary system by grouping the intermediate classes: Sf + sf + Fs → SF; Sp + sp + Ps → SP; Pf + pf + Fp → PF. The number of classes in the whole classification is thus reduced to 10. In this paper, however, all 20 classes have been used, to demonstrate the maximum resolution.

## Mapping methodology

Preliminary airphoto interpretation is used to map zonal trends. Control sites are then selected on traverses across these zones for assessment by SCUBA divers. The control sites are circular and of a size appropriate for the map scale and resolution required. For 1:10 000 maps, areas of 50 m diameter have generally been used, except where photopatterns indicated smaller but distinct facies zones. Details are recorded on underwater slateboards (Figs. 2c, 4) and later transferred to a magnetic tape file for processing. Additional information is acquired from dive traverses on the reef margin slopes.

The main limitation to photo-interpretation is the decreasing resolution with increasing water depth (Fig. 3), because light penetration is dependent on water clarity, surface texture, and sun angle. Bathymetric profiles offer a limited extension to interpretation for depths that preclude SCUBA surveys. Ideally, submersible traverses or side-scan sonar techniques have greatest potential in these deeper zones.

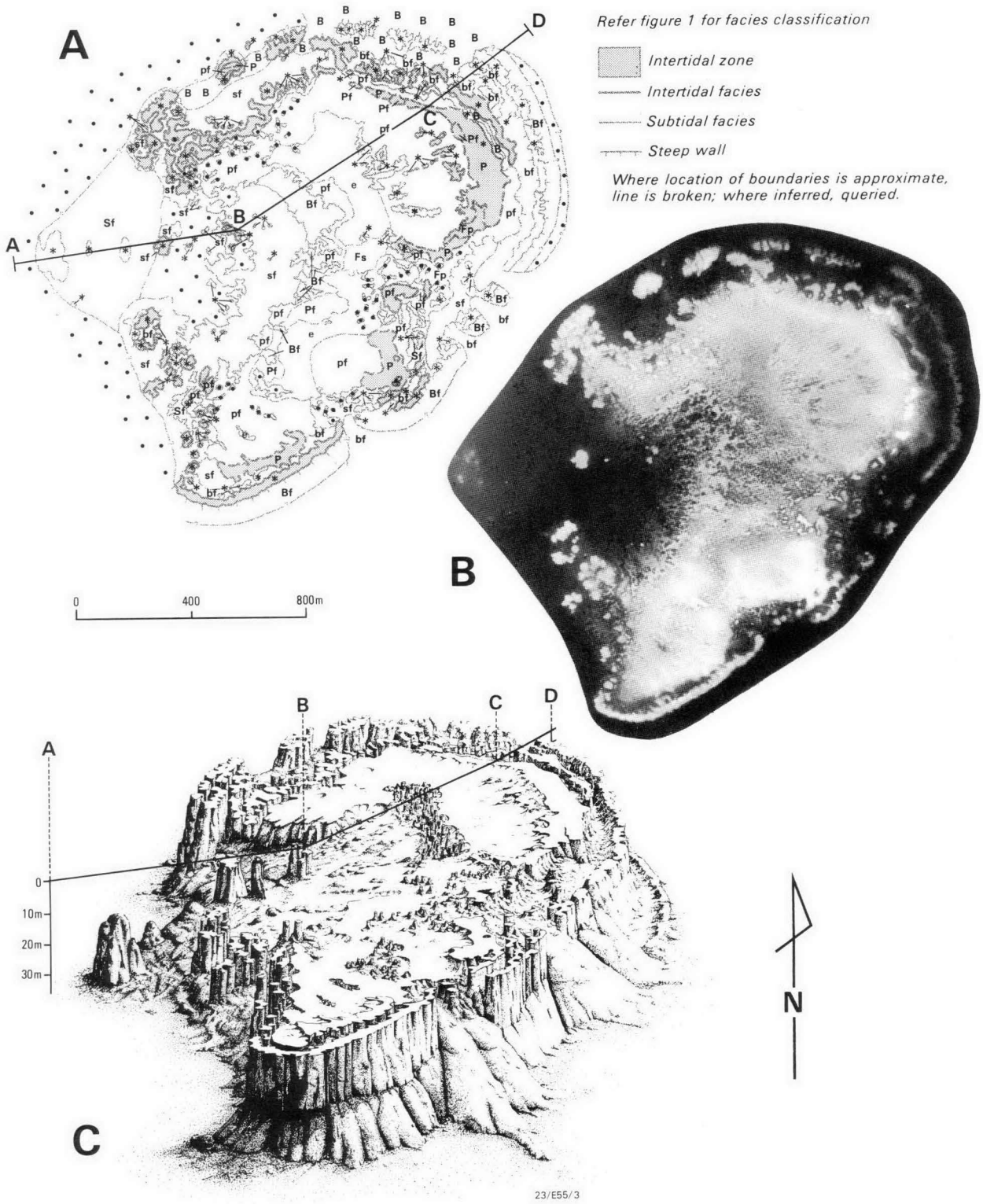


**Figure 3.**
A–Surficial facies map of Viper Reef, using classification in Figure 1 (from BMR, 1982). Comparison of the facies distribution with airphoto features shows the transtional nature of facies on gentle slopes and more distinct boundaries on steeper slopes. B–Aerial photograph of Viper Reef. C–Three dimensional view of Viper Reef, demonstrating bathymetric features of the reef (from BMR, 1982). The contrast between the steep-walled windward margin and the gently sloping leeward sediment wedge is a feature common to many reefs in this region.

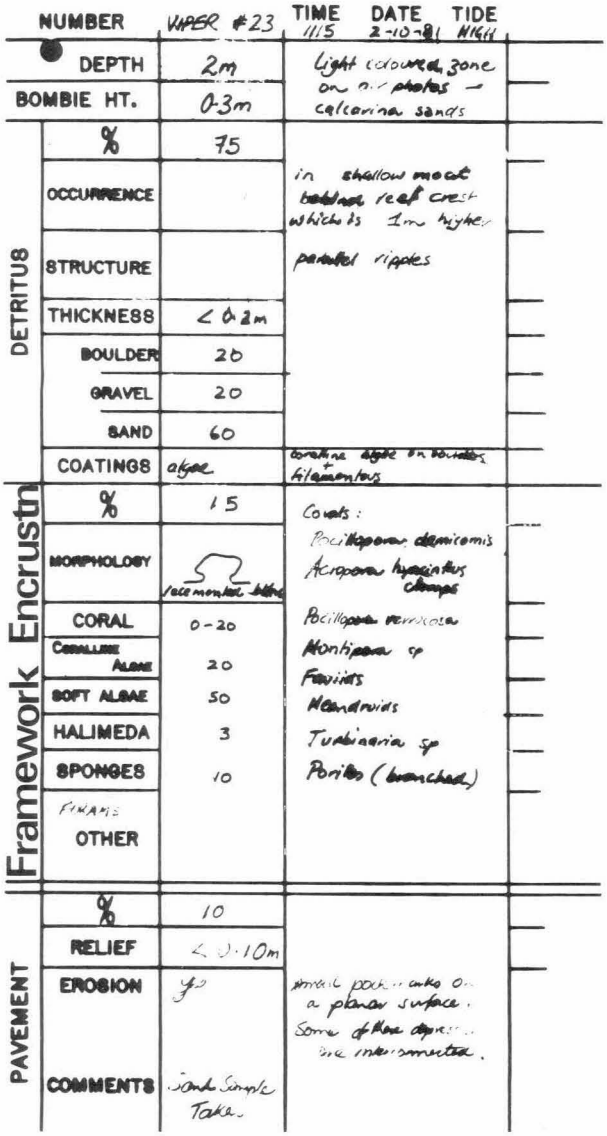


**Figure 4. Data inventory on slateboard used for each dive-control site.**
In addition to percentage cover of surficial types, descriptive elements including coral species are recorded for later compilation of species distribution.

End-member percentage abundance at each control site is plotted on the ternary system to determine the entropy-based facies type. The resolution of end-member distribution varies with map scale. Entropy levels are proportionally higher at smaller map scales. It has been found that, at any scale, resolution of mapping decreases with increasing water depth. Depending on the proposed usage of the map, resolution may be either standardised over the whole map, which requires acceptance of the lowest level of resolution, or be kept at various levels to preserve detailed information in shallower environments.

If the maps are printed in four colours, one for each detrital type and the other end members, the other facies are represented by intermediate colours (BMR, 1982). Where surficial facies are not superimposed on detailed bathymetry, tidal zones can be differentiated with different line weights on or between facies boundaries. Supratidal (above highest astronomical tide), intertidal, and subtidal (below low-water datum) zones are differentiated in Figure 3a.

## Viper Reef

Located at 18°52′30″S, 148°08′45″E, on the edge of the continental shelf, east-northeast of Townsville in the central Great Barrier Reef, Viper Reef is about 2 km long and roughly curved about an east-northeast axis (Fig. 3a, b). The south-eastern arm of the reef front is longer and more continuous than the northern front. The windward (east to southeast) main reef front (Fig. 2a) and the outer ridges (Fig. 5) are separated by deep, steep-sided moats with detrital floors (Fig. 3c) and are completely covered by framework encrustation. Leeward (west) of the reef front is a flat pavement zone (Figs. 3a, 5), which delineates the shallowest windward zone. This pavement is partly covered by low-relief shoals of boulder/cobble detritus. Further leeward, this pavement, which is at first variably encrusted with framework, slopes gently westward, through transitional detrital facies, to more framework encrustation interspersed with boulder/cobble detritus and then to a high-entropy reef flat. At depths greater than 5 m, the floor becomes predominantly sand (Figs. 2c, 3a). This example demonstrates that in areas of subdued relief the boundaries of most surficial facies are diffuse. Facies boundaries are sharper in areas of higher relief, where they generally coincide with breaks in slope at the base of steep walls (Fig. 3a, c).

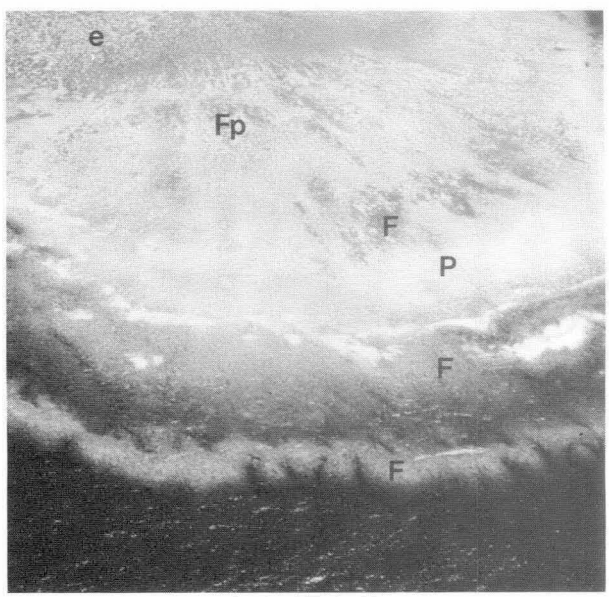


**Figure 5. Oblique aerial view of Viper Reef from the windward side, showing distinct outer ridges (F), moats, main reef crest (F), pavement (P) and transition (Fp) to increasing entropy (e) on the reef flat.**

## Discussion

The correlation of mixtures of substrate types with entropy zones gives a classification that can categorise both variation of the reef surface and the relative dominance of substrate types.

The surface of Viper Reef has been effectively classified by 13 of the possible 20 classes (Fig. 3a). Using the simplified classification, only 8 classes would be needed. Other reefs from the same region as Viper Reef show different substrate variation and facies proportions. For example, Wheeler Reef (BMR, 1982) is classified with 12 of the possible 20 classes, including one not present on Viper Reef. East Stanley Reef (BMR, 1982) requires 15 classes, including two not on either Viper or Wheeler Reefs. Between these three reefs in one province, there is significant variation of substrate type and

distribution that is not solely related to geomorphology. With a broader comparison of reefs, this variation would undoubtedly be greater.

Many zonation schemes, mostly based on geomorphology, have been applied to the description and mapping of reefs, and various disciplinary schemes have used a mixture of unrelated terms (e.g. Adey, 1975; Goreau, 1959; Hopley, 1982; Longman, 1981; Maxwell, 1968). These zone classifications offer easily comprehended generalisations for particular scales and, in some cases, specific provinces. However, their application to consistent quantitative mapping is very limited.

An additional problem with geomorphological categories is their lack of standardisation. Geomorphological nomenclature in the Great Barrier Reef has been extremely varied, and a generally accepted standardisation is yet to be resolved (Kuchler, in press, a). Without standardisation of terms there is little scope for meaningful comparative analysis of reefs beyond that of the nomenclature itself!

In contrast, the entropy-based classification has three distinct advantages in addition to its internal consistency.

1) It is applicable over a large range of scales, as it can accommodate different levels of resolution. LANDSAT imagery is presently being assessed for its applicability to regional mapping of the Great Barrier Reef (Jupp & others, 1981; Kuchler, in press, b), and the simplified entropy classification with only 10 classes has been successfully applied to this imagery by using an additional parameter, water depth, to allow correlation of substrate type with LANDSAT spectral classes.

2) Because of its simplicity and the minimal subjectivity in differentiating end members, the classification can be used for local, regional, or worldwide comparisons. It is the practicality of such standardisation that Stoddart (1969) saw as essential for comparing reef studies and the recognition of variations at local and regional scales. Comparison of gross sedimentological and ecological factors is possible with surficial facies, regardless of the details of biotic elements in the reef community.

3) It can also be applied to the subsurface and to ancient reefs, where the biota and communities were quite different. For this application, sampling needs to be modified to accommodate differences in preservation of pavement, a two- dimensional feature, and detritus and framework encrustation, which are preserved as three-dimensional bodies. From the geological viewpoint, it offers a practicable descriptive and genetic basis for comparison of surficial facies with those preserved in the subsurface. Classifications with morphological criteria are limited in that they can only be applied to the subsurface if the reef structure and its over-all relief are known or if morphological features are first interpreted in the context of specific substrate associations.

## Conclusions

An entropy classification of surficial facies, using framework encrustation, pavement, and detritus as end members, can be used for mapping coral reefs at all scales and degrees of resolution, and for comparisons between reefs. Facies derived from this classification can be superimposed on bathymetric, biological, morphological, and other classifications, offering a powerful and objective approach for communicating the character and complexity of reef surfaces.

## Acknowledgements

Funding for survey work in this study was, in part, from an Australian Marine Sciences and Technologies Advisory Council grant. Assistance with survey facilities and logistic support were provided by the Great Barrier Reef Marine Park Authority, Townsville. I thank K. Heighway, P. Davies, J. Marshall, and B. West for assistance with the dive surveys and for their constructive comments that helped develop this mapping technique. G. Wilford, P. Davies, J. Marshall, I. McIntyre, and an anonymous reviewer offered helpful advice on the manuscript. The text figures were drafted by Gail Young and R. Anderson.

## References

Adey, W.H., 1975 — The algal ridges and coral reefs of St. Croix. Their structure and Holocene development. *Atoll Research Bulletin*, 187.

Bates, R.L., & Jackson, J.A. (editors), 1980 — Glossary of geology. Second edition. *American Geological Institute, Falls Church, Virginia.*

BMR, 1982 — Great Barrier Reef surficial cover facies maps: Wheeler, Viper, and East Stanley Reefs, Queensland, 1:10 000. *Bureau of Mineral Resources, Canberra.*

Forgotson, J.M. Jr, 1960 — Review and classification of quantitative mapping techniques. *American Association of Petroleum Geologists, Bulletin*, 44, 83–100.

Friedman, G.M., & Sanders, J.E., 1978 — Principles of sedimentology. *Wiley Interscience, New York.*

Goreau, T.F., 1959 — The ecology of Jamaican coral reefs 1. Species compositon and zonation. *Ecology*, 40, 67–90.

Hopley, D., 1982 — The geomorphology of the Great Barrier Reef. *Wiley Interscience, New York.*

Jupp, D.L.B., Mayo, K.K., Kuchler, D.A., Heggen, S.J., & Kendall, S.W., 1981 — Remote sensing by Landsat as support for management of the Great Barrier Reef. *Proceedings, Landsat '81 Conference, Canberra, Australia*, 9.5.1–9.5.6.

Kuchler, D.A., in press, a — Geomorphological nomenclature: reef cover and zonation, Great Barrier Reef, Australia. *Great Barrier Reef Marine Park Authority, Technical Report.*

Kuchler, D.A., in press, b — Classification system: reef cover and zonation, for use with remotely sensed data, Great Barrier Reef, Australia. *Great Barrier Reef Marine Park Authority, Technical Report.*

Longman, M.W., 1981 — A process approach to recognizing facies of reef complexes. *In* Toomey, D.F. (editor), European fossil reef models. *Society of Economic Paleontologists and Mineralogists Special Publication*, 30, 9–40.

Maxwell, W.G.H., 1968 — Atlas of the Great Barrier Reef. *Elsevier, Amsterdam.*

Pelto, C.R., 1954 — Mapping of multicomponent systems. *Journal of Geology*, 62, 501–511

Stoddart, D.R., 1969 — Ecology and morphology of Recent coral reefs. *Cambridge Philosophical Society Biological Review*, 44, 433–498.

BMR Journal of Australian Geology & Geophysics, 8, 313–322


# POLLUTION OF A FRACTURED ROCK AQUIFER BY PETROL — A CASE STUDY

G. Jacobson

Shallow groundwater aquifers are susceptible to pollution by various contaminants. Amongst them, refined petroleum products are a serious hazard, because of their immiscibility with water, and the explosive and combustible nature of their more volatile constituents. Groundwater has been polluted by leaked or spilled petrol at two locations in Canberra in the Australian Capital Territory. At one location, seepage of the pollutant into the basement of a building caused a fatal explosion in 1977. Investigation by drilling showed that the pollution plume was pancake-shaped and floated on the water-table in a fractured mudstone aquifer; the plume extended over 5000 $m^2$ and was up to 4.5 m thick. Remedial action has been undertaken for five years by pumping groundwater from a deep bore to depress the water-table, and removing the petrol that collects in the cone of depression with a skimming device. About 40 per cent of the original spill of about 32 000 litres has been removed, and the source traced to leakage from a nearby service station. At a second site, a pollution plume of petrol occurs on the water-table in cavernous limestone and affects about 300 $m^2$. At this locality, petrol has entered the basement of a building as a result of a rising water-table after heavy rain. The two incidents are due to a combination of circumstances, which include the location of underground fuel tanks in an area with a shallow water-table and in close proximity to buildings with basements extending below the water-table.

## Introduction

In February 1977, a fatal explosion and fire occurred in the basement of a building in Canberra City in the Australian Capital Territory (Fig. 1). A plumber who had been welding pipes in the basement was killed in the explosion, and his assistant was injured. Because of the presence of explosive vapours and liquids, the building was closed for several months. The explosive fluids were identified as being mainly petrol, and the hydrogeology of the area surrounding the building was investigated with particular reference to the occurrence of the petrol in association with groundwater.

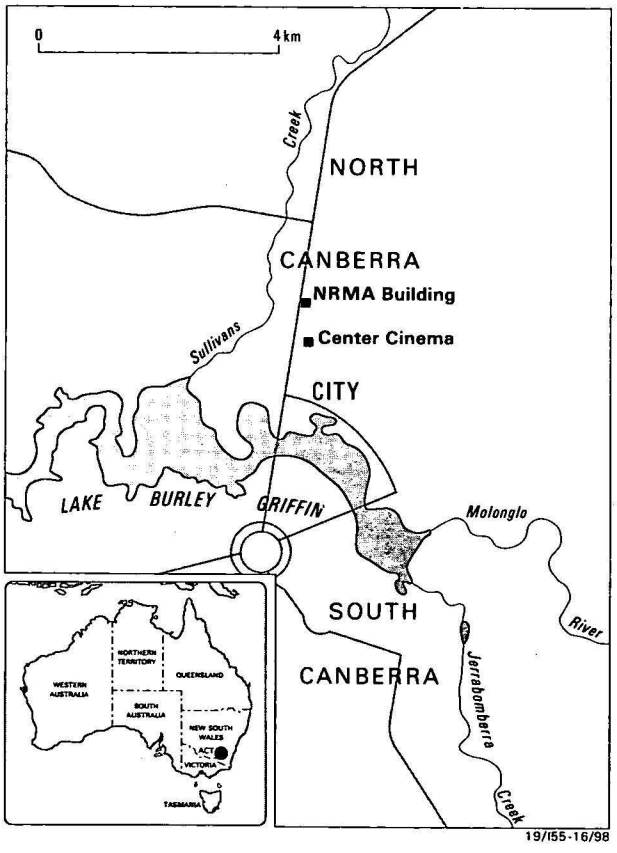


**Figure 1. Locality map.**

Investigations into the extent of the pollution plume and its probable source continued throughout 1977 and 1978 and enabled the design of remedial works. Surveillance of the area and monitoring of the remedial system have been maintained since then. The explosion and fire were the subject of a coroner's inquest in 1977 and subsequent litigation.

In September 1978, hydrocarbons with explosive vapours were reported in the drainage sump of a second building, in Braddon, about 600 m away (Fig. 1). This was investigated in 1979, and again resulted in the identification of groundwater pollution by petrol.

## Groundwater pollution by refined petroleum products

Groundwater pollution by refined petroleum products apparently has not previously been reported in Australia. The nature of the problem is, however, known from published case histories in the United States (Matis, 1971; Osgood, 1974; Williams & Wilder, 1971) and Canada (Clean Environment Commission, 1974; Hall & Quam, 1976). It has also been studied in Europe, where several case histories have been presented at symposia (Cole, 1974; Hepple, 1971; International Association of Hydrogeologists, 1978). The number of reported cases is increasing. Most overseas reports relate to the pollution of domestic water supplies; some are concerned with the explosive or fire hazard created by petrol fumes accumulating in basements.

Groundwater aquifers may become polluted by petroleum products in several ways, including surface spillages being washed into the ground or entering the ground through drains, the indiscriminate dumping of waste products, and leakage from underground storage tanks and fuel pipelines. Investigation of the situation is complicated when there are a number of service stations or other facilities that may contribute to the pollution.

In a typical case, when the petroleum product is spilled or leaked, it migrates downwards, by gravity. It may be adsorbed by soil before it reaches the water-table. Heavy oils do not readily penetrate the soil, while lighter fractions, in particular petrol, move through it more readily than water does. The distance a spill may travel depends also on the quantity released; the product leaves a coating on the soil particles as it

moves through successive layers, and is gradually reduced until movement virtually stops. Large spills travel further than small spills, and lighter fractions travel further than heavier fractions.

The spilled or leaked petroleum product need not reach the water-table itself in order to contaminate it. A rise in the water-table following rainfall may concentrate the petroleum product on the water-table, or heavy rains may flush it down to the water-table. Once the pollutant reaches the water-table, it penetrates the saturated zone, forming a recharge mound (Fig. 2); it also spreads laterally on top of the water-table. As the water-table rises and falls so does the petroleum product on top of the water.

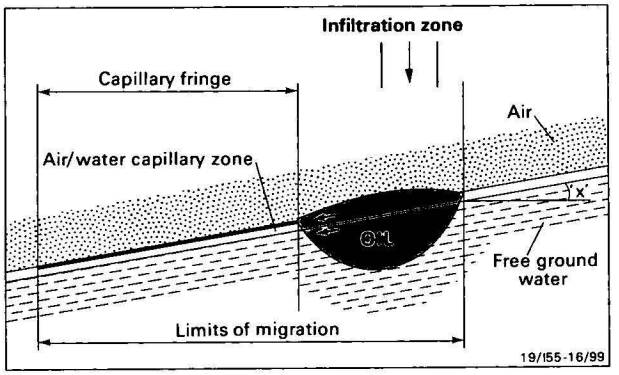


**Figure 2. Migration of hydrocarbons along a water table (after van Dam, 1967).**

Free hydrocarbons float directly on groundwater in a well; however, in the surrounding aquifer, there is a three-layer relationship in which the free hydrocarbons are separated from the groundwater below by a capillary fringe containing both water and hydrocarbons. Petroleum products that become distributed through the soil as part of the capillary fringe are not readily dislodged and their removal cannot be assured. Spreading of the pollution plume takes place mainly in the capillary fringe, and mainly in the direction of the hydraulic gradient. This has been demonstrated by model tests in porous materials (Schwille, 1967) and also theoretically (van Dam, 1967). It has been confirmed by the present field investigations in fractured rock aquifers in Canberra.

The seriousness of the pollution is affected by the solubility in water of the components of the petroleum product. Thus, the lighter hydrocarbon fractions have more components that are soluble than do heavier fractions. Soluble components are able to migrate with the water and release vapours, which may collect in sewers or basements. Fortunately, petrol vapours can readily be detected by smell at concentrations below the level of explosion hazard, and in many cases explosions can be prevented by monitoring. However, a hazardous condition may persist for a long time, during which a building will remain unfit for occupation unless the explosive vapours are evacuated.

## Central Canberra — the hydrogeological environment

The subsurface geology of central Canberra is known from records of building-site investigations (Henderson, in press). Quaternary alluvium covers the area surrounding the first building affected, the Center Cinema (Fig. 3) and fills a shallow depression that probably represents an old water course. The alluvium is 3–6 m deep and consists mainly of clay, 2.5–4 m thick, which overlies clayey to sandy gravel,

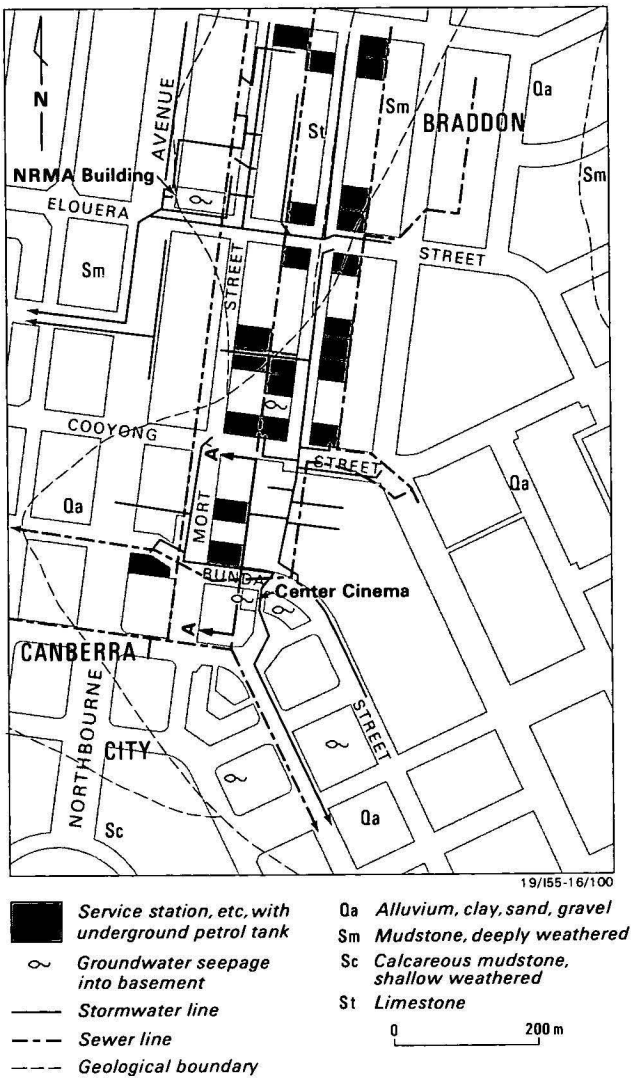


**Figure 3. Geology and hydrology of central Canberra.**

0.5–2 m thick. The bedrock beneath the alluvium at the first site is deeply weathered, fractured Silurian mudstone; at the second site, the NRMA (National Roads and Motorists' Association) building, it is cavernous Silurian limestone.

Groundwater occurs in the basal gravel of the alluvium, in the fractured mudstone, and in the limestone. The perched alluvial aquifer contains water intermittently after significant rainfall; it is unconfined and a water-table is evident. The fractured rock aquifer is continuous throughout the area: it is semi-confined beneath the alluvial cover, and water-levels in bores indicate the potentiometric surface to be about 4 m below the ground surface.

The groundwater catchments probably reflect the topographic catchments. The general direction of stormwater drainage in the catchment containing the Center Cinema building is southwards towards Lake Burley Griffin, and in the catchment containing the NRMA building it is westwards towards Sullivan's Creek (Fig. 3). Groundwater flow is probably also in these directions. The groundwater is of potable quality, and there are slight differences in its chemistry between the two sites, reflecting differences in rock type. At the Center Cinema, the groundwater contains about 200 mg/L total dissolved solids and is a bicarbonate/chloride water, with sodium the dominant cation. At the NRMA building, the groundwater contains about 330 mg/L and is a bicarbonate water, with calcium the dominant cation.

The area is urban and surfaces are paved; groundwater recharge is, therefore, mainly through leakage from stormwater drains. The stormwater drains are open-jointed, laid in trenches 0.5–1.5 m deep, and provide a ready path for groundwater infiltration. Groundwater recharge is, therefore, rapid after rainfall. The mean annual rainfall in Canberra is about 620 mm, fairly evenly distributed throughout the year.

The area is sewered by sealed pipes laid in trenches 3–5 m deep. The pipe bedding and backfill materials are sandy and more permeable than the surrounding alluvium. Intersections of trenches where stormwater drains cross sewer pipes allow particularly rapid infiltration of water underground.

The area contains more than 20 service stations and motor vehicle workshops in an area of 20 ha (Fig. 3), and there are more than 60 underground petrol tanks, all of which are potential sources of pollution. The tanks are set 3–4 m below ground level, which is close to the base of the alluvium. They are generally bedded in sand, which provides a ready path for the infiltration of leaked or spilled petrol.

## The first incident

### Investigation of the groundwater regime

Following the explosion and fire in February 1977, the groundwater regime in the vicinity of the Center Cinema building was investigated by diamond drilling and the setting of 37 open-tube piezometers (Fig. 4). Five piezometers were completed with slotted casing in the alluvium, and in the remaining drillholes, the alluvium was sealed off and slotted casing was set in the fractured mudstone to a depth of 11 m.

Groundwater was encountered in all the bores, although the five alluvial bores are often dry. The potentiometric surface in the fractured mudstone aquifer is depressed at the Center Cinema building (Fig. 4), and the main groundwater flow is from the north towards the building.

A cross-section (Fig. 5) illustrates the relationship between the potentiometric surfaces of the two aquifers. That of the mudstone aquifer slopes gently towards the building; the water-table in the alluvial aquifer is slightly higher and near the building it merges with the potentiometric surface of the mudstone aquifer.

Water entering the ground in the northern part of the catchment reaches the alluvial aquifer first and flows in accord with the water-table gradient towards the Center Cinema building. The building excavation acts as a sump for groundwater moving in the alluvium and also collects inflow from the underlying mudstone aquifer. The hydraulic gradients near the building are maintained by pumping from foundation drainage sumps. Monitoring of the piezometers has shown that water-levels in the alluvium are quicker to respond to rainfall than those in the mudstone.

Permeability tests in the alluvial bores, using the slug injection method, gave a mean hydraulic conductivity of 0.45 m/day. In the fractured mudstone aquifer, permeability tests, using the auger hole recovery method, gave a mean value of 0.05 m/day. The mean transmissivity of the mudstone aquifer was estimated, from the results of pumping, at 7.4 $m^2$/day, with a more transmissive component in the NE–SW direction. These hydraulic parameters were used in the assessment and design of remedial works.

Fluorescent dye tracing experiments between boreholes proved the hydraulic continuity of the aquifers; the velocities of the

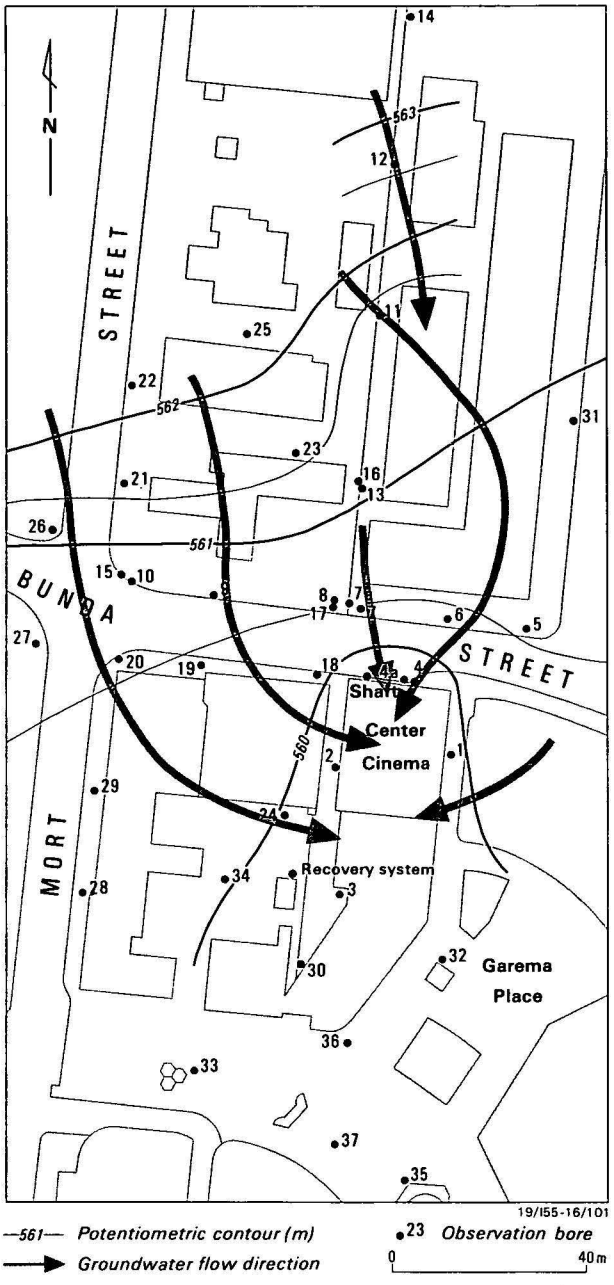


**Figure 4. Potentiometric contours of the fractured mudstone aquifer, and groundwater flow direction, July 1977.**

dye pulse ranged from 0.6 to 8.8 m/day (Smith & Jacobson, 1981). Some dye remained in the aquifers for at least one year and, with each recharge event, a new pulse of dye was transmitted to the observation bores.

## The Center Cinema building

A plan and cross-sections of the Center Cinema building foundations are shown in Figure 6. The building excavation is about 8 m deep, and extends through 4–5 m of alluvium into weathered and fractured mudstone. There is some rubble and slipped material next to the building.

The concrete slab foundations were located well below the water-table, and a foundation drainage system was installed to relieve uplift pressure. Groundwater is drained by a herring-bone system of rubble drains beneath the concrete slab, into two sumps. From these the water is pumped intermittently into stormwater drains outside the building.

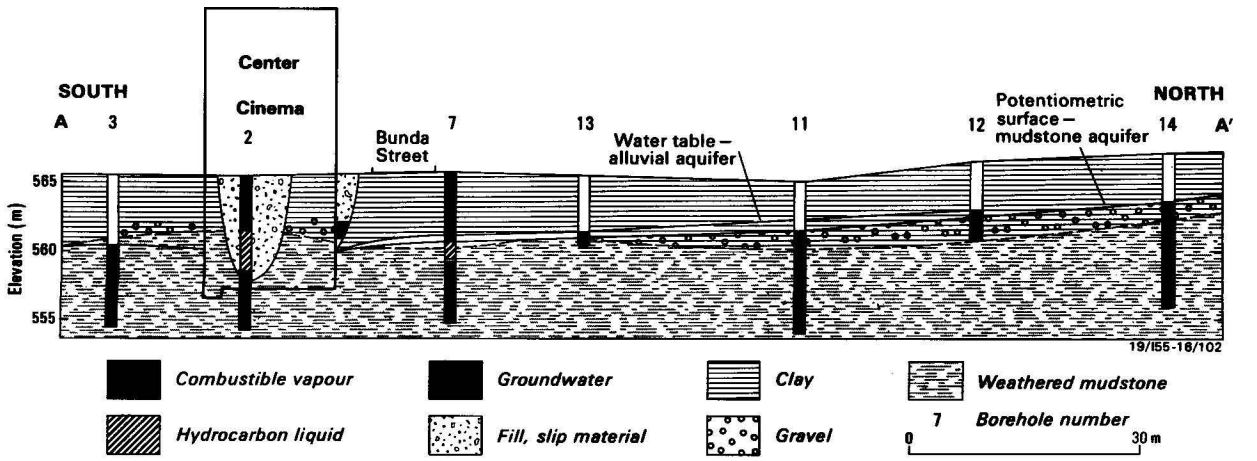


**Figure 5. Hydrogeological section through the Centre Cinema area.**
Line of section A — A' shown on Figure 3.

The total groundwater flow into the building was measured during March 1977 at about 10 $m^3$ per day. Petrol was present with the groundwater, particularly in the west drainage sump.

The scene of the fatal explosion was the north sump, which houses sewage ejection equipment, and is not connected to the foundation drainage system. At the time of the explosion, two vents, about 4 cm diameter, penetrated the north wall at 2.6 and 3.0 m, respectively, above the floor of the sump. The vents were installed some time after construction, to drain groundwater from outside the basement wall of the building and relieve condensation problems. For several months after the explosion, fluid levels outside the north wall were monitored by observation through plastic tubes attached to the vents in the wall. A layer of petrol persisted on top of the water through March and April 1977. As the fluids rose after each rainfall event, fumes entered the building through the vents and built up to danger level within the sump. Once the rising water had pushed the petrol layer above the level of the top vent, the high concentration of combustible gas dissipated quickly. Groundwater was also seen to enter the north sump through cracks in masonry and concrete at floor level.

A stormwater main in front of the Center Cinema was found to be blocked and was cleared a few days after the incident. The blockage probably contributed to high groundwater levels outside the north wall of the building.

The explosion is attributed to the following circumstances. The Center Cinema building occupies a deep excavation that lies across the path of natural groundwater flow from the north and northwest. Pumping of water from the drainage sumps maintains a cone of depression in the water-table, on which petrol moved to, and became trapped against, the walls of the building. The cone of depression became effectively a sump for the collection of petrol. Fumes were first reported in the building in mid-1976, as a result of petrol entering either the groundwater drainage system or the sewage ejection pit. The explosion occurred in the sewage ejection pit, where petrol fumes entered through the apertures in the wall or through fractures in the concrete and masonry.

## The pollution plume

Petrol with explosive vapours was encountered in two bores in the deepest part of the alluvium (4a and 7a on Fig. 7), in ten bores in fractured mudstone (3, 4, 7, 9, 16, 17, 19, 23, 24 and 30), and in a bore in fill material close to the Center Cinema (bore 2). In most cases, because of the injection of large quantities of water during drilling, it took several weeks for the petrol to enter the bores and establish a column that indicated the thickness of petrol-saturated ground.

Potentiometric contours and groundwater flow directions in July 1977 are shown in Figure 4. The pollution plume was regarded as a lens of petrol floating on the water (Holzer, 1976), which had the effect of raising the fluid surface above the potentiometric surface of the groundwater. The potentiometric contours in Figure 4 were drawn from the corrected fluid surface levels, using Australian oilfield data to relate water/hydrocarbon saturation ratios to the height of the petrol column above the water table. The flowlines were then constructed to intersect the modified potentiometric contours at right angles, and thus indicate the movement paths of underground fluids in the area.

The thickness of the petrol column in piezometers was monitored weekly, using a mechanical fluid-level measuring device to obtain the depth to the top fluid surface, and an electrical water-level gauge to obtain the depth to the petrol/water interface. The extent of the pollution plume was shown by isopachs of petrol thickness in drillholes (Fig. 7).

In July 1977, the pollution plume extended over an area of 5.3 ha, beneath several buildings. The thickest part, about 4.5 m, was close to bore 9 in Bunda Street. The plume was roughly pancake-shaped with an elongated fringe extending southwards from Bunda Street.

Subsequent monitoring for several months indicated southwards spread of the pollution plume (Fig. 7) along the direction of groundwater flow. During this time, the thickness of the petrol column in bore 24 increased to more than one metre (Fig. 8) and a number of bores presented traces of petrol for the first time.

To estimate the volume of petrol in the ground it was necessary to assume a value for porosity, which is the percentage volume of pores and fractures in the rock. A value of 1.3 per cent was estimated from measurements of joints in drill cores. However, values of 0.15–1.0 per cent were estimated by relating porosity to the flow velocity of the dye tracer in different parts of the groundwater system near the Center Cinema. For purposes of computation, a value of 1.0 per cent porosity was assumed.

Both water and petrol were, and are, present in the pollution plume. The over-all percentage of petrol in the pollution plume was calculated at 41 per cent, using Australian oilfield data for water/hydrocarbon saturation ratios. In July 1977, the volume

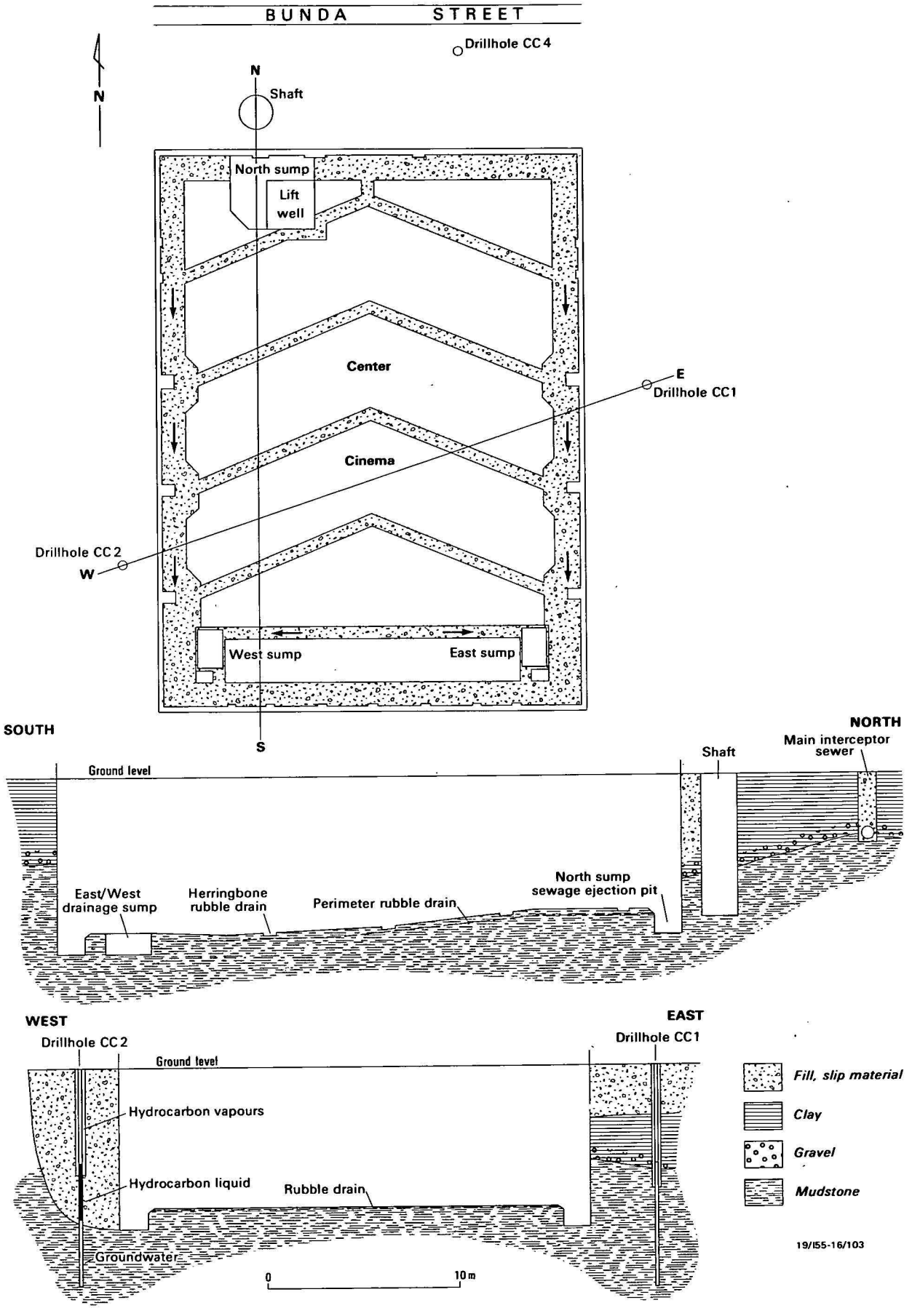


**Figure 6. Foundation plan and sections, showing drainage system of Center Cinema.**

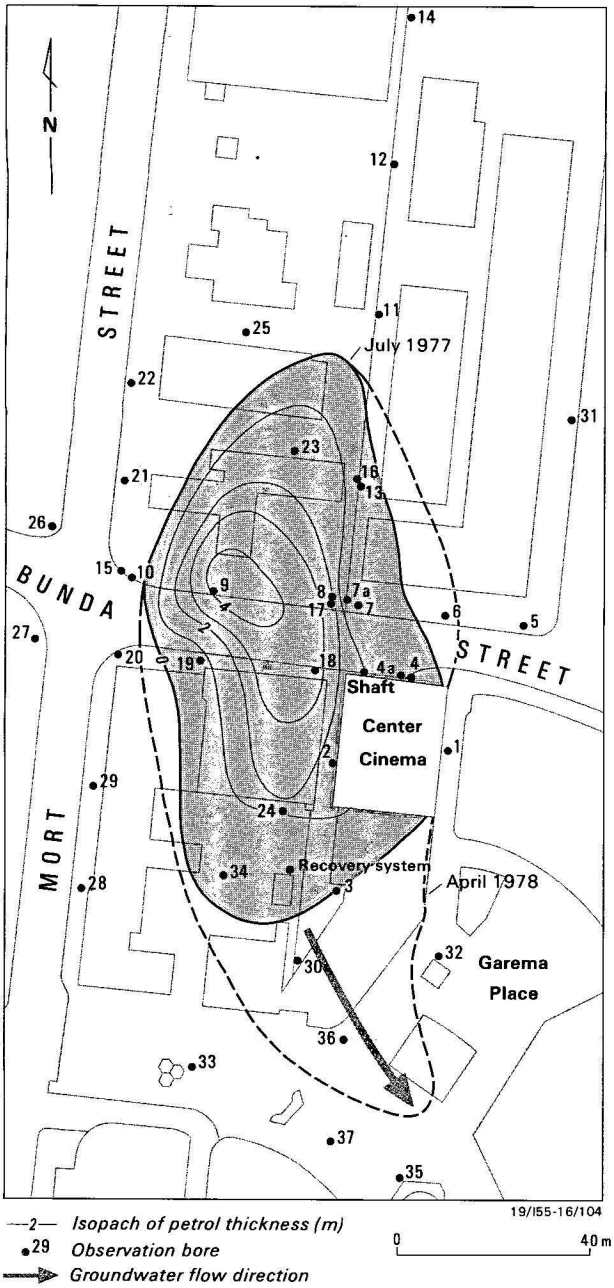


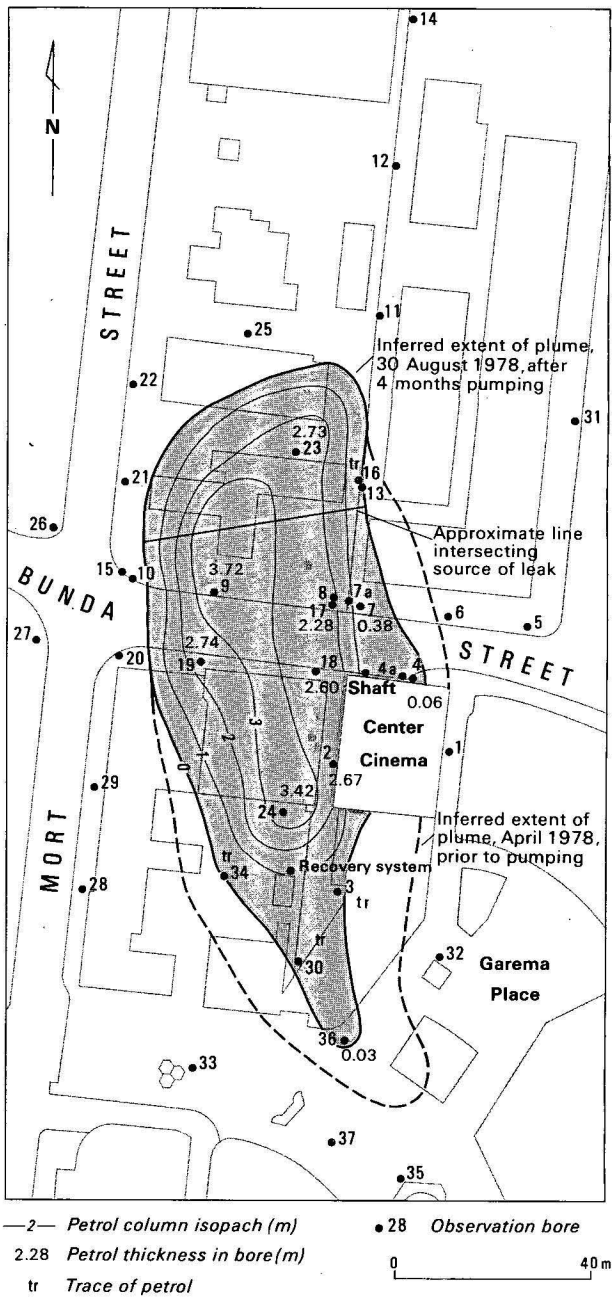


**Figure 7. Isopachs of petrol thickness in observation bores, July 1977, and drift of the pollution plume to April 1978.**

of rock containing the pollution plume was estimated at about 7800 $m^3$ and, assuming 1.0 per cent porosity, the volume of fluids in the plume was estimated at 78 000 L, of which about 32 000 L was petrol.

## Source of pollution

Hydrocarbons from the Center Cinema building and nearby bores were analysed by the BMR Petroleum Technology Laboratory, and comparisons were made with analyses of petrol from local service stations. The principle analytical methods used were gas-liquid chromatography, distillation, specific gravity, refractive index, and evaporation tests.

The results showed that the samples taken from the Center Cinema consisted mainly of petrol, with small amounts of dissolved heavier hydrocarbons present in some samples. The samples from the bores consisted of fresh super-grade petrol

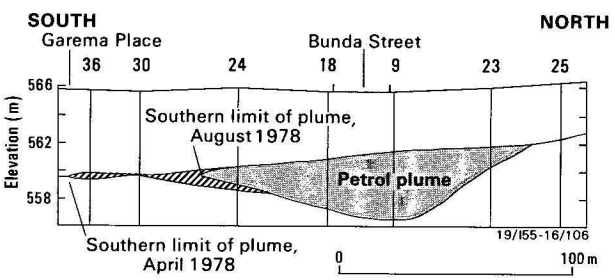


**Figure 8. Petrol thickness in observation bores, August 1978, after 4 months of pumping.**

that had retained its volatile components and was, therefore, considered to have travelled underground from a nearby source. Comparison of the bore samples with petrol samples from local service stations showed similarities to two brands of super-grade petrol sold in the area. The analytical evidence

indicated that the petrol was derived from a leaking underground installation rather than a surface spillage. It was not possible, however, to positively identify the source from the analyses.

Hydrogeological observations relevant to the origin of the petrol concerned the extent and thickness of the pollution plume (Fig. 7). It was considered that the maximum thickness of the petrol, at bore 9, must be close to the point of infiltration.

The theoretical maximum distance that the hydrocarbon plume would move up the hydraulic gradient from the point of infiltration of the petrol was calculated. According to van Dam (1967, p.85), the limit of up-dip migration, I, is given by $I = (e - c)/\tan x$, where e is the elevation of the top of the hydrocarbon lens, c is the elevation of the groundwater potentiometric surface projected through a point below e, and tan x is the hydraulic gradient of the potentiometric surface (Fig. 2). The variables on the right hand side of the equation were derived from investigation data (Fig. 4). Thus, in the vicinity of bore 9, the limit of up-dip migration, $I = 0.58/0.02$ m = 29 m.

As bores 22, 25, and 11 had remained free of petrol since monitoring began, the up-dip limit of the pollution plume was considered to be between bores 23 and 25. A line across the slope of the hydraulic gradient 29 south of the limit of the plume was considered likely to intersect the source of the leak (Fig. 9). This line is midway between bore 23 and bore 9, and the source of the petrol was probably close to the line within the 3-m isopach. This location is the site of underground petrol storage tanks at a service station close to the affected building.

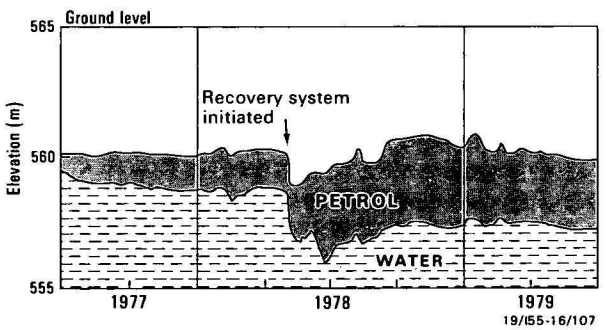


**Figure 9. Petrol thickness in observation bore 24.**

## Remedial works

Remedial measures were undertaken by the owners of the building; the basement and drainage sumps were sealed off and ventilated.

Outside the building, on the north side, a shaft was constructed in August 1977 to drain and collect petrol; petrol is removed from the shaft once a fortnight by suction pump. Later, concern about the drift of the pollution plume beneath the city centre led to the design of a remedial pumping system. This system was installed near the south end of the pollution plume in April 1978. It consists of a deep borehole to depress the water-table by continuous pumping and an adjacent recovery well (Fig. 10). Petrol moves slowly on the depressed water-table towards the recovery well, where it is skimmed off by a stainless steel conveyor belt and transferred to an underground tank.

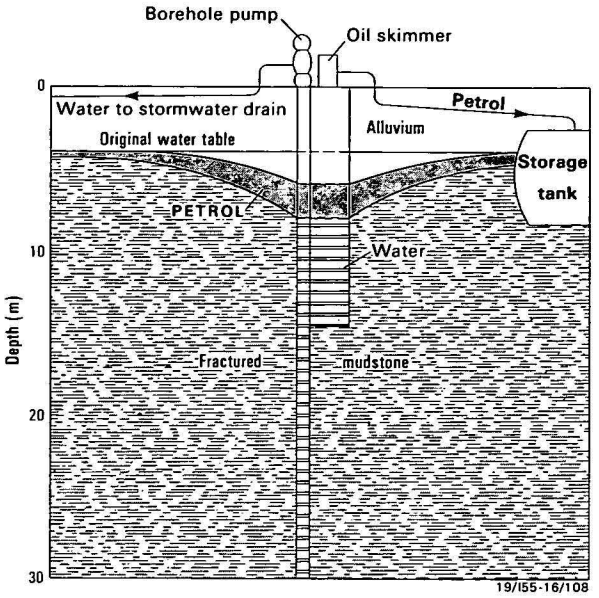


**Figure 10. Petrol removal system.**

Figure 11 shows the potentiometric contours of the mudstone aquifer and groundwater flow directions after two weeks' operation of the pumped-bore removal system. A cone of depression developed over almost the entire pollution plume with groundwater flowing radially inwards towards the pumping bore. This cone of depression has been maintained since 1978, with the exception of short periods of pump repair.

Petrol-column isopachs based on observation bores after about four months pumping are shown in Figure 9. The effect of the pumping has been to draw petrol towards the pumping bore, especially from the southern end of the pollution plume. A total of 1100 L of petrol was removed in the first four months; in addition, an unknown amount was removed as vapour through the ventilation system. Some petrol has been removed with water from the building's drainage sumps, and a small amount has been removed from the shaft. The southwards drift of the pollution plume has been arrested. Figure 12 shows the isopachs of petrol thickness in observation bores in October 1982. It is estimated that about 40 per cent of the original spill has been removed. The bulk of the remaining petrol has migrated southwards towards the pumped-bore removal system.

## The second incident

The NRMA building in Braddon has a sump that collects groundwater inflow to the foundation drains of the building. The sump was installed when the building was constructed in 1969, after groundwater had flowed into the excavation. In September 1978, petrol entered the sump after heavy rain on three occasions and explosive vapours were present.

The investigation at this site included six drillholes to depths of 12–17 m, which were equipped with slotted plastic casing to serve as fluid-level monitoring bores. Five of them, bores 1, 3, 4, 5, and 6 (Fig. 13), encountered irregularly weathered, cavernous limestone with clay and gravel cave-fillings. Drillhole 2 intersected clay and gravel to a depth of 12 m without reaching bedrock.

Groundwater was encountered in all six drillholes; the water-table is 4–5 m below ground surface and slopes gently to the west. A cross-section through the building (Fig. 13) shows that

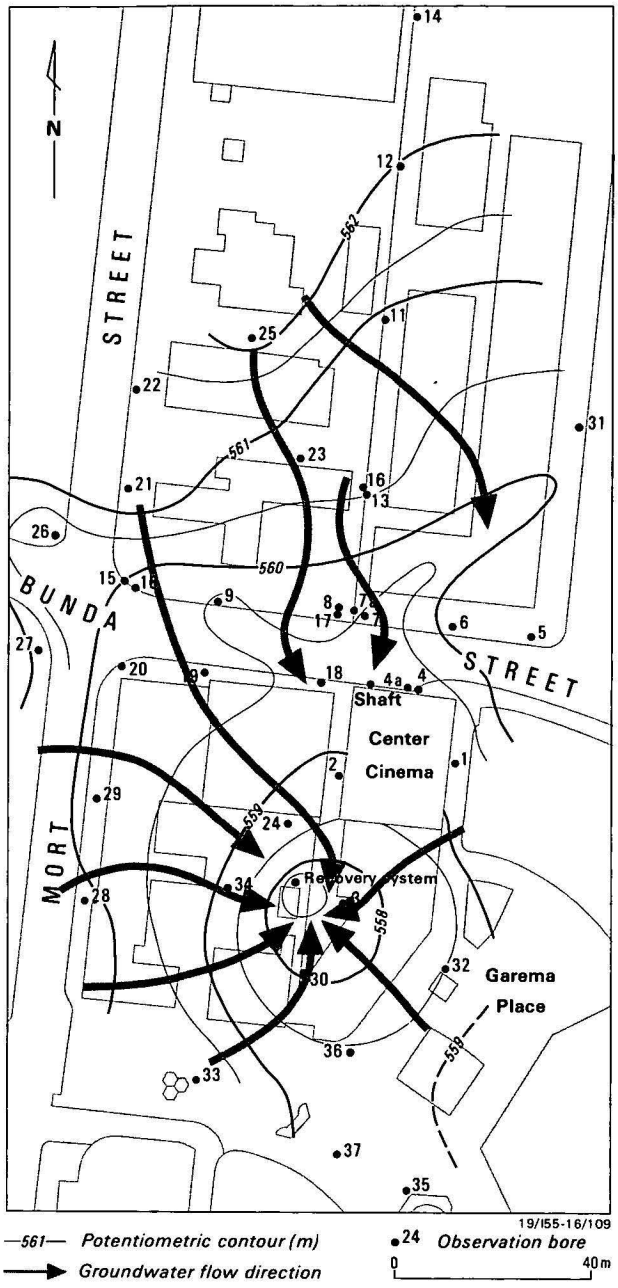


Figure 11. Potentiometric contours of the mudstone aquifer, and groundwater flow direction, after two weeks of pumping.

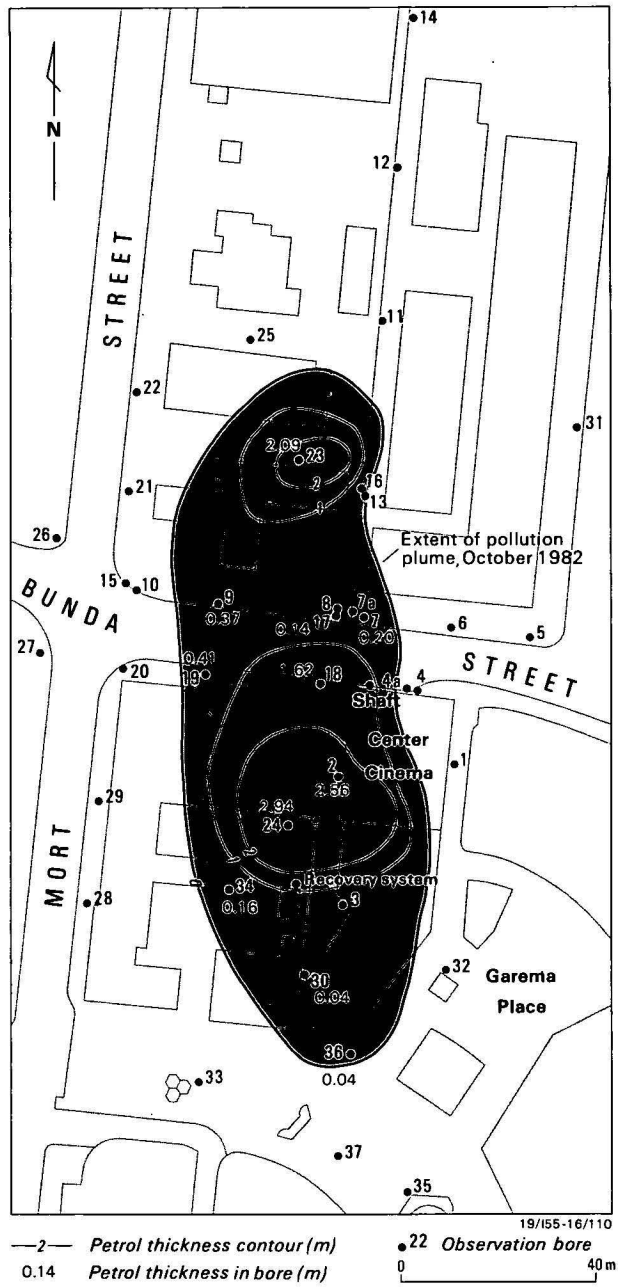


Figure 12. Thickness of petrol pollution plume, October 1982.

the water-table is, at times of high rainfall and groundwater recharge, close to the level of the foundation drains.

## The pollution plume

Petrol has been observed on top of the water-table in three of the observation bores. It was observed in bore 1 soon after drilling, and the column of petrol has since ranged in thickness from 0.84 m to 0.30 m late in 1982. In bore 2, petrol thickness has ranged from 0.53 to 0.13 m late in 1982. In bore 3, the petrol thickness has ranged from 0.49 m to 0.30 m late in 1982. The decline in petrol thickness is regarded as indicating that petrol is no longer being added to the pollution plume.

The pollution plume is believed to be continuous between the bores that contain measurable quantities of petrol, and probably extends for some distance laterally beyond them. The inferred extent of the pollution plume in February 1980 was about 300 $m^2$ (Fig. 13). The total volume of petrol-saturated rock was estimated as about 200 $m^3$, and the total amount of petrol in the pollution plume was about 2000 L.

In March 1979, the water-table and the petrol floating on top of it were just below the level of the foundation drains along the west side of the building. A rise in the water-table brought petrol into the drains and thence into the sump on three occasions in September 1978. It has not occurred since, possibly because subsequent years have been relatively dry and groundwater-levels have remained low.

The inferred extent of the pollution plume includes an underground petrol tank in the building's own car park, and this tank and its fittings have been considered the most likely source of petrol. The tank was excavated in November 1979, and petrol was observed in the excavation. However, tests on the tank did not detect any leakage. The most likely source of the petrol is

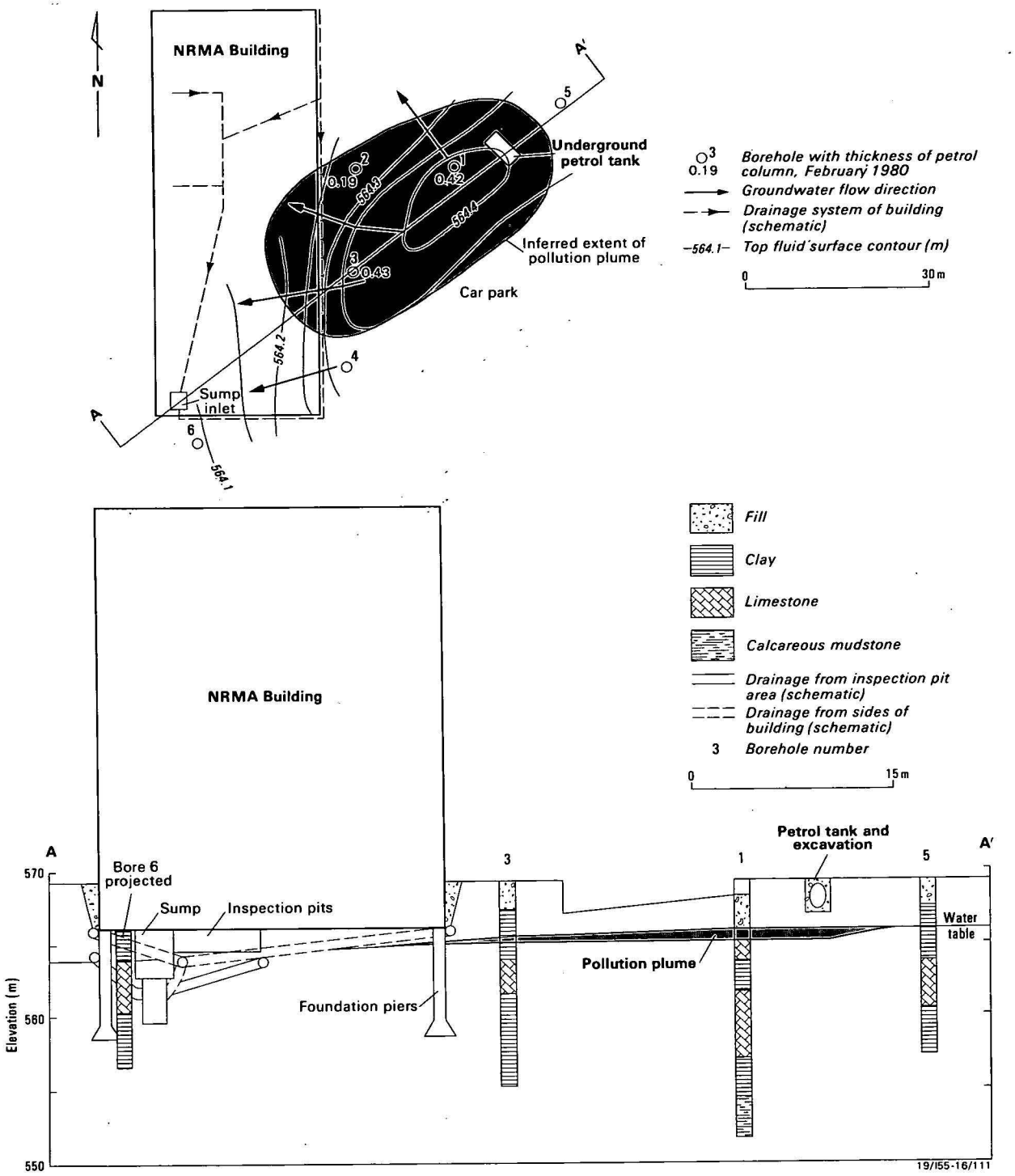


**Figure 13. Petrol pollution plume, NRMA building.**

spillage caused by overfilling; the petrol probably infiltrated readily through backfill around the tank, and eventually down to the water-table, where it floated and spread laterally.

Ventilation has been installed in the drainage sump by the building's owners in order to ensure the safety of the building. The conditions that caused the inflow of petrol could recur when the groundwater aquifer is recharged after prolonged heavy rain. The pollution plume is slowly being attenuated by natural drift down the hydraulic gradient.

## Discussion

The two affected buildings in central Canberra are probably in different groundwater catchments and the pollution plumes at the two sites are not connected. The two incidents are similar in that, at each site, the extent and thickness of the pollution plume indicate that the petrol is derived from a local source, within 50 m. Also both buildings have basements below the water-table that are dewatered by internal pumping.

The large number of underground fuel tanks concentrated in a relatively small area (Fig. 3) raises the probability of other, as

yet undetected, leakages or spillages of petrol in the area. Petrol pollution plumes and deep basements below the water-table are a lethal combination; the removal of service stations may remove sources of future pollution, but will not remove the petrol that is already underground. In this area, the foundations of buildings that penetrate the water-table are likely to encounter petrol as well as groundwater, and buildings should be designed to exclude both. Alternatively, the buildings should be founded above the water-table. The implication for urban planning is that, in an area with a shallow water-table, service stations should be dispersed rather than concentrated or their petrol storage facilities should be above ground.

The prognosis for remedial works in cases of this kind is not hopeful; removal systems have to be maintained for many years and will only be partly effective. In one of the Canberra incidents, a substantial proportion of petrol has been removed, but the rate of removal is now very slow. In at least two well-documented incidents in the United States, about 20 per cent of the spilled or leaked petrol was removed in an initial period of 1 to 3 years by means of tile drains (Holzer, 1976) or skimming wells (Williams & Wilder, 1971).

It is inevitable that underground fuel storage tanks and pumping systems will corrode in time, and leak. It is also inevitable that spillages of fuel will occur during filling operations. Every service station or other establishment with underground fuel tanks doubtless has its pollution plume, which will only be detected by investigations following the recognition of leakage. The incidents documented in Canberra may be only the tip of an iceberg! The difficulty of recovering spilled or leaked petroleum products from the aquifer means that strict preventative measures are vital for present installations, and that legislation for future control of the placement of underground fuel tanks is essential if this form of pollution is to be prevented.

## Acknowledgements

These investigations involved teamwork over several years. Colleagues that assisted at various times included E.G. Wilson, P.D. Hohnen, and W.R. Evans with hydrogeological studies of the Center Cinema pollution plume and possible recovery techniques, J.R. Kellett with the NRMA building investigation, B.A. McKay and Z. Horvath with analyses of hydrocarbons, A.W. Schuett and R. McPake with monitoring. The fluorescent dye tracing experiments were done in collaboration with D. Ingle Smith, Centre for Resource and Environmental Studies, Australian National University. The investigations were made for the Department of the Capital Territory, in close cooperation with W. Southwell, Flammable Liquids Inspector, and C. Thompson, City Engineer. The remedial works and the investigation drilling were funded by the National Capital Development Commission, and the construction and maintenance of the remedial works was done by the Department of Housing and Construction.

## References

Clean Environment Commission, 1976 — Preliminary report on contamination of underground water sources by refined petroleum products. *Ground Water*, 14, 36 –44.

Cole, J.A. (editor), 1974 — Groundwater pollution in Europe. Proceedings of a conference organised by the Water Research Association in Reading, England, September 1972. *Water Information Center Inc., Port Washington, New York.*

Hall, P.L. & Quam, H., 1976 — Countermeasures to control oil spills in Western Canada. *Ground Water*, 14, 163 –169.

Henderson, G.A.M., in press — Central Canberra, A.C.T., 1:10 000 Engineering Geology Map and Explanatory Notes. *Bureau of Mineral Resources, Australia.*

Hepple, P. (editor), 1971 — Water pollution by oil. *The Institute of Petroleum* and *Elsevier, London.*

Holzer, T.L., 1976 — Application of groundwater flow theory to a subsurface oil spill. *Ground Water*, 14, 138 –145.

International Association of Hydrogeologists, 1978 — Proceedings of the international symposium on ground water pollution by oil hydrocarbons, Prague, June 1978. *Stavebni Geologie, Prague.*

Matis, J.R., 1971 — Petroleum contamination of groundwater in Maryland. *Ground Water*, 9, 57–61.

Osgood, J.O., 1974 — Hydrocarbon dispersion in groundwater: significance and characteristics. *Ground Water* 12, 427–36.

Schwille, F., 1967 — Petroleum contamination of the subsoil — a hydrological problem. *In* Hepple, P. (editor), The joint problems of the oil and water industries. *The Institute of Petroleum* and *Elsevier, London*, 23 –54.

Smith, D.I. & Jacobson, G., 1981 — The application of fluorescent dye techniques to groundwater pollution problems with special reference to studies in Canberra. *In* Lawrence, C.R., & Hughes, R.J. (editors), Proceedings of the groundwater pollution conference, Perth, 1979. *Australian Water Resources Council, Conference Series*, 1, 182 –198.

van Dam, J., 1967 — The migration of hydrocarbons in a water-bearing stratum. *In* Hepple, P. (editor), The joint problems of the oil and water industries. *The Institute of Petroleum* and *Elsevier, London*, 55–88.

Williams, D.E., & Wilder, D.G., 1971 — Gasoline pollution of a groundwater reservoir — a case history. *Ground Water*, 6, 50 –54.

BMR Journal of Australian Geology & Geophysics, 8, 323–328 

# VOLCANIC CORE OF NIUE ISLAND, SOUTHWEST PACIFIC OCEAN

P.J. Hill

The results of a gravity and magnetic survey of Niue Island, a raised atoll in the southwest Pacific Ocean, indicate that volcanic rocks underlie the coral limestone capping at a depth of 300–400 m below sea level. A roughly flat-topped, dome-shaped dense volcanic core, is present beneath the southwest of the island. The core has a lateral density contrast of 0.20 t/m$^3$ and a reverse magnetisation of 3.0 A/m, and is believed to be of basaltic composition. An early–middle Miocene age is inferred for the volcanic pedestal. The asymmetric location of the core within the island is thought to be evidence for large-scale landslide activity, particularly on the west and south flanks of the seamount.

## Introduction

Niue Island is a raised coral atoll in the southwest Pacific Ocean (Fig. 1). It is roughly circular, about 18 km across, and rises steeply from an ocean depth of 4–5 km. It is the only significant landmass for hundreds of kilometres, its nearest neighbours being Samoa, 500 km to the north, and Tonga, 400 km to the west.

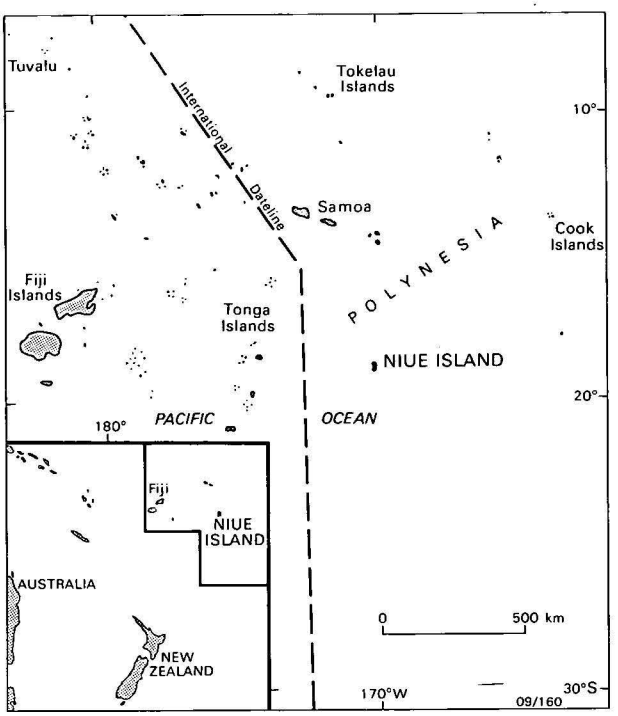


**Figure 1. Location of Niue Island.**

In 1979, an investigation of Niue's groundwater resources was conducted by the Bureau of Mineral Resources on behalf of the Australian Development Assistance Bureau (Jacobson & Hill, 1980a,b). Geophysical input to the investigation took the form of vertical electrical soundings (with current electrode separations to 3200 m) and detailed gravity and magnetic surveys of the island (Hill, 1982).

Very little was known about the presumed volcanic substructure of Niue Island (Schofield, 1959). Basement rock is not exposed on the island and, to date, only coralline limestone and dolomite have been intersected during water-bore and mineral exploration drilling. The gravity and magnetic surveys were aimed at determining the depth and structure of the basement.

## Tectonic setting and geology

Niue is located near the edge of the Pacific plate, which, at the Tonga Trench about 270 km to the west, is being by subducted beneath the Australian plate at a rate of about 9 cm/yr. The present-day tectonism of the area is well illustrated by the seismicity (Fig. 2), virtually all the activity being associated with the under-thrusting of the Pacific plate. Relative stability of the Pacific crust away from the plate boundary is indicated by the low incidence of earthquakes. Tensional fracturing of the flexing lithosphere sub-parallel with the subduction zone may account for the minor activity present within the outer 300 km of the Pacific plate. Insufficient seismic data are available to allow any definite deductions to be made on recent tectonic activity at Niue.

The geomorphology of Niue is shown in Figure 3. The raised former Mutalau Lagoon at the centre of the island is about 35 m above sea level. The enclosing ancient atoll rim, the Mutalau Reef, is about 25 m higher. Dubois & others (1975) proposed that the Quaternary uplift of Niue has been due to the upward bulge of the lithosphere before its subduction at the Tonga Trench (Fig. 2). Coralline limestone/dolomite is the only rock exposed on the island (Schofield, 1959) and drilling to depths up to 300 m at a number of locations (Fig. 3) has revealed only limestone and dolomite, no volcanics. Fossil dating of cores from depths to 220 m in exploration drillhole DH4 indicate a middle to late Miocene age (G.C.H. Chaproniere *in* Jacobson & Hill, 1980a).

## Acquisition, reduction, and presentation of data

Gravity and magnetic observations were generally made along roads and tracks on the island, with stations spaced at about 300-m intervals. A 6.5 km magnetic traverse out to sea from Alofi was also undertaken. Total survey coverage consisted of 547 gravity stations and 305 magnetic stations. With the inclusion of results of magnetic work done in 1978 by Mr J. Barrie (Avian Mining Pty Ltd), using a BMR magnetometer, the number of magnetic stations selected for analysis was increased to 870. All were read with a proton precession magnetometer; no diurnal corrections were made.

Except for the relatively steeply rising coastal fringe, most of the island is of low relief with a shallow depression of a former lagoon in the interior. Consequently, topographic corrections for land relief are small. Elevation control for the gravity stations is good (Hill, 1982): about 90 per cent of the stations have heights accurate to 0.5 m (corresponding to possible Bouguer anomaly error of about 1μm/s$^2$); the remainder have an elevation accuracy within 2 m.

The Niue gravity network was tied to a base station established by the New Zealand Department of Scientific and Industrial Research in Alofi between 1959 and 1963 (Robertson, 1965). Observed station values were converted to modified Bouguer anomalies by applying latitude (using the 1930 International Gravity Formula), elevation, and terrain corrections (for above sea-level topography). A density of 2.1 t/m$^3$ for the coralline

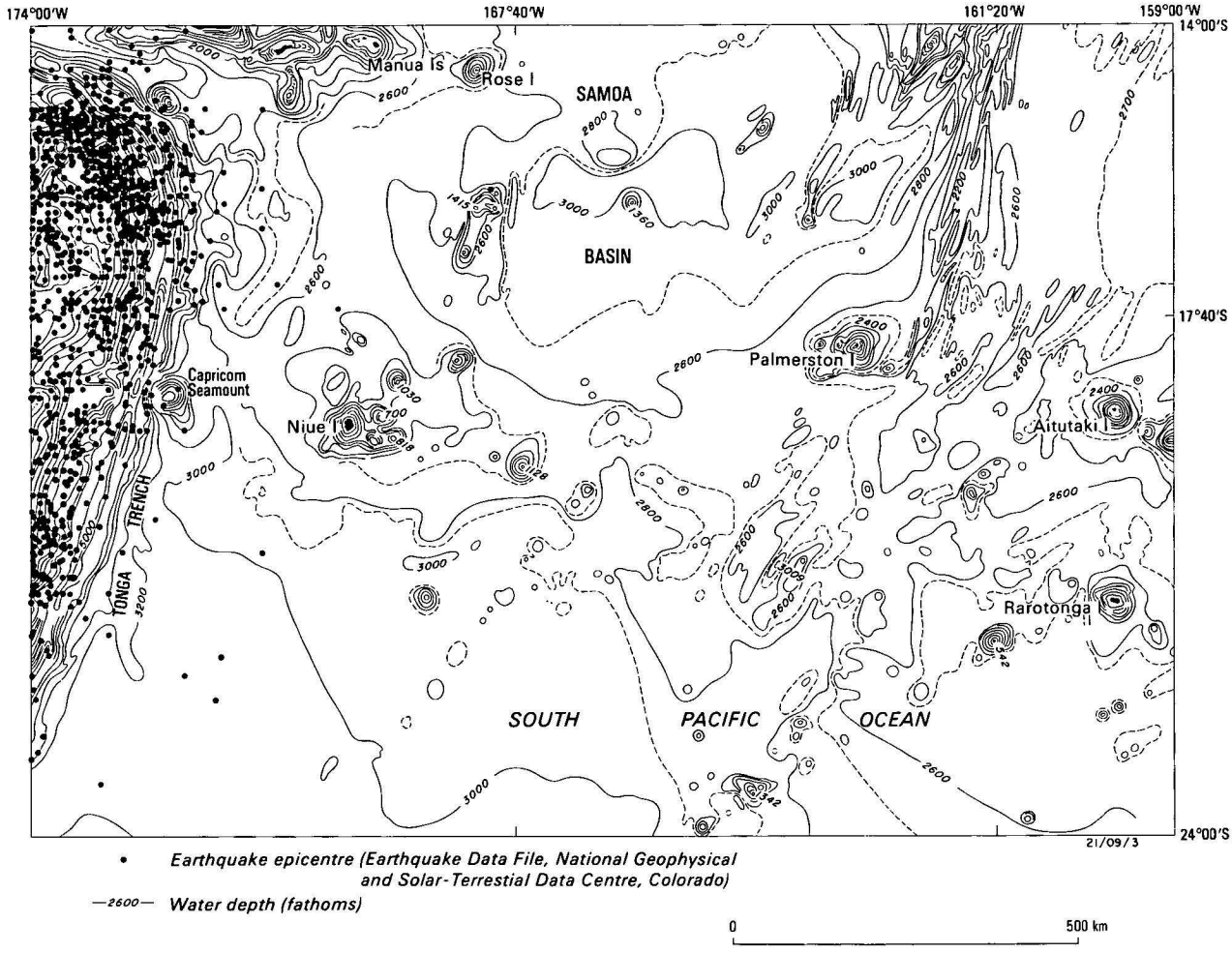


**Figure 2. Seismicity and bathymetry.**
Base from *Bathymetry of the South Pacific*, Charts 12 (1974) and 13 (1973), Scripps Institution of Oceanography. Computer plot of epicentres provided by A.S. Murray (BMR).

limestone, indicated by laboratory measurements on core samples, was adopted for the reductions.

The data were further processed to remove the effect of the island pedestal's submarine relief, so that any anomalous internal density distributions would be highlighted. To do this it was necessary to assume a density model for the pedestal below sea level. Strange & others (1965), working in the Hawaiian Ridge region, assumed increasing density with depth, and a similar approach was taken in the case of Niue (Table 1). The density increase is mainly attributed to compaction by the overlying material and the reduced vesicle space of volcanics deposited at depth.

Bathymetric contours (Brodie, 1966) corresponding to the depths in Table 1 were approximated by a set of polygons. Sub-routines from the Fortran program of Spies (1975), based on the method of Talwani & Ewing (1960), were used to calculate the gravity effect of the island pedestal (to 4000 m depth) at each gravity station.

The final gravity and magnetic results were plotted as contour maps (Figs 4, 5, 6) using a computer program developed by Murray (1977) — a grid spacing of 0.2 minutes (about 360 m) was chosen.

## Main features of the gravity and magnetic fields

A broad gravity high is located in the southern part of the island. The anomalies, corrected for the island pedestal, range from about $-180\mu m/s^2$ in the north to $+130\mu m/s^2$ in the south.

**Table 1. Increase of volcanic pedestal density with depth.**

| *Depth (m)* | *Density contrast (relative to sea water*, t/m³)* |
|---|---|
| 0 | 1.35 |
| 250 | 1.40 |
| 500 | 1.45 |
| 750 & 1000 | 1.50 |
| 1500 & 2000 | 1.60 |
| 2500 | 1.65 |
| 3000 | 1.70 |
| 3500 & 4000 | 1.75 |

* sea water = 1.03 t/m³.

The magnetic field is depressed at the centre of the island, and there is a relatively steep rise in the total field towards the south, from about 41 180 nT in the central west to about 41 940 nT at the southern coast.

Both the gravity and magnetic fields exhibit steeper gradients in the south of the island around Avatele, indicating a shallower source depth there.

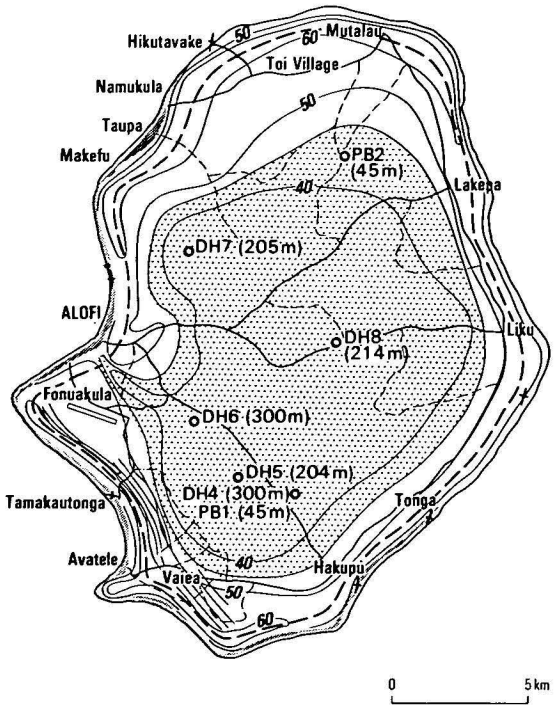


**Figure 3. Geomorphology and drill hole locations.**

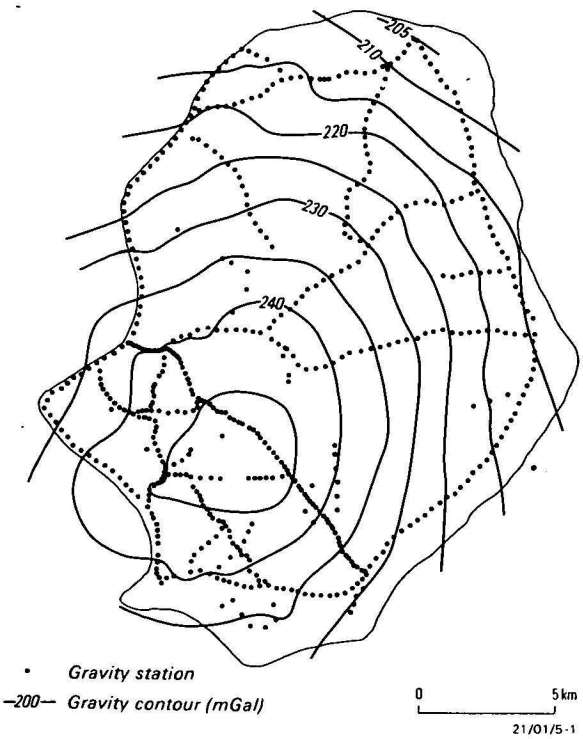


**Figure 4. Modified Bouguer anomalies.**


**Figure 5. Residual Bouguer anomalies after correction for the island pedestal.**

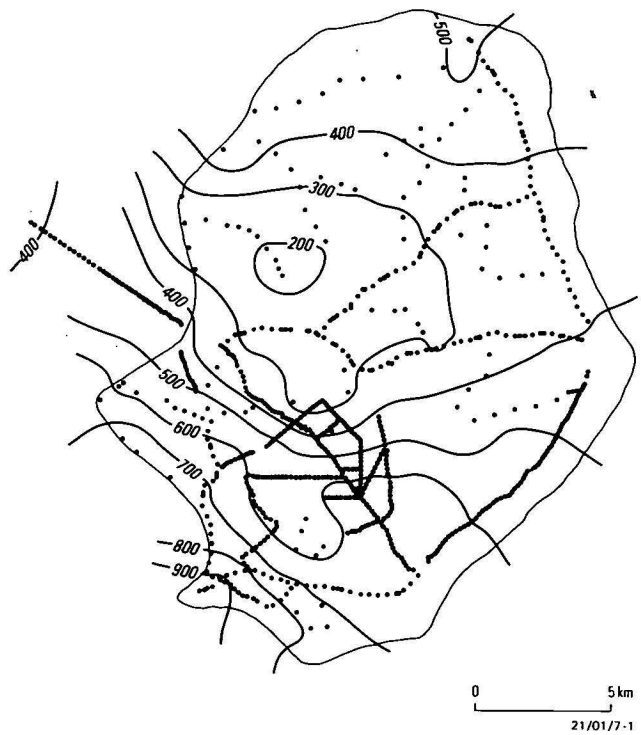


**Figure 6. Total magnetic intensity.**

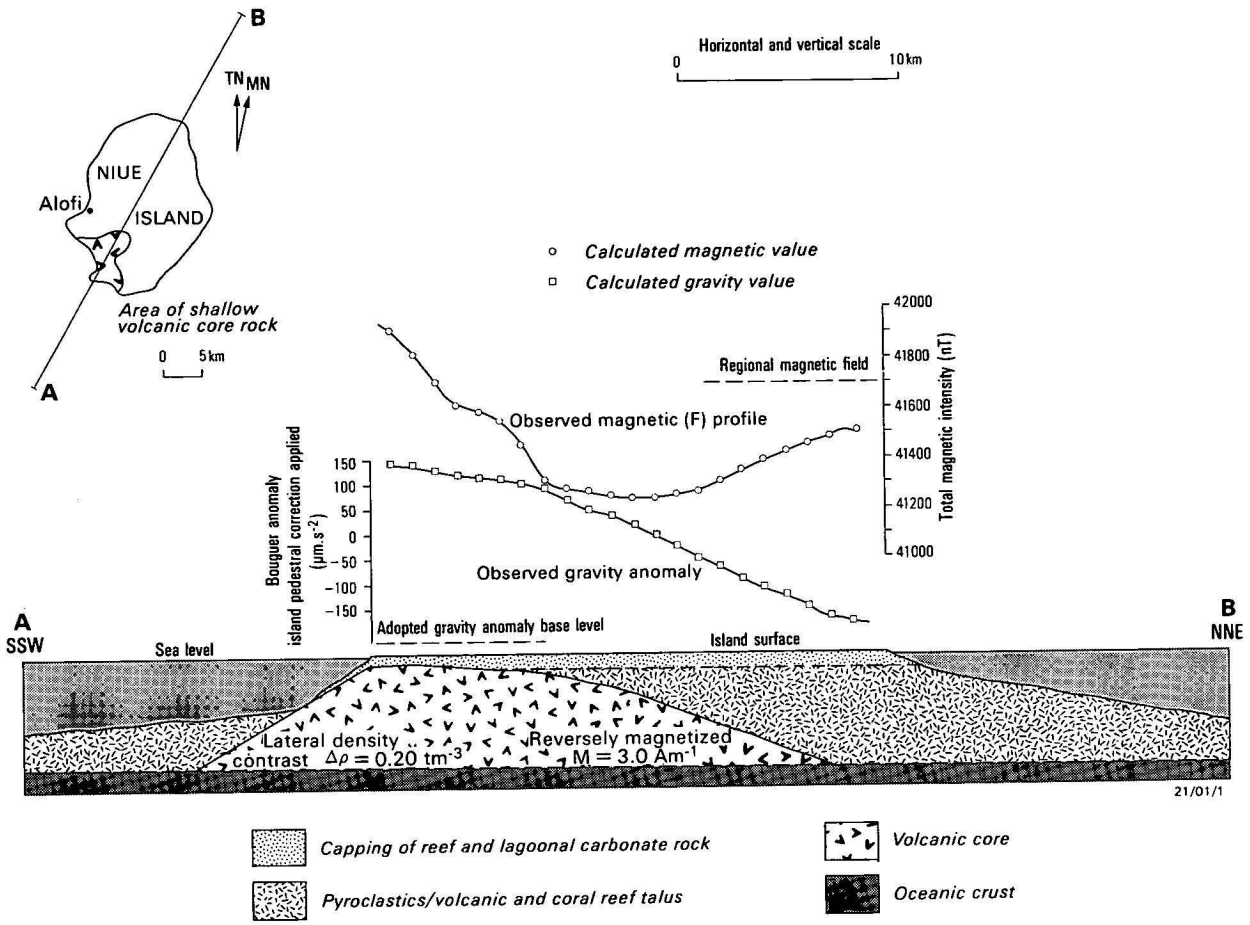


**Figure 7. Interpreted volcanic substructure of Niue Island.**

## Analysis of results

The geophysical results suggest a dense, reversely magnetised volcanic core centred in the southwest of the island, and the configuration and geophysical parameters of this have been modelled as follows. A SSW–NNE section through the centre of the island was selected for analysis (section AB in Fig. 7). For both the magnetic and gravity cases the core was modelled as a two-dimensional body of polygonal cross-section (Talwani & others, 1959; Heirtzler & others, 1962). Optimisation of the fit between observed and calculated profiles was assisted by a computer inversion routine applied to the geometric model parameters (i.e. coordinates of the polygon vertices). Trial and error forward modelling was used to evaluate the other parameters.

The regional geomagnetic field at Niue (1979) has the following components: total field (F), 41 700 nT; declination (D), 13.4°E; inclination (I), –37.5° (Charts of the Earth's magnetic field. Epoch 1975.0; published by Defence Mapping Agency, Hydrographic Centre, Washington).

For the modelling it was assumed that, in the horizontal plane, the core's magnetisation vector was aligned with, but opposite in direction to, the Earth's geomagnetic field. That this is a valid assumption, as an approximation at least, is evidenced in Figures 5 & 6 by the N–S (geomagnetic) trends of local magnetic highs, magnetic lows, and gravity highs associated with particular subsurface sources.

The cross-section of Figure 7 shows the interpreted substructure of Niue Island. The model represented provided the best fit to the observed data: standard deviations of the calculated values from those observed were magnetics, 14 nT, and gravity, 13μm/s$^2$.

Interpreted geophysical parameters of the volcanic core are: (1) lateral density contrast 0.20 t/m$^3$ — density increases with depth from 2.6 t/m$^3$ for the upper core to 3.0 t/m$^3$ at a depth of 4 km; (ii) reverse magnetisation of magnitude 3.0 A/m; and (iii) inclination of magnetisation vector is 137.5° (cf. geomagnetic field inclination of –37.5°).

The volcanic core is centred in the southwest of the island in the vicinity of Avatele and lies at a depth of 300–400 m below sea level. The top of the core is fairly flat, but irregular in outline. There appear to be three lobes extending to the northeast, southeast, and northwest (inset, Fig. 7). The size of the area underlain by relatively shallow core rock is about 20 km$^2$. The core lithology is thought to consist of basic (to ?ultrabasic) intrusives and pillow lavas.

## Discussion

The volcanic core is roughly flat-topped at about 350 m below sea level, and it is inferred that the original volcano was truncated to this level by wave-base and sub-aerial erosion. Later subsidence would have led to the growth of coral reefs and deposition of reefal sediments on and adjacent to the volcanic platform. With continued subsidence, as the lithosphere cooled, the coralline limestone capping would have grown upwards eventually to produce the Mutalau Reef and lagoon, now exposed by Quaternary uplift.

The material around the core is believed to consist of pyroclastic deposits, and volcanic and coral reef talus, but there is no significant expression of this in the magnetic contours (Fig. 6). Several explanations can be advanced to account for this. The material may contain or consist of (i) inherently non-magnetic or weakly magnetic rock types (i.e. low magnetic susceptibility) such as carbonates and acid to ?intermediate tuffs; (ii) weakly reverse-magnetised volcanics, the magnetic effect of which is counteracted by opposing induced magnetisation; (iii) clastic deposits of low to ?moderate susceptibility (e.g. volcanic talus, pyroclastics). Although the clasts may have been derived from parent rock possessing an appreciable remanent magnetisation, any residual effects of this magnetisation at the surface would be nullified by the post-transport chaotic re-orientation of the individual clasts.

The interpreted depth of the volcanic core is consistent with the drilling results, as no volcanics have been intersected so far. Furthermore, vertical electrical soundings (Jacobson & Hill, 1980a) gave no indication of dense volcanic core rock shallower than about 400 m. Relatively large electrode separations were used (out to 292–400 m for the Wenner arrays and AB/2 = 1100–1600 m for the Schlumberger arrays). However, the effective depth of investigation is reduced on Niue, owing to the very low resistivity (about 2 ohm-m) of a salt-water saturated layer beneath the freshwater aquifer. The apparent resistivity values show no increase at large current electrode spacings, as would be expected if dense volcanic rocks existed at shallow depth. No deep electrical sounding data are available for the area in the southwest of the island, where gravity and magnetic results indicate relatively shallow core rock (Fig. 7).

The fact that the volcanic core is not located in the centre of the island suggests that large sections of the volcano's flanks were removed by landslides, particularly in the southwest, where the bathymetry indicates steep submarine slopes adjacent to his coast. This theory is reinforced by the embayed nature of the southern and western coastlines of the island. Schofield (1959) commented similarly, though he believed that the volcanic centre lay in the central west of the island.

## Age of the Niue volcano

The fact that the core's magnetisation and the present geomagnetic field are closely aligned, though opposite in polarity, suggests that the volcanic foundation of Niue is of Late Tertiary age.

The best estimate of the inclination of the magnetisation of the core gave a value 5° steeper than that of the geomagnetic field alignment. This difference may be explained, at least partly, by the northerly drift of Niue on the Pacific plate. In the region of Niue the absolute motion of the Pacific plate is approximately 10 cm/yr in the direction 300° (A.S.P.G., 1981). If it is assumed that the plate motion has remained essentially unaltered, an apparent 5° steepening of the magnetisation vector would imply emplacement of Niue's core at about 11 Ma.

A number of other atolls and guyots have been studied, and their average sinking rates estimated at 1000–1600 m/50 Ma (Wood & Hay, 1970; Menard, 1964). The geophysical data indicate that the coralline capping on Niue is about 400 m thick, and hence an age of 12.5–20 Ma is inferred for the volcano. BMR palaeontological age determinations gave a middle–late Miocene age for drill-core samples from a depth of about 200 m. Therefore, the volcanic pedestal of Niue is probably early–middle Miocene.

## Comparison with other magnetic and gravity studies in the SW Pacific region

Gravity and magnetic surveys of a number of the Cook Islands east of Niue (Robertson 1967a, b; Woodward & others, 1970; Lumb & others, 1973) have indicated that, for most of the islands studied, the observed data are compatible with a structural model consisting of an uncompensated island platform of density 2.35 t/m$^3$, containing a core of density 2.87 t/m$^3$ and radius equal to the radius of the island at sea level. Although a model with a more complex density distribution and structural configuration is proposed for Niue, the parameters are basically similar to those of the Cook Islands model.

Bipolar magnetic anomalies were recorded in the Cook group for islands that are isolated and resting on a flat ocean floor (Rarotonga, Manihiki, and Mangaia); complex patterns are associated with those located on ocean-floor rises. Attempts to model the observed data by assuming homogenous internal magnetisation of the islands proved to be generally unsatisfactory. Reasonable fits were obtained for the islands with bipolar anomalies, and for these, values of 2.0–5.0 A/m were calculated for the internal magnetisation. The interpreted value for the volcanic core of Niue is 3.0 A/m.

## Conclusions

The coralline capping of Niue Island is underlain by middle–lower Miocene volcanics at a depth of 300–400 m below sea level. The volcanics include a dense basaltic core, located beneath the southwest of the island, with a lateral density contrast of 0.20 t/m$^3$ and reverse magnetisation of 3.0 Am.

## Acknowledgements

I thank the Directors and staff of the Niue Public Works Department and Department of Justice, Lands and Survey for their cooperation and willing assistance, particularly in relation to the extensive gravity station levelling surveys. I am also grateful to Mr J. Barrie of Avian Mining Pty Ltd for making his 1978 magnetic data available.

## References

A.S.P.G., 1981 — Plate-tectonic map of the Circum-Pacific Region. South-West Quadrant. *American Society of Petroleum Geologists, Tulsa, Oklahoma.*

Brodie, J.W., 1966 — Niue Island provisional bathymetry. *New Zealand Oceanographic Institute, Wellington. Island Series*, 1:200 000.

Dubois, J., Launay, J. & Recy, J., 1975 — Some new evidence on lithospheric bulges close to island arcs. *Tectonophysics*, 26, 189–196.

Heirtzler, J.R., Peter, G., Talwani, M. & Zurflueh, E.G., 1962 — Magnetic anomalies caused by two-dimensional structure: their computation by digital computers and their interpretation. *Lamont Geological Observatory (Columbia University). Technical Report* 6.

Hill, P.J., 1982 — Gravity and magnetic survey of Niue Island, 1979. *Bureau of Mineral Resources, Australia, Record* 1982/40.

Jacobson, G. & Hill, P.J., 1980a — Groundwater resources of Niue Island. *Bureau of Mineral Resources, Australia, Record* 1980/14.

Jacobson, G. & Hill, P.J., 1980b — Hydrogeology of a raised coral atoll — Niue Island, South Pacific Ocean. *BMR Journal of Australian Geology & Geophysics*, 5, 271–8.

Lumb, J.T., Hochstein, M.P., & Woodward, D.J., 1973 — Interpretations of magnetic measurements in the Cook Islands, South-west Pacific Ocean. *In* Coleman, P.J. (editor), The Western Pacific — island arcs, marginal seas, geochemistry. *University of Western Australia Press, Nedlands, W.A.*

Menard, H.W., 1964 — Marine geology of the Pacific. *McGraw Hill, New York.*

Murray, A.S., 1977 — A guide to the use and operation of program CONTOR. *Bureau of Mineral Resources, Australia, Record* 1977/17.

Robertson, E.I., 1965 — Gravity base stations in the south-west Pacific Ocean. *New Zealand Journal of Geology and Geophysics*, 8, 424–39.

Robertson, E.I., 1967a — Gravity effects of volcanic islands. *New Zealand Journal of Geology and Geophysics*, 10, 1466–83.

Robertson, E.I., 1967b — Gravity survey in the Cook Islands. *New Zealand Journal of Geology and Geophysics*, 10, 1484–98.

Schofield, J.C., 1959 — The geology and hydrology of Niue Island, South Pacific. *New Zealand Geological Survey Bulletin 62*.

Spies, B.R., 1975 — A Fortran program for calculating the gravity effect of a three-dimensional body of arbitrary shape. *Bureau of Mineral Resources, Australia, Record* 1975/4.

Strange, W.E., Woollard, G.P. & Rose, J.C., 1965 — An analysis of the gravity field over the Hawaiian Islands in terms of crustal structure. *Pacific Science* 19, 381–89.

Talwani, M., Worzel, J.L. & Landisman, M., 1959 — Rapid gravity computation for two-dimensional bodies with application to the Mendocino sub-marine fracture zone. *Journal of Geophysical Research*, 64, 49–59.

Wood, B.L. & Hay, R.F., 1970 — Geology of the Cook Islands. *New Zealand Geological Survey Bulletin* 82.

Woodward, D.J. & Hochstein, M.P. 1970 — Magnetic measurements in the Cook Islands, South-West Pacific Ocean. *New Zealand Journal of Geology and Geophysics*, 13, 207–24.

BMR Journal of Australian Geology & Geophysics, 8, 329–337


# GEOTHERMAL GRADIENTS AND HEAT FLOW IN AUSTRALIAN SEDIMENTARY BASINS

J.P. Cull & D. Conley

Geothermal gradients in Australian sedimentary basins have been calculated from data obtained from water bores in the Great Artesian Basin and oil exploration wells. The data are subject to several types of systematic error, but statistical trends have been extracted, using values of thermal conductivity obtained from sediment compaction models. Estimates of heat flow from the Great Artesian Basin are consistent with the configuration of the major aquifer systems. Oil well data confirm the regional trends obtained from previous investigations, but previously recognised anomalies in southeast Australia are no longer evident. Temperatures at a depth of 40 km range from 320°C to 380°C for the Precambrian terrain and from 470°C to 550°C for the Phanerozoic. These results are modified by sediment cover. A 1 km thickness causes additional heating, with temperatures raised by 16–40°C.

## Introduction

Three heat-flow provinces have been defined for the Australian continent (Fig. 1; Sass & Lachenbruch, 1979). Each can be considered to have a characteristic composition and tectonic history. A representative continental geotherm can be constructed for each on the assumption of an exponential decrease in heat production as a function of depth. Distributions of this type are consistent with the model proposed by Lachenbruch (1970) to explain observed linear relationships between surface heat flow and surface heat production in basement rocks. However, few data have been obtained to confirm these results in basin strata.

All heat-flow data obtained in Australia have been compiled in standard format, rating the principal facts of each determination (Cull, 1982). The results have been used to suggest correlations with other geophysical data (Cull & Denham, 1979) and to provide estimates of temperature at mantle depths (Sass & Lachenbruch, 1979). Anomalies can be attributed to heat generated by orogenic movements, episodic intrusions, hydrothermal convection, or differential erosion.

Thermal models based on an extended data base can be used to locate fault systems, fold closures, dome structures, coal field boundaries, and mineral deposits subject to exothermic reactions due to hydration or oxidation. More general constraints can be imposed on models of basin evolution. Levels of hydrocarbon maturation can be calculated from estimates of total heating time related to depth of burial (e.g. Falvey & Middleton, 1981).

Borehole temperatures have been measured in Australia for many years during routine logging of oil wells by private companies. Many of the data have been submitted to the Bureau of Mineral Resources, under the terms of the Commonwealth Petroleum Search Subsidy Acts. In addition, numerous water bores have been logged in hydrological surveys conducted by BMR. Temperature gradients obtained at the sites indicated in Figure 1 have now been integrated with the existing heat-flow data in an attempt to define thermal anomalies in greater detail.

## Thermal parameters

Values of heat flow (Q, $mW/m^2$) are calculated from the expression $Q = \lambda\beta$, where $\beta$ (degrees C/km) is the geothermal

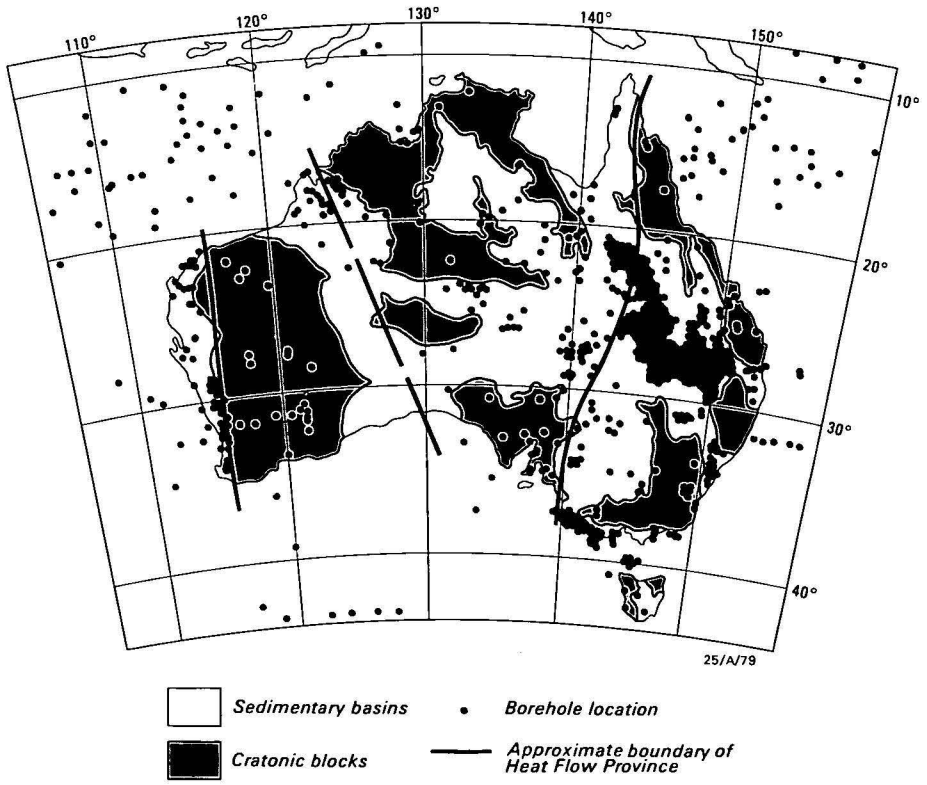


**Figure 1. Location of boreholes used for determinations of thermal gradient.**

gradient and λ (W/m/K ) is the thermal conductivity of the rocks in which the gradient is established. A linear gradient implies a constant thermal conductivity and a uniform stratigraphy. These conditions are seldom satisfied together and complex temperature profiles are frequently encountered in regions of constant heat flow.

Thermal conductivities have been measured in Australia primarily on core samples taken from holes drilled in hard rock for mineral exploration. The range of values is shown in Figure 2. The distribution is approximately normal with a mean value of 3.3 ± 0.1 W/m/K (standard error of mean). However, thermal conductivity data for basin sequences are comparatively rare. Estimates are readily available for coal measures at depths less than 1000 m (Cull & Denham, 1979; Hyndman, 1967), but there have been no routine measurements of conductivity on core from the deeper oil wells. Consequently, representative values must be assigned using other techniques.

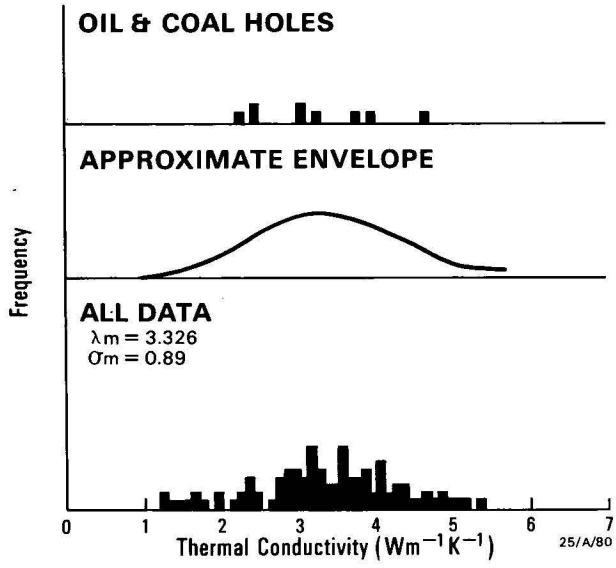


**Figure 2. Histogram of thermal conductivities used in determinations of heat flow in Australia (Cull, 1982).**

Reasonable estimates of conductivity for basin sequences can be based on sonic-log determinations of porosity (e.g. Yorath & Hyndman, 1983), but Falvey & Middleton (1981) adopted a more general approach, basing their estimates on the assumption of progressive compaction of sediments (with consequent loss of porosity). Representative values of conductivity are indicated by the solid curve in Figure 3 together with the only comprehensive oil well data in Australia (taken from Sass, 1964). Although there is considerable scatter, which can be related to changes in stratigraphy, the data support the general trend of the compaction model. The model suggests representative values of conductivity in the range 2.0–3.0 W/m/K, significantly less than the values obtained for basement.

The effect of lateral gradations in thermal conductivity can be demonstrated in Figure 4. Results are based on finite difference solutions for equilibration of heat in 2 dimensions (Carslaw & Jaeger, 1959, p.466). Although the regional heat flow is assumed to be constant, the geothermal gradient at any location is difficult to predict. Perturbations are related not only to variations in thermal conductivity, but also to refraction of heat associated with basement topography. In general, a basement high enhances heat flow and increases geothermal gradients. Refraction at the margins of a basin may be even more complicated, according to the geometry of the contact. A graben contact may generate a discontinuity in heat flow, and gradients within the basin will be generally reduced.

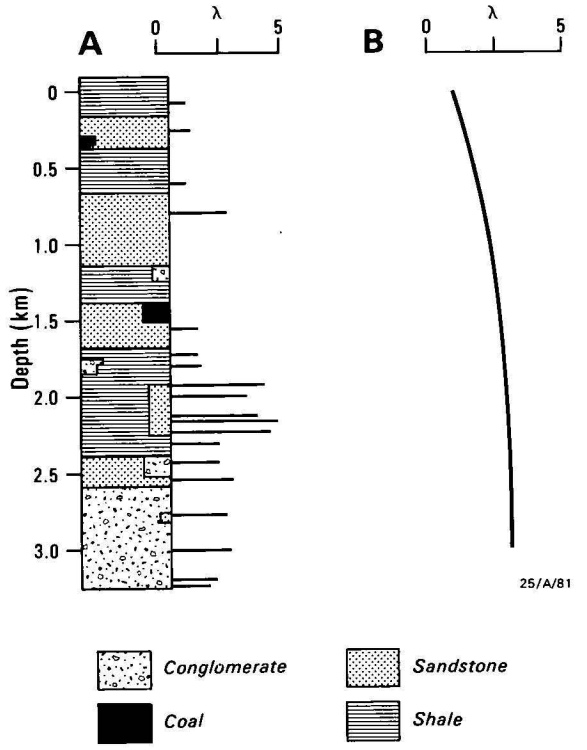


**Figure 3. Variation in thermal conductivity of sediments with depth of burial.**
(A) Core samples according to Sass (1964); (B) Compaction model calculated according to Falvey & Middleton (1981).

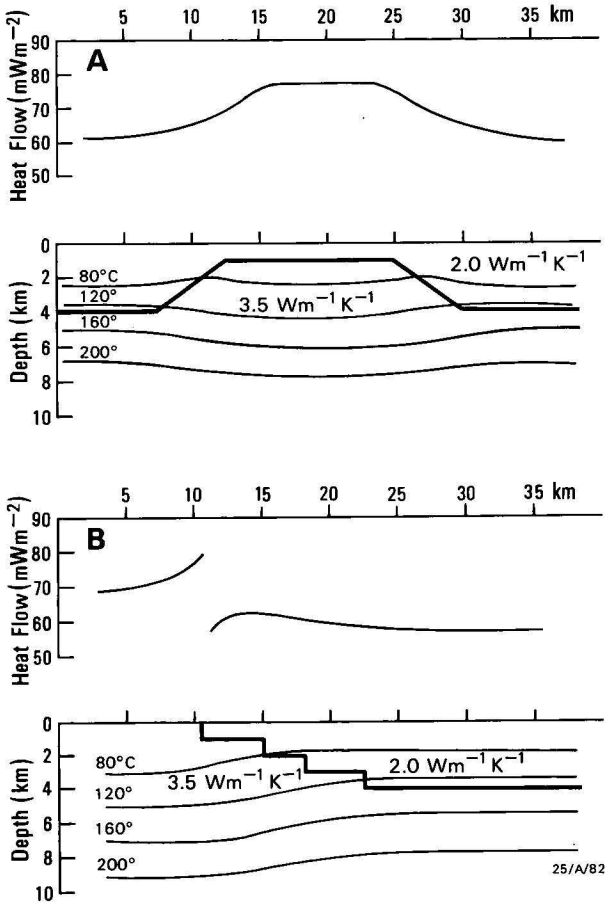


**Figure 4. Refraction of heat caused by variations in conductivity associated with (A) a rise in basement topography and (B) truncation of sediments at a basin margin.**

Many other anomalies in heat flow can be related to refraction of heat near materials of contrasting conductivity. However, detailed structural models are rare and corrections for refraction are difficult to formulate. Other perturbations are related to variations in climate, involving natural and cultural modifications to the surface temperature (Cull, 1983). Consequently, current values of heat flow based on apparent values of the geothermal gradient must be averaged in order to obtain reasonable estimates of regional trends.

## Water temperatures in the Great Artesian Basin

The Great Artesian Basin occupies about one-fifth of the Australian land mass. It extends across parts of Queensland, New South Wales, South Australia, and the Northern Territory (Fig. 5). The basin contains up to 3000 m of sediments forming a large synclinal structure; it is uplifted and exposed along its eastern margin, and tilted southwest. Hydrological models have been considered by Habermehl (1980), who identified major aquifers in continental quartzose sandstones of Triassic, Jurassic, and Cretaceous age. The intervening confining beds consist of siltstone and mudstone; a thick sequence of argillaceous marine sediments of Cretaceous age forms the main confining unit.

Environmental isotope analysis shows that the artesian water is of meteoric origin. Large flow rates may generate significant thermal perturbations unrelated to thermal conductivity. In particular, forced convection may be associated with aquifer recharge along the eastern marginal zone; large-scale groundwater movement is generally towards the southwestern, western, and southern margins. Natural discharge occurs from springs in these areas, and most are connected with structural features. Aquifer thicknesses range from several metres to several hundred metres, and average groundwater velocity in the eastern marginal parts is 1–5 m/yr.

About 4700 artesian wells have been drilled to depths as great as 2000 m, but average depth is near 500 m. Individual flows exceeding 10 000 $m^3$/day have been recorded. The temperature of water in wells tapping aquifers in Lower Cretaceous and Jurassic sediments generally ranges from about 30°C to 50°C, but, in many areas of the basin, temperatures at the well head are as much as 100°C. Water is discharged from mound springs along the western margin at temperatures ranging from about 20°C to 40°C.

Bottom-hole temperatures were recorded in 940 water bores logged by BMR between 1966 and 1978 (Polak & Horsfall, 1979). All geophysical logging was done at least one year after drilling; consequently, the temperature recorded next to the source aquifer should be in long-term equilibrium. However, temperatures in the upper section of each bore are disturbed by water flow during production phases and continuous temperature profiles prove difficult to interpret.

Polak & Horsfall (1979) noted extreme variations in the geothermal gradient for the Great Artesian Basin. Estimates range from 15.4°C/km to 102.6°C/km, with a mean of 48°C/km. More than 75 per cent of such estimates exceed the global average of 33°C/km (as calculated by Polak & Horsfall, 1979), and the excess heat was assumed to result from anomalous basement radioactivity. However, Habermehl (1980) recognised that high gradients occur (1) where shallow basement rocks are present, (2) adjacent to some major faults, and (3) near some discharge areas. These correlations suggest seepage between aquifers at different levels.

Vertical migration of groundwater implies a major departure from the normal quasi-linear geothermal gradient. Models based solely on thermal conduction can no longer be assumed, and estimates of temperature must be based on determinations of regional heat flow. To avoid these complications in the

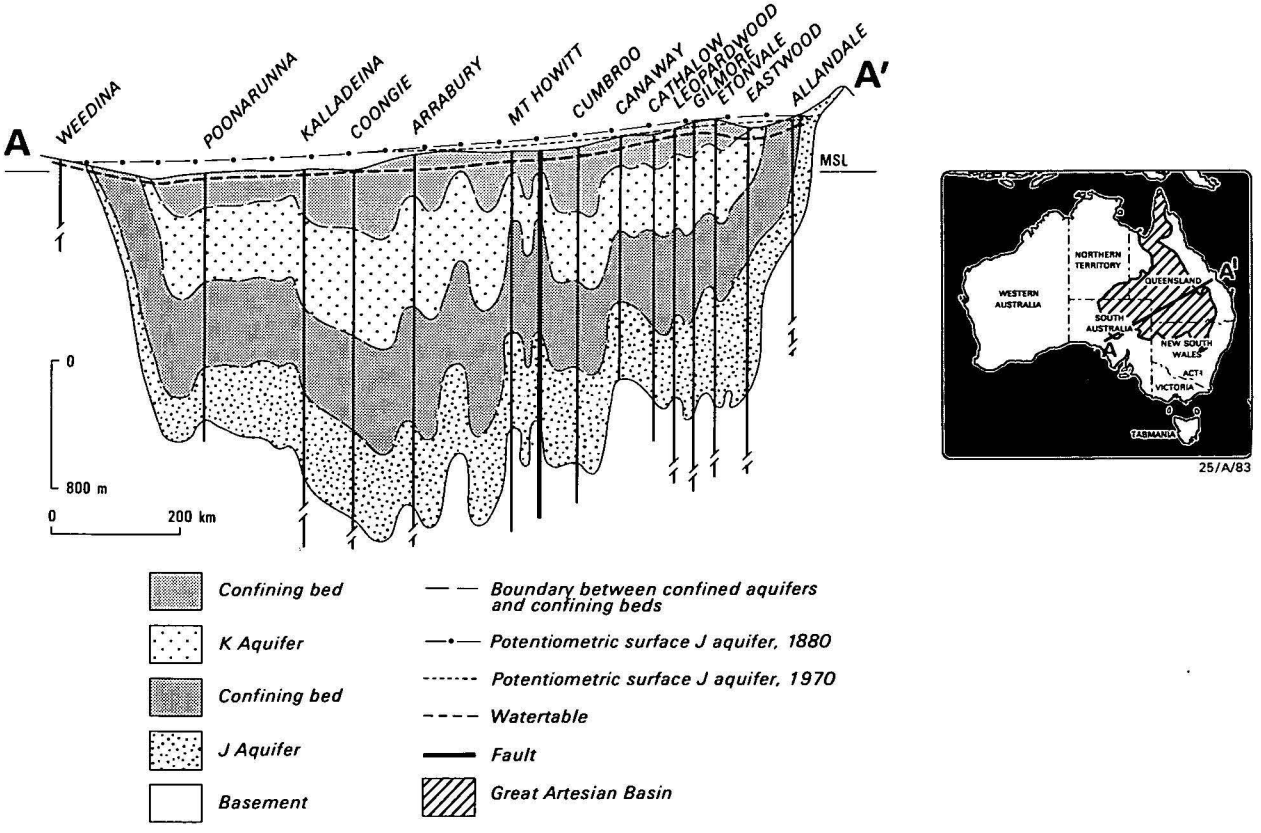


**Figure 5. Aquifer configurations in the Great Artesian Basin (after Habermehl, 1980).**

current analysis, qualitative selection criteria were adopted, based on the generalised aquifer configuration proposed by Habermehl (1980). Essentially, any data within 100 km of Jurassic outcrop were rejected on the assumption that the associated aquifers in such a region are normally steeply dipping (Fig. 5). In particular, the zones of discharge are comparatively narrow, causing enhanced migration velocities accompanied by convective instability. Data indicating discontinuities in temperature at major fault systems can be similarly rejected.

Temperatures recorded at a constant depth reflect both the geothermal gradient and the mean annual surface temperature. Surface temperatures in the Great Artesian Basin range from 18°C to 28°C, according to latitude. Consequently, borehole temperatures must be adjusted to a common level by subtracting the relevant surface value from each borehole measurement prior to statistical analysis of a combined data set. Bottom-hole temperatures corrected for variation in air temperature are presented in Figure 6. Considerable scatter is apparent, but the mean gradient of 38.6 ± 0.1°C/km is closer to the world average of 33°C/km than are the results of Polak & Horsfall (1979).

The extrapolated gradient does not pass through the origin defined by the mean annual air temperature. However, the resulting anomaly of 5.9 ±0.6°C is consistent with positive intercepts ranging about 3.0°C observed elsewhere (Howard & Sass, 1964). Anomalies of this type can normally be attributed to a greenhouse effect at the air/earth interface, but the higher values in Figure 6 may indicate that quasi-linear geothermal gradients are a poor approximation in the Great Artesian Basin.

Thermal conductivities normally vary with depth, and any change in lithology is accompanied by a change in the geothermal gradient. However, models of basin formation involving progressive compaction of sediments have been suggested in studies of oil maturation (Falvey & Middleton, 1981). Compaction can be expected to generate a gradual increase in conductivity accompanied by a decrease in geothermal gradient. The suggested trend in thermal conductivity can be expected to generate several linear segments of decreasing geothermal gradient consistent with the data in Figure 6. Two primary zones of conductivity can be identified, corresponding to an interval of maximum curvature centred near 1000 m (Fig. 3). Representative values of thermal conductivity can be assigned if the random variations related to minor changes in lithology are ignored. The compaction model predicts a mid-range value of 2.0 W/m/K for thermal conductivity of sediments at depths less than 1000 m, and 2.5 W/m/K for greater depths.

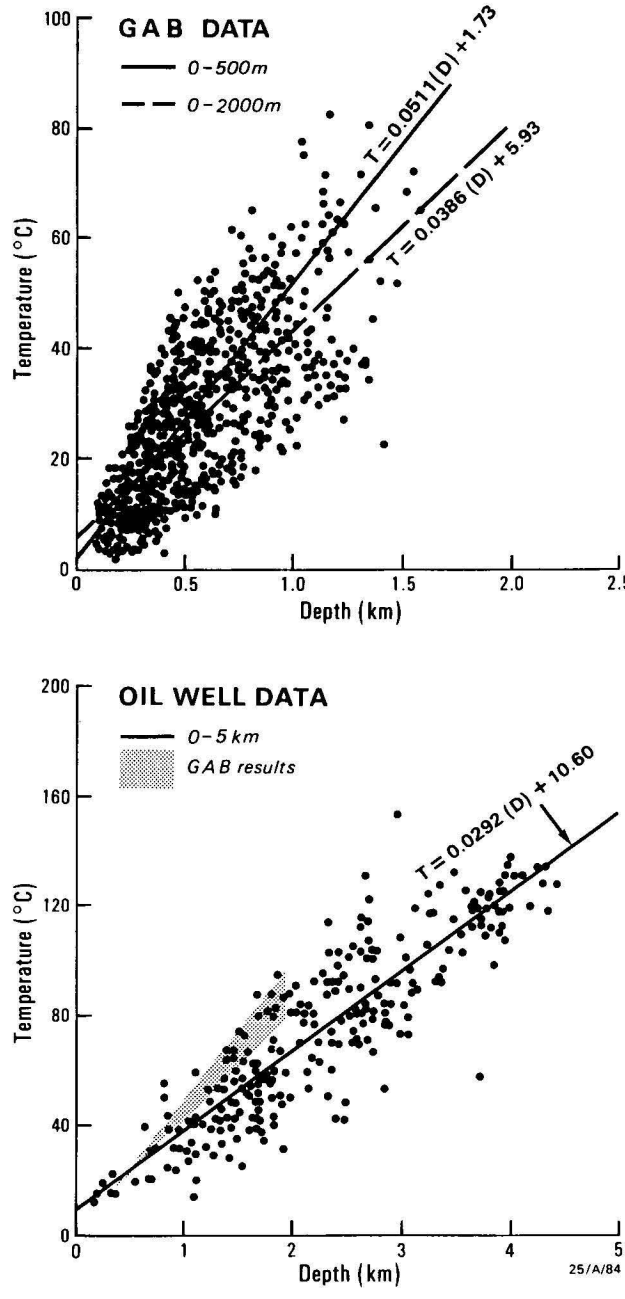


**Figure 6. Borehole temperatures for water bores in the Great Artesian Basin (GAB) and oil exploration wells in all basins, corrected for variations in mean annual air temperatures.**
The stippled area of GAB results in the lower diagram corresponds to the area between the trend lines in the upper diagram.

## Oil exploration wells

Bottom-hole temperatures are measured as a matter of routine during the drilling of oil exploration wells. Many of these data are contained in the completion reports submitted to BMR under the terms of the Commonwealth Petroleum Search Subsidy Acts (Nicholas & others, 1980). Site locations are indicated in Figure 1. Data quality is highly variable, according to logging procedure and instruments available. However, selected data have been used for estimates of heat flow (Cull & Denham, 1979; Middleton, 1979) and for studies of maturation history (Burne & Kantsler, 1977). Applications of this type require detailed examination of the data to isolate major sources of error prior to formulation of more complex geological models.

In general, bottom-hole temperatures are considered to be minimum estimates of the true formation temperature. Normal geothermal gradients become modified by relative cooling caused by the circulation of drilling muds introduced at surface temperatures. Both empirical and exact methods of compensation have been proposed by log analysts, and adequate results have been demonstrated (e.g. Lachenbruch & Brewer, 1959; Oxburgh & others, 1972; Middleton, 1979). However, corrections cannot be applied to the majority of data, because the necessary observations of relaxation times are rarely documented.

Errors in the raw data were recognised by Nicholas & others (1980) during compilation of a geothermal data base. However, they adopted a pragmatic approach in order to simplify the presentation. To determine the geothermal gradients, uncorrected bottom-hole temperatures, taken from wireline

logs of petroleum exploration wells, were plotted on temperature/depth graphs, and a best-fit straight line was drawn through present-day surface temperature (from meteorological charts) for onshore wells and assumed sea-bed temperature for offshore. This method provides a rapid means of estimating representative gradients and broad regional trends. However, absolute values may be in error by more than 20°C (Middleton, 1979).

Estimates of temperature obtained from oil wells appear to be of similar quality to those obtained from water bores in the Great Artesian Basin. Calculations of error in the average gradient are similar, even though the depth range is greatly extended (Fig 6). Actual gradients appear to be slightly less than those indicated by the water bore data, but the intercept is slightly greater. This result is consistent with the concept of increased thermal conductivities at greater depth as a result of greater compaction of the sediment pile.

The data compiled by Nicholas & others (1980) have now been combined with more recent data in the Eromanga Basin (V. Passmore, BMR, personal communication 1983) for individual calculations of the geothermal gradient. Representative values of thermal conductivity, calculated from the compaction model, result in linear gradients at depths greater than 1000 m. Increased rates of curvature in thermal conductivity at shallow depth result in a progressive shift in the surface intercept during extrapolation (Fig. 6) of increasingly deeper segments of the temperature plot. Consequently, an additional correction (+3°0) was added to the mean surface temperature prior to calculations of gradient at depths greater than 1000 m. Contours based on averages over a 1° grid are presented in Figure 7. Observations of heat flow (Cull 1982) have been used to extend the contours beyond the basins margins by providing temperature gradients for the Precambrian and other cratonic blocks. However, because of a lack of precision in estimates of marine conductivity, no controls were imposed at shoreline boundaries.

## Estimates of heat flow

Although geothermal gradients can be used directly in mineral exploration and structural analysis, models of global tectonism are more generally constrained by observations of heat flow. These observations can be used to provide estimates of total energy expenditure within the Earth. Temperatures at any depth are seldom constant over geological time and a complete thermal history must be based on assessing transient perturbations in models constrained by observations of heat flow. The geothermal gradients presented in Figure 7 now provide an opportunity to expand the current heat flow data base.

Heat-flow trends presented by Cull (1982) can be defined in greater detail by including estimates from oil and water well data. However, heat flow ($mW/m^2$) is defined as the product of the thermal gradient (°C/km) and thermal conductivity (W/m/K). Adequate estimates of thermal conductivity at each site should result in values of heat flow that are constant with depth. In addition, any lateral discontinuity should be rare. Corrections can be formulated to allow for compaction of sediments, but more serious anomalies are generated in the transition to the hard rock margins.

Random sources of error in estimates of thermal conductivity can be identified with changes in lithology. Consequently, detailed stratigraphic logs are required for precise determinations of heat flow. However, regional trends can be defined using contours based on statistical reduction (Murray, 1977). The data presented in Figure 7 are transformed on the assumption of constant thermal conductivities at depths greater than 1000 m. Data at shallower depths are excluded. Values of 2.5 and 3.5 W/m/K were adopted for the near-surface thermal conductivity of sedimentary and crystalline rocks, respectively. The marine data reported by Cull & Denham (1979) were accepted without modification.

Estimates of heat flow at each location in Figure 1 are presented in Figures 8 & 9. The character of individual determinations is

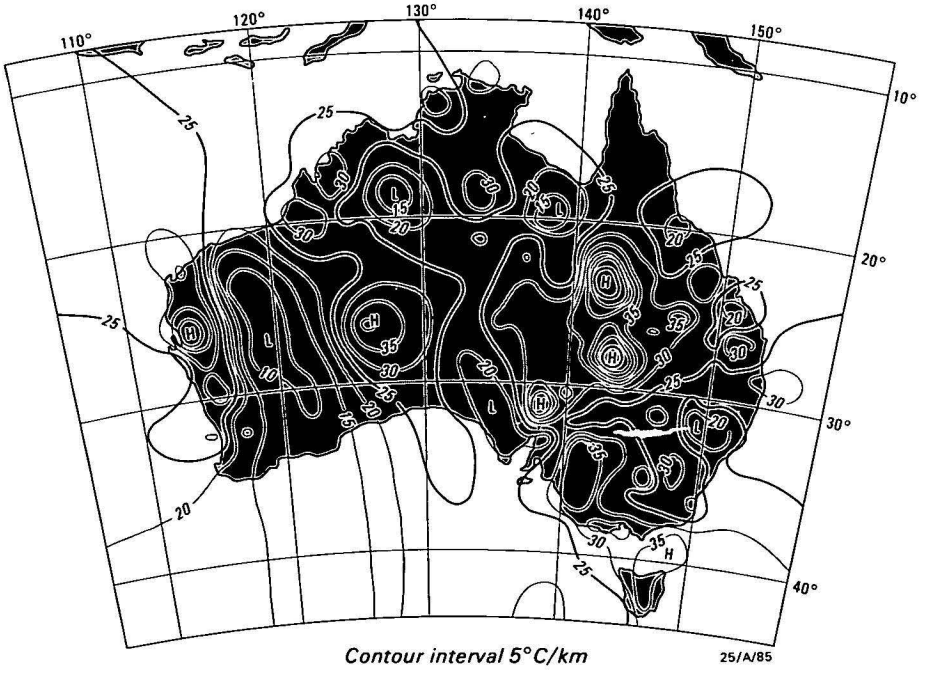


**Figure 7. Variation in the geothermal gradient, based on averages over a 1° grid.**

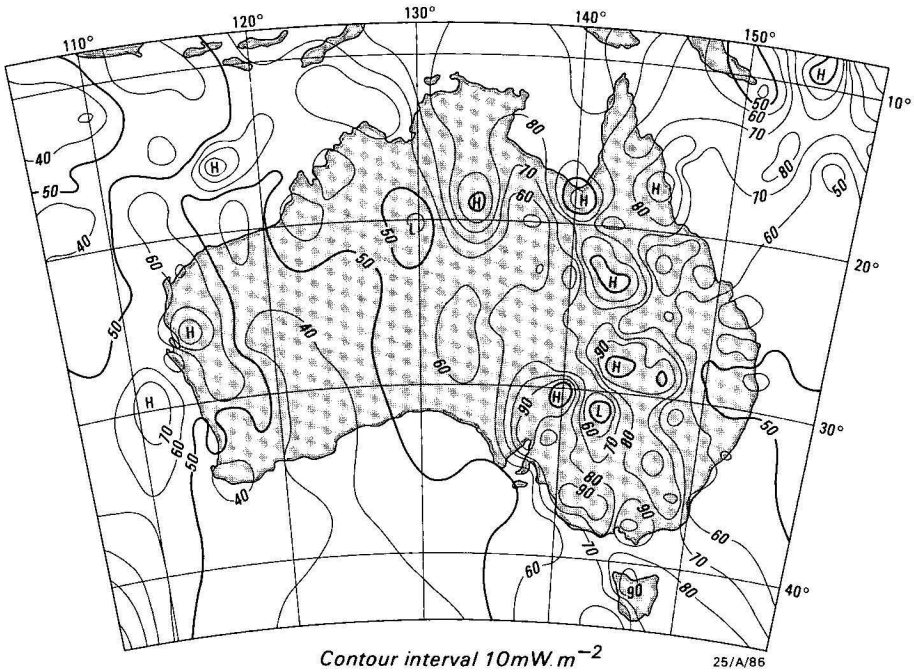


**Figure 8. Estimated heat flow, based on transformation of the geothermal gradients in Figure 7.**
Marine data from Cull (1982). Contours based on averages over a 1° grid.

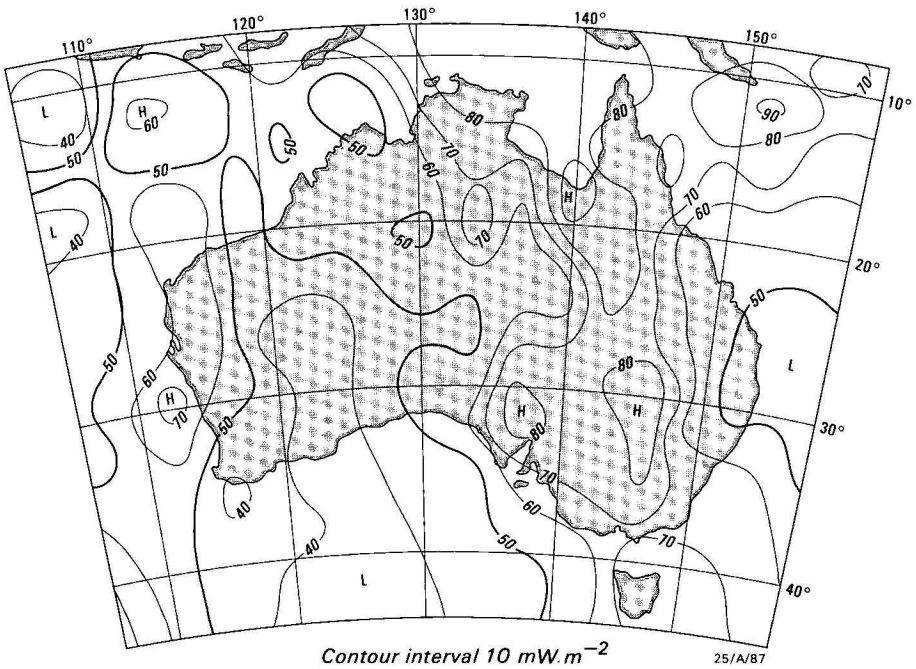


**Figure 9. Heat flow contours based on averages over a 3° grid.**

preserved, using contours based on averages over a 1° grid, and regional trends are indicated by contours on a 3° grid. The previous trends reported by Cull (1982) are confirmed, but extreme values in the southeast are no longer evident and a general high is revealed in central Queensland.

Anomalous values of heat flow in southeast Australia have been assumed to indicate episodic transient heating related to the mechanisms of large-scale crustal intrusion (Sass & Lachenbruch, 1979). Models were based on correlations with hot-spot migration indicating southwards younging of volcanism (Wellman & McDougall, 1974). However, the extreme values of heat flow used to define critical short-wavelength anomalies in the south may now require revision.

## Temperature profiles

An extrapolation of near-surface geothermal gradients presented in Figure 7 implies large-scale melting in the upper mantle, contrary to seismic evidence. An adequate reduction in the gradient requires a model based on enhanced conductivity with depth and a progressive depletion of heat-producing

elements. These factors are combined in the expression $d(\lambda\beta) / dz = -A$, where $\lambda(z)$ is the thermal conductivity and $A(z)$ is the rate of heat production per unit time per unit volume.

To estimate $\lambda(z)$ and $A(z)$ it is essential to consider individual geological profiles. Thermal conductivities vary with depth, depending on composition and temperature. Uniform values in the range 2.5–3.0 W/m/K can be adopted as representative of the lower crust (e.g. Davies & Strebeck, 1982), but near-surface values are more erratic. In particular, sedimentary basins must be distinguished from major cratons. Sedimentary basins contain thick sequences of erosion products transported from surrounding topographic highs. It has been demonstrated above that conductivities of 2.5 W/m/K are appropriate at depths greater than 1000 m, but corresponding estimates of heat production are rare. Radioelements concentrated near the surface of the original crystalline basement are redistributed in complex patterns (e.g. Rogers & Richardson, 1964), depending on the subsidence history of each basin. However, heat production should still be related to the total volume of sediments rather than the depleted basement. Consequently, observations of heat production in basin sequences are similar to estimates for exposed basement in Australia (Facer & others, 1980; Middleton, 1979).

The distribution of heat sources in crystalline rocks can be described by the expression $A(z) = A(0)\exp(-z/D)$, where $A(0)$ is the heat production at the surface and D is a characteristic unit of length (Lachenbruch, 1970). This distribution is consistent with observations of a linear relationship in which heat flow is found to be proportional to heat production in surface outcrop. This relationship is described by the expression $Q(0) = q^* + A(0)^*D$, where $Q(0)$ is the surface heat flow and $q^*$ is the residual heat flowing into the crust from mantle sources unrelated to radioelement distributions. However, other non-linear distributions have been proposed (e.g. Allis, 1979; Hyndman & others, 1968) and simple correlations have been disputed (e.g. Smith & others, 1979).

Linear relationships have been used by Sass & Lachenbruch (1979) to define three major heat-flow provinces in Australia. A primary distinction can be made between the West Australian Shield (WAS) and the Central Australian Shield (CAS). Values of $q^*$ and D used for calculations of temperature are extracted from Sass & others (1976). Geothermal gradients calculated according to Pollack (1965), are illustrated in Figure 10. Models for the Western Australian Shield are characterised by lower values of heat flow and smaller values of D compared to models for the Central Australian Shield. As a result, temperatures in the West Australian Shield range from 320°C to 380°C at depths of 40 km, compared to 470–550°C at similar depths in the Central Australian Shield.

Modifications to the computed geothermal gradient are required in regions of substantial sediment cover. A uniform layer of lower conductivity (2.0 W/m/K) and constant heat production, equal to half the basement value, has been added to the previous exponential distributions to approximate a basin structure. Temperatures at the base of the crust are increased by as much as 16°C for each 1 km increment in Western Australian Shield sediment thickness and 40°C for similar increments in Central Australian Shield sediments (Fig. 11).

Estimates of temperature in eastern Australia are complicated by episodes of recent tectonism. Sass & Lachenbruch (1979) defined a third heat-flow province for Australia, based on departures from the Q/A trends in central Australia. However, Clark (1980) has demonstrated that simple linear correlations are inappropriate in regions such as eastern Australia, which

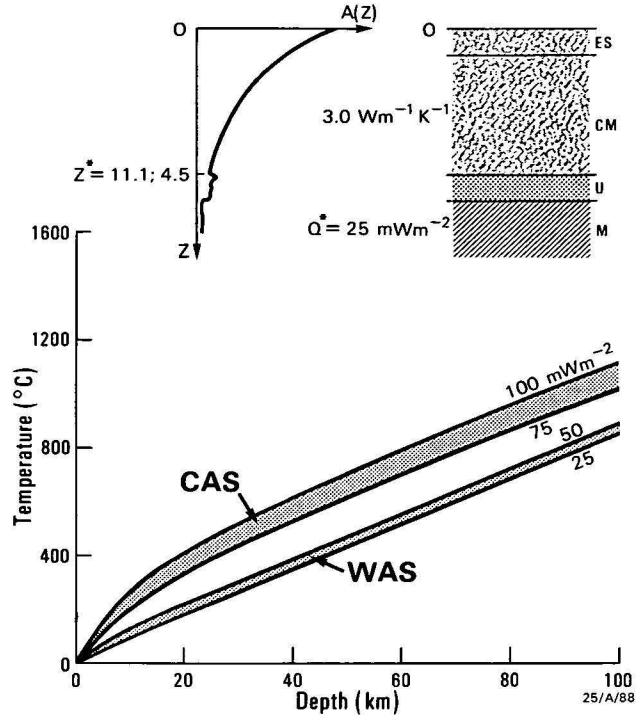


**Figure 10. Temperature profiles based on exponential distribution of heat-producing elements in lithosphere of conductivity 3.0 W/m/K.**

Temperature ranges indicated by shaded sections correspond to surface heat production of 4.32–6.58 $\mu W/m^3$ and 0–5.33 $\mu W/m^3$ for the Central Australian Shield (CAS) and Western Australian Shield (WAS), respectively. ES, erosion surface; CM, crustal melting; U, underplating; M, mantle.

have been subject to recent episodes of uplift and erosion (Wellman, 1979). In addition, critical anomalies in heat flow are rejected in the current analysis. Consequently, the results for the Central Australian Shield are assumed to apply for all areas of Phanerozoic cover.

There are no in-situ measurements of temperature to confirm the results of the conduction models at depths greater than 5 km. However, petrological data provide indirect evidence. Garnet-lherzolite nodules found in kimberlite are assumed to be representative of upper mantle xenoliths. For each nodule the temperature and pressure at the depth of origin can be readily estimated from the compositions of coexisting mineral assemblages (Davis & Boyd, 1966).

Consequently, a palaeogeotherm can be constructed to provide constraints for the more detailed conduction models.

Data obtained from xenoliths in eastern Australia were summarised by Ferguson & others (1979). Their temperature/depth estimates are illustrated in Figure 12. Extreme near-surface gradients are required to accommodate the xenolith data. However, Ferguson & others (1979) emphasised that nodules are generated during periods of anomalous tectonic activity, resulting in significant thermal transients. Consequently, nodule palaeotemperatures may be considered to represent maximum temperatures at the sampling depth, possibly associated with mechanisms of crustal underplating (Sass & others, 1976). In such circumstances, conduction models can be used only to define the extent of mass mobility within the mantle.

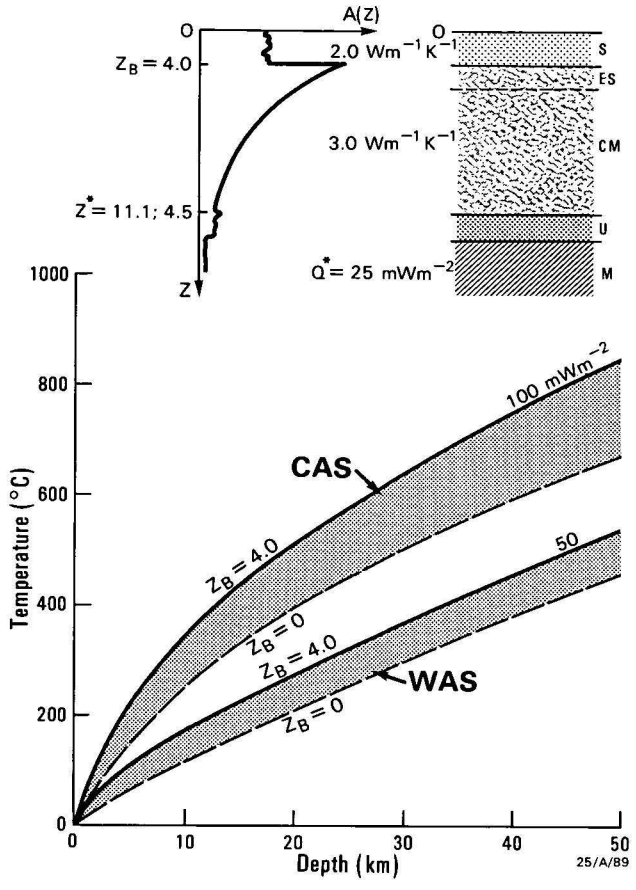


**Figure 11. Temperature profiles for crustal section with basin sequence of thickness $Z_B$.** Surface layers of conductivity 2.0 W/m/K and heat productivity equal to half the basement value added to the models of Figure 10. S, sediments; ES, erosion surface; CM, crustal melting; U, underplating; M, mantle.

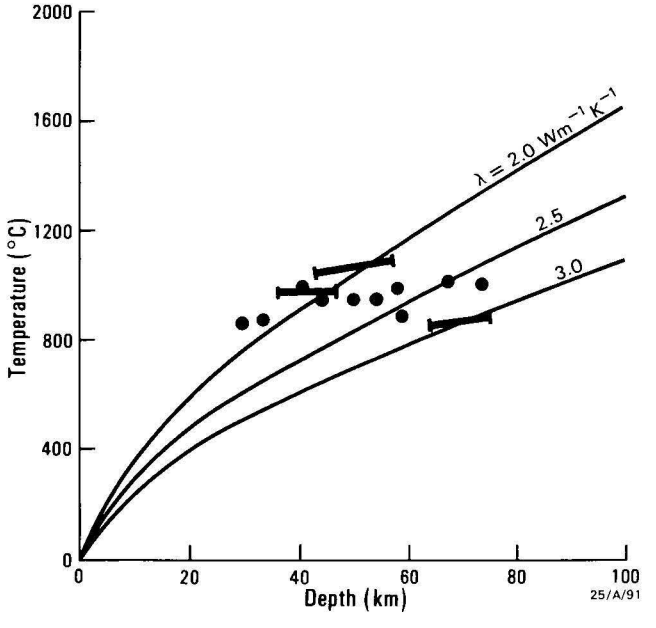


**Figure 12. Palaeotemperatures derived from xenolith data (Ferguson & others, 1979) compared to results from conduction models (solid curves) extrapolated from the upper crust.**

## Conclusions

Temperatures obtained for sedimentary basins during routine well logging must be treated with extreme caution. Apart from perturbations associated with drilling, there are several structural and stratigraphic corrections required before representative gradients can be estimated. Appropriate values for thermal conductivity can be obtained from sediment compaction models, but other geological constraints must be fully assessed for any regional analysis.

Estimates of heat flow from the Great Artesian Basin are consistent with the configuration of the major aquifer systems. Low values of heat flow are observed along the zones of recharge in the east and corresponding highs are generated in the west. Geothermal gradients in other areas are also subject to perturbations unrelated to thermal conductivity. Anomalies can be generated by vertical groundwater flow associated with fracture patterns and streaming near basement structures.

Oil well data confirm the regional trends obtained in previous investigations of heat flow, but local anomalies can be related to refraction in areas of contrasting conductivity. There is no evidence for abrupt changes in heat flow at the basin margins and, consequently, graben contacts appear to be rare. Anomalies in southeast Australia are no longer evident in the combined data set, contrary to models of crustal tectonism based on mechanisms of recent melt intrusion.

## References

Allis, R.G., 1979 — A heat production model for stable continental crust. *Tectonophysics*, 57, 151–165.

Burne, R.V., & Kantsler, A.J., 1977 — Geothermal constraints on the hydrocarbon potential of the Canning Basin, Western Australia. *BMR Journal of Australian Geology & Geophysics*, 2, 271–288.

Carslaw, H.S., & Jaeger, J.C., 1959 — Conduction of heat in solids. *Oxford University Press.*

Clark, S.P., 1980 — Comments on erosion, uplift, exponential heat source distribution and transient heat flux — by T.C.Lee. *Journal of Geophysical Research*, 85, 2694–2695.

Cull, J.P., 1982 — An appraisal of Australian heat flow data. *BMR Journal of Australian Geology & Geophysics*, 7, 11–21.

Cull, J.P., 1983 — Cultural changes to ground temperature and geothermal gradients. *Search*, 14, 101–103.

Cull, J.P., & Denham, D., 1979 — Regional variations in Australian heat flow. *BMR Journal of Australian Geology & Geophysics*, 4, 1–13.

Davies, G.F., & Strebeck, J.W , 1982 — Old continental geotherms : constraints on heat production and thickness of continental plates. *Geophysical Journal of the Royal Astronomical Society*, 69, 623–634.

Davis, B.T.C., & Boyd, F.R., 1966 — The join $Mg_2SiO_4$ — $CaMgSi_2O_6$ at 30 kb pressure and its application to pyroxenes from kimberlite. *Journal of Geophysical Research*, 71, 3567–3576.

Facer, R.A., Cook, A.C., & Beck, A.E., 1980 — Thermal properties and coal seams of the southern Sydney Basin, New South Wales : A palaeogeothermal explanation of coalification. *International Journal of Coal Geology*, 1, 1–17.

Falvey, D.A., & Middleton, M.F., 1981 — Passive continental margins: evidence for a prebreakup deep crustal metamorphic subsidence mechanism. *Oceanologica Acta, Proceedings of 26th IUGG SP*, 103–114.

Ferguson, J., Arculus, R.J., & Joyce, J., 1979 — Kimberlite and kimberlitic intrusives of southeastern Australia: a review. *BMR Journal of Australian Geology & Geophysics*, 4, 227–241.

Habermehl, M.A., 1980 — The Great Artesian Basin, Australia. *BMR Journal of Australian Geology & Geophysics*, 5, 9–38.

Howard, L.E., & Sass, J.H., 1964 — Terrestrial heat flow in Australia. *Journal of Geophysical Research*, 69, 1617–1626.

Hyndman, R.D., 1967 — Heat flow in Queensland and Northern Territory, Australia. *Journal of Geophysical Research*, 72, 527–539.

Hyndman, R.D., Lambert, I.B., Heier, K.S., Jaeger, J.C., & Ringwood, A.E., 1968 – Heat flow and surface radioactivity measurements in the Precambrian Shield of Western Australia. *Physics of the Earth and Planetary Interiors*, 1, 129–135.

Lachenbruch, A.H., & Brewer, M.C., 1959 — Dissipation of the temperature effect in drilling a well in Arctic Alaska. *U.S. Geological Survey, Bulletin*, 1083C, 73–109.

Lachenbruch, A.H., 1970 — Crustal temperature and heat productivity: implication of the linear heat flow relation. *Journal of Geophysical Research*, 75, 3291–3300.

Middleton, M.F., 1979 — Heat flow in the Moomba, Big Lake and Toolachee gas fields of the Cooper Basin and implications for hydrocarbon maturation. *Bulletin of the Australian Society of Exploration Geophysicists*, 10, 149–155.

Murray, A.S., 1977 — A guide to the use and operation of program Contor. *Bureau of Mineral Resources, Australia, Record* 1977/17.

Nicholas, E., Rixon, K., & Haupt, A., 1980 — Uncorrected geothermal map of Australia. *Bureau of Mineral Resources, Australia, Record* 1980/66.

Oxburgh, E.R., Richardson, S.W., Turcotte, D.L., & Hsui, A., 1972 — Equilibrium borehole temperatures from observations of thermal transients during drilling. *Earth and Planetary Science Letters*, 14, 47–49.

Polak, E.J., & Horsfall, C.L., 1979 — Geothermal gradients in the Great Artesian Basin, Australia. *Bulletin of the Australian Society of Exploration Geophysicists*, 10, 144–148.

Pollack, H.N., 1965 — Steady heat conduction in layered mediums : the half space and sphere. *Journal of Geophysical Research*, 70, 5645–5648.

Rogers, J.J.W., & Richardson, K.A., 1964 — Thorium and uranium contents of some sandstones. *Geochimica et Cosmochimica Acta*, 28, 2005–2011.

Sass, J.H., 1964 — Heat flow values from Eastern Australia. *Journal of Geophysical Research*, 69, 3889–3893.

Sass, J.H., & Lachenbruch, A.H., 1979 — The thermal regime of the Australian continental crust. *In* M.W. McElhinny (editor), The Earth — Its origin, structure and evolution. *Academic Press*.

Sass, J.H., Jaeger, J.C., & Munroe, R.J., 1976 — Heat flow and near surface radioactivity in the Australian continental crust. *U.S. Geological Survey, Open File Report* 76-250.

Smith, D.C., Nuckels, C.E., Jones, R.C., & Cook, G.A., 1979 — Distribution of heat flow and radioactive heat generation in Northern Mexico. *Journal of Geophysical Research*, 84, 2371–2379.

Wellman, P., 1979 — On the Cainozoic uplift of the southeastern Australian highland. *Journal of the Geological Society of Australia*, 26, 1–9.

Wellman, P., & McDougall, I., 1974 — Cainozoic igneous activity in Eastern Australia. *Tectonophysics*, 23, 49–65.

Yorath, C.J., & Hyndman, R.D., 1983 — Subsidence and thermal history of Queen Charlotte Basin. *Canadian Journal of Earth Science*, 20, 135–159.

BMR Journal of Australian Geology & Geophysics, 8, 339–349 

# A HEAVY-MINERAL SURVEY OF THE FORSAYTH AREA NORTHEAST QUEENSLAND

Allan G. Rossiter*

A heavy-mineral survey of the Forsayth 1:100 000 Sheet area, northeast Queensland, is described. The suitability of the technique for detecting gold, tin, and probably uranium mineralisation in the region has been established. The heavy-mineral method is also useful in the interpretation of sieved-sample surveys, and can provide valuable input to geological and metamorphic mapping programs.

## Introduction

In 1972, the Bureau of Mineral Resources and Geological Survey of Queensland began a detailed investigation of the geology and mineralisation of the Georgetown region in northeast Queensland. Orientation geochemical studies in 1972–3 (Rossiter, 1975) were forerunners to a regional stream-sediment survey of the Forsayth 1:100 000 Sheet area, combining both sieved-fraction and heavy-mineral samples, in 1974. The regional stream-sediment coverage was designed to delineate broad areas where detailed exploration should be concentrated and to establish a sound framework on which to base future work. The results of the sieved-fraction sampling were discussed by Rossiter & Scott (1978).

The Georgetown region has a semi-arid to monsoonal climate. The mean annual rainfall is about 800 mm and the average daily maximum temperature is about 33°C. Most of the region is covered by savannah woodland dominated by small eucalypts : large trees are generally found only along watercourses. As a consequence of the seasonal rainfall, most streams are dry during the winter: active dissection of the upland areas occurs during the wet season, however, and recently worked sediment is abundant in nearly all stream beds. Permanent waterholes occur almost exclusively on only the largest rivers.

The Newcastle Range is the most prominent topographic feature, and consists mainly of resistant Palaeozoic felsic volcanic rocks. It is flanked to the east and west by moderately hilly country occupied by Precambrian granitic and metamorphic rocks.

The results of the first systematic geological investigation of the Forsayth 1:100 000 Sheet area were published by White (1962, 1965). More recently, detailed mapping has been carried out by Bain & others (1976), and the following notes are based on their work. The regional geology has been described by Withnall & others (1980).

The oldest rocks in the area are the ?Middle Proterozoic Einasleigh Metamorphics and Robertson River Formation (Fig. 1), which may be correlatives. Both comprise multiply deformed, regionally metamorphosed sandstone-siltstone-shale sequences: the former underwent upper amphibolite (and minor granulite) grade metamorphism with greenschist overprinting in places; metamorphism of the latter ranged from greenschist to upper amphibolite facies. During and shortly after deposition of the Robertson River Formation numerous small mafic intrusions (and probably some flows) were emplaced: the amphibolite in the Einasleigh Metamorphics may be related.

The metamorphic rocks are intruded by three major granitic bodies (the Forsayth, Copperfield, and Robin Hood Batholiths) and many smaller plutons. The Forsayth and Copperfield Batholiths are ?Middle Proterozoic and both contain a number of phases. The Robin Hood Batholith may be considerably younger (?Silurian–Devonian) and is remarkably uniform.

*17 Churchill Avenue
Bright, Victoria 3741

Continental felsic volcanics of the Carboniferous Newcastle Range Volcanics and the Permian Agate Creek Volcanics overlie the Precambrian rocks of the region. Plugs and dykes of rhyolite and microgranite, presumably related to the volcanics, are widespread. Jurassic and Cretaceous marine and non-marine sediments cap many hills in the region.

Mineral deposits are numerous in the Forsayth Sheet area (Withnall, 1976; Bain & Withnall, 1980), although there is no mining on a significant scale at present. The gold deposits of the Forsayth Goldfield occur mainly as small fissure reefs within the Forsayth Batholith. Copper-lead-zinc mineralisation within the Einasleigh Metamorphics in the northeast corner of the area is confined to a single stratigraphic level (Bain & Withnall, 1980) and is probably syngenetic in origin. Small stratigraphically controlled lead-silver deposits occur close to the top of the Robertson River Formation southwest of Forsayth.

Although tin production has been negligible, large stream-sediment tin anomalies are associated with the Newcastle Range Volcanics and overlying sediments (Rossiter & Scott, 1978), and the region holds some promise for the discovery of economic tin deposits. The presence of Maureen-type uranium-molybdenum-fluorine mineralisation (O'Rourke, 1975; Bain, 1977) associated with the Palaeozoic igneous sequences (and their basal sediments) cannot be discounted entirely. Gold deposits in the Oakville and Percyville districts in the south of the area are spatially related to similar rocks, and there may be a genetic relationship as well (Bain & Withnall, 1980).

## Sample collection and processing

### Field procedures

The bulk of the sampling was carried out during July, 1974, using a Hughes 500 helicopter with a three-man crew (pilot, geochemist-navigator, and field hand). For ease of navigation the sampling loops were designed where possible to follow a major stream, and landings were made at points where tributaries entered. At each locality (Fig. 2) the aircraft remained on the ground for 2–5 minutes, while one or two 5–10-kg samples were taken. Active sediment from near the centre of the stream channel was collected where this was possible: each sample was a composite of three or four scoops a few metres apart. Four loops of about twenty sample sites each could be completed in a day, using about 4 hours flying time. In all, 1121 samples were collected, giving an overall sample density of about one per 2.5 $km^2$.

The helicopter was able to maintain vertical performance carrying its crew of three, about 150 kg of samples, and sufficient fuel for the return to base camp: however, it was found better to complete loops in difficult terrain in the cool of the morning, when the aircraft performed best. Normally, little difficulty was experienced in landing close to the predetermined sample sites, and it was necessary to move a site closer to a clearing in fewer than 5 per cent of cases. Only rarely was a ground traverse to a sample point needed to maintain adequate sampling coverage.

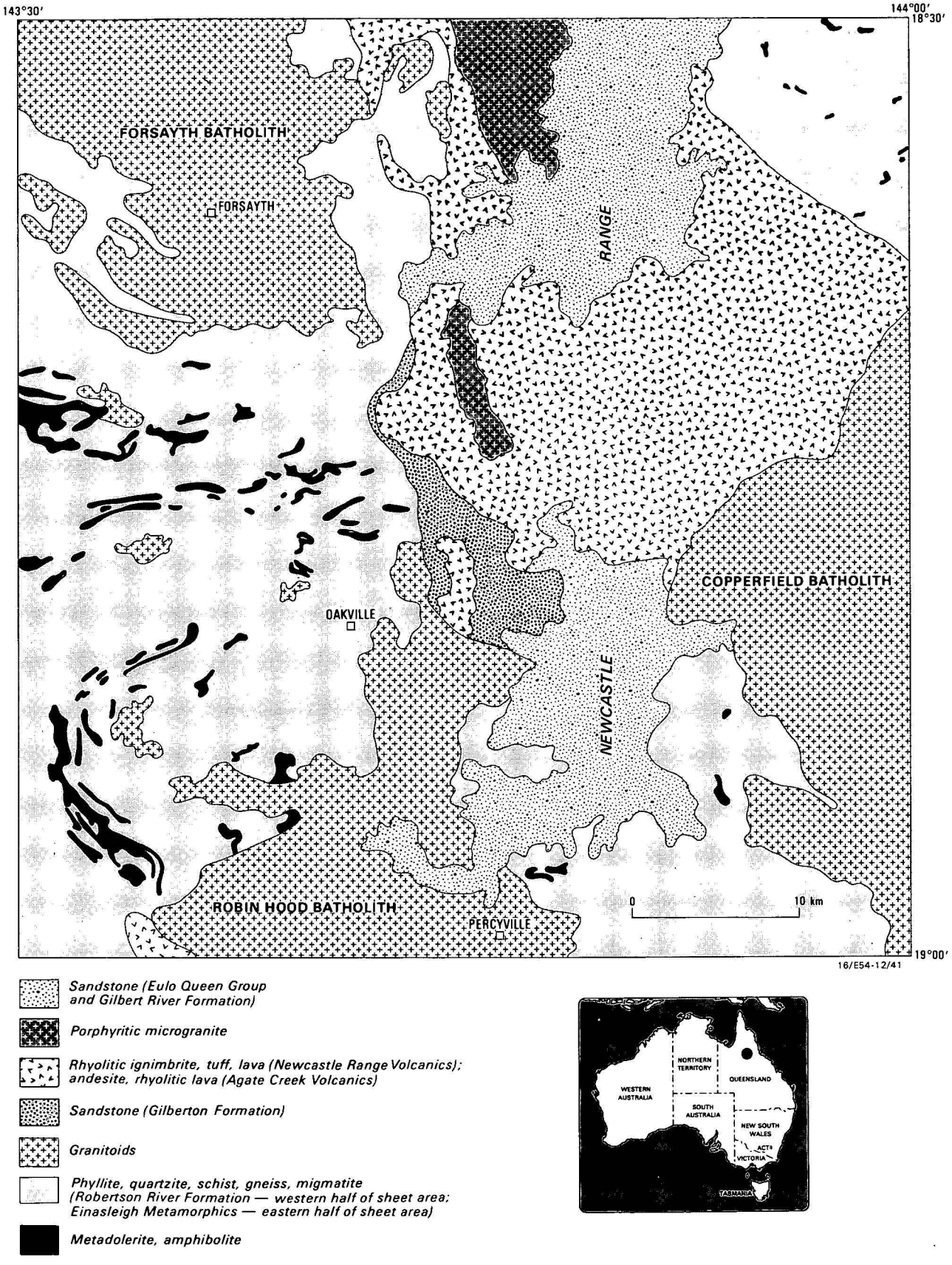


**Figure 1. Main rock types.**
Simplified from Rossiter & Scott (1978) and modified to take account of Withnall & others (1980).

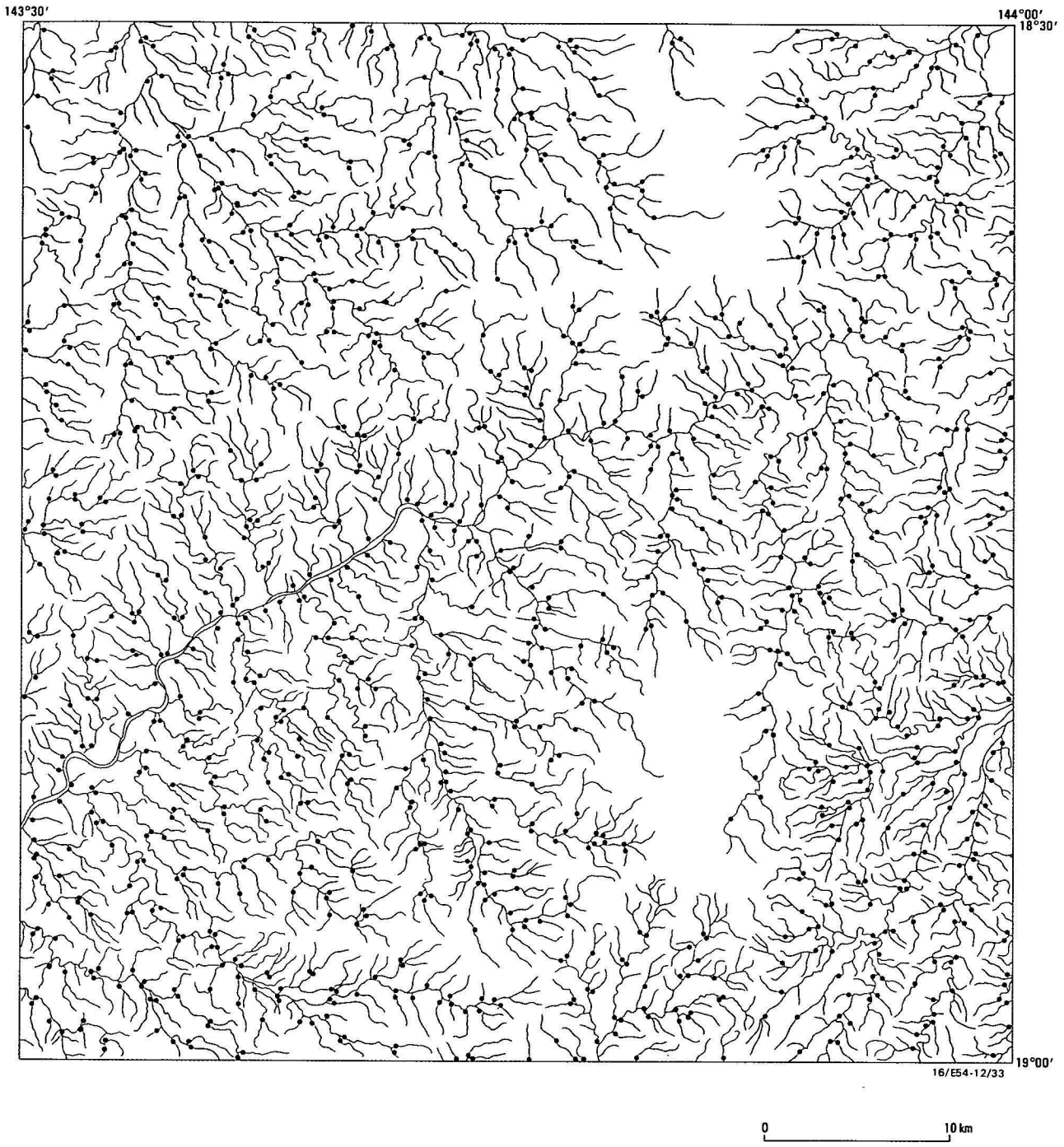


**Figure 2. Sample localities.**

At the base camp, each sample was passed through a series of non-contaminating sieves and panned in a prospector's dish* (Fig. 3A). The camp was beside a permanent waterhole and abundant water was available for panning. The heavy minerals were transferred from the pan to a Petri dish and dried in the sun. They were then packed in plastic vials for shipment to the laboratory.

## Laboratory procedures

From the field, the samples were sent to the Australian Mineral Development Laboratories for static tetrabromoethane separation. Most of the quartz and feldspar were removed by this procedure, although some fragments, which had presumably stuck to denser grains, persisted in the concentrates. Muscovite and biotite have specific gravities similar to that of tetrabromoethane (2.96), but, owing to their flaky habit, these minerals seldom sank in the heavy liquid.

All subsequent processing of the samples was carried out in the Bureau of Mineral Resources laboratories (Fig. 3B). Firstly, a hand magnet was used to remove magnetite, which was common in most concentrates. The heavy minerals were then checked for anomalous radioactivity on a gamma-ray spectrometer to see if monazite was present. Next, the samples were passed through a Franz isodynamic separator set at a side slope of 10° and a forward slope of 20°. An initial pass at 0.2 or

*A Wilfley table was used successfully in later surveys.

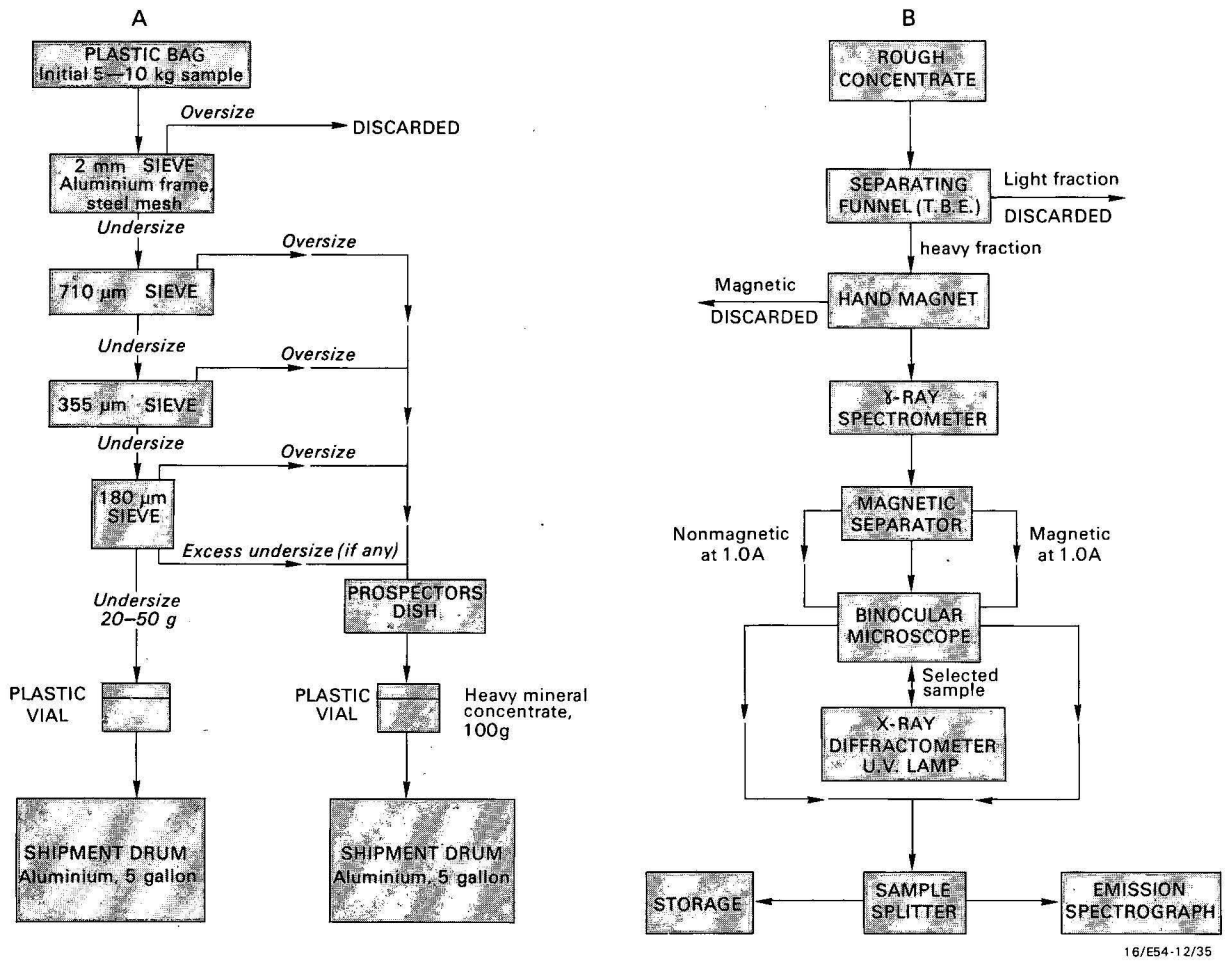


**Figure 3. Flow charts of sample treatment in the field (A) and laboratory (B).**

0.4 A (the lower current was used if there was any tendency for magnetic minerals to clog the separator) removed ilmenite and garnet, and a further pass at 1.0 A extracted minerals such as epidote, monazite, hornblende, and tourmaline.

The magnetic and non-magnetic fractions were then examined under a binocular microscope fitted with a zoom lens. Generally, the non-magnetic fraction, which contained most of the minerals of economic interest, was small enough for checking to be completed in 15–30 minutes. Any grains that could not be readily recognised were removed with a needle and identified by X-ray diffraction. Selected samples were examined under short (<300 nm) and long-wavelength (300–400 nm) ultraviolet light to check for the presence of fluorite, scheelite, etc. The fractions were then recombined and passed through a sample splitter: one split was crushed and analysed by emission spectrograph for antimony, barium, bismuth, cobalt, chromium, copper, gold, lanthanum, lead, molybdenum, niobium, silver, strontium, tin, tungsten, yttrium, and zinc; the other was stored for later reference.

## Discussion of results

Of the minerals identified in the Forsayth concentrates only nine (about one-third) can be considered to be of any economic consequence. Gold, fluorite, cassiterite, and anglesite appear to be the only direct indicators of mineralisation present. Monazite and epidote can be classified as having indirect economic significance, as checking heavy-mineral samples for these species would prove useful in the interpretation of data obtained from future sieved-sample surveys in the region. Andalusite, staurolite, and sillimanite might be useful exploration indicators if the presence of mineralisation (or the possibility of its detection) was somehow related to the metamorphic grade of the host rocks.

## Minerals of direct economic significance

**Gold.** Gold occurs as rounded, irregular grains in the concentrates: a brassy colour often suggests the presence of some copper in solid solution. Malleability is the best test for a suspect grain. Not surprisingly, about 40 per cent of the samples containing gold came from the Forsayth Goldfield area (Fig. 4), but auriferous concentrates were obtained from many other parts of the region as well.

To smooth the data, the Sheet area was divided in twenty-five equal cells and a moving average analysis of the number of gold-bearing samples in each cell was carried out, using a square four-cell window with a 50 per cent lateral overlap. The results are shown in Figure 4: gold concentrations in the northwest and southwest of the study area are strongly highlighted. Cells in which there has been little or no mining activity and which contain three of more gold-bearing samples are indicated in the inset and exploration for previously undetected gold lodes in these areas might be successful. However, the gold so indicated in the north-central and southeast parts of the area may be shedding from Mesozoic sediments after being eroded from the Forsayth and Percyville Goldfields, respectively.

The occurrence of gold in two streams draining only Newcastle Range Volcanics supports the contention of Bain & Withnall

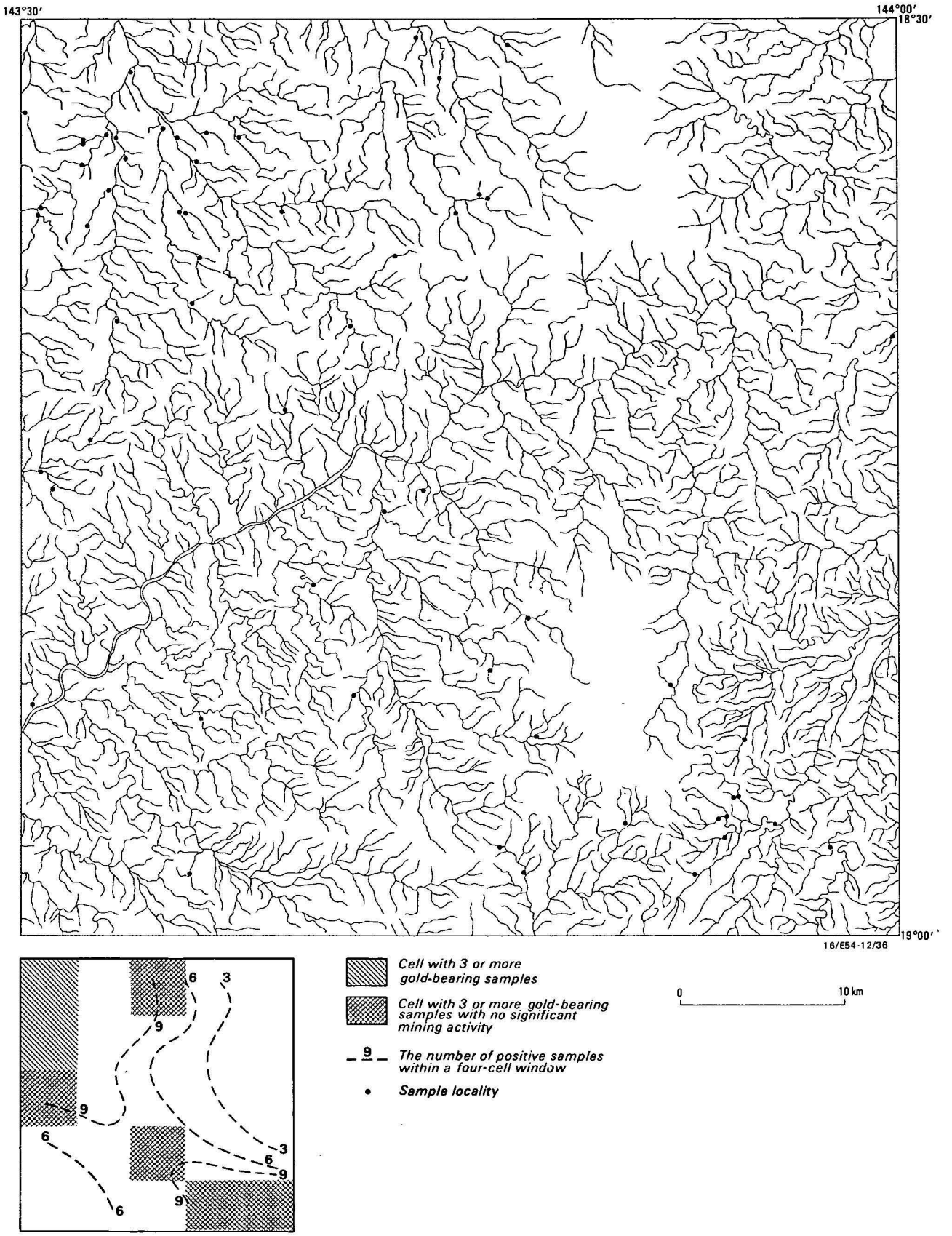


**Figure 4. Distribution of gold-bearing heavy-mineral samples.**

(1980) that many of the gold deposits of the region are related to Late Palaeozoic volcanic activity. It is also possible, however, that the gold in the two samples came from fossil placers in Mesozoic rocks now removed by erosion.

**Fluorite.** Fluorite is mentioned here as it has some potential for indicating uranium mineralisation of the Maureen type. It generally occurs in the Forsayth concentrates as equidimensional, colourless–white grains with purple blotches. Green grains are occasionally present in streams draining the Forsayth Batholith. Fluorite can sometimes be distinguished under the ultraviolet lamp by a purplish-blue fluorescence: this effect is more pronounced under long-wavelength radiation.

The distribution of fluorite in the Forsayth concentrates is shown in Figure 5. The main concentration of this mineral is near the northwestern corner of the area and is obviously associated with rocks of the Forsayth Batholith. Cells with more than one fluorite-bearing sample are shown in the inset. Of these, the one in the centre of the area is perhaps the most interesting, as Carboniferous sediments prospective for uranium mineralisation are conspicuous here. Company exploration in this area, however, has not located any mineralisation of economic significance.

**Cassiterite.** The cassiterite in the Forsayth heavy-mineral samples is fine-grained and difficult to identify microscopically. Figure 6 is based on spectrographic analyses of the concentrates. As tin rarely enters the crystal lattices of many heavy minerals — sphene and micas are notable exceptions (Hamaguchi & Kuroda, 1969), but these are not abundant in the Forsayth samples — tin analyses can be taken as fairly reliable indicators of the presence of cassiterite. Where the mineral could be confidently distinguished under the microscope it was present as small, equidimensional brown grains.

Samples that probably contain cassiterite are largely confined to the northeast quarter of the area, where Newcastle Range Volcanics and Mesozoic sediments crop out. It appears that the mineral has originated from both mineralisation in the Newcastle Range Volcanics and locally-derived fossil placers at the base of the Mesozoic sequence. If the cassiterite shedding from the Mesozoic had a distant source, large amounts of this mineral would be expected in all other parts of the area where rocks of this age are represented. However, apart from a slight concentration in the south-central part of the study area, such an effect is not observed. The large tin anomalies outlined by the sieved-sample survey (Rossiter & Scott, 1978) and the present study have not been thoroughly evaluated by exploration companies.

**Anglesite.** Anglesite has been noted in a few concentrates from the Forsayth Goldfield, but is not readily recognisable under the microscope. Spectrographic lead determinations do not help, as samples rich in monazite contain anomalous lead derived from radiogenic decay. In addition, the anglesite present does not appear to fluoresce under ultraviolet light. It was thought that anglesite might prove a useful indicator of gold mineralisation, but, because of the problems mentioned above, this did not prove to be the case.

## Minerals of indirect economic significance

**Monazite.** Monazite is abundant in the Forsayth heavy-mineral concentrates (Fig. 7). It occurs as smallish, rounded, colourless to yellow and red grains, and is easily detected by gamma-ray measurements. Monazite is particularly common in streams draining the Forsayth Batholith and the Einasleigh Metamorphics. It is noticeably scarce in areas occupied by Newcastle Range Volcanics and low-grade Robertson River Formation rocks.

Monazite can be considered to have some economic significance, as it produces geochemical and radiometric anomalies that are not related to uranium mineralisation. During a stream-sediment survey for uranium, it is necessary to have a technique for discounting anomalies caused by monazite. The examination of heavy-mineral samples and the consideration of analytical data for elements such as cerium and thorium (Rossiter & Scott, 1978) can both be used for this.

**Epidote.** Epidote is very common in the Forsayth concentrates, but the mineral varies greatly in appearance. Most commonly, it occurs as large yellowish-green grains, often having striated crystal faces. In streams draining mafic igneous rocks within the Robertson River Formation the epidote grains are similar, but light brown. Small, rounded, yellow epidote grains are abundant in areas where Einasleigh Metamorphics crop out: white and pink varieties occur on occasions.

Brown epidote has some economic interest as an indicator of mafic igneous rocks in the Forsayth area. Such rocks produce copper anomalies in sieved samples taken downstream from them and, if these are to be distinguished from copper enrichment related to mineralisation, heavy-mineral work or scrutiny of analytical data for elements such as cobalt, nickel, and chromium is necessary.

**Andalusite, staurolite, sillimanite.** Andalusite is present as large, rounded, transparent grains, ranging from colourless to pink: numerous black inclusions are diagnostic. There is also an opaque, light grey-brown variety. Staurolite occurs as largish, equidimensional crystals, varying from orange to red-brown. Conchoidal fracturing can be seen in places, but none of the cruciform twins that characterise staurolite in other areas was observed. Sillimanite is present mainly as large, white to grey, sometimes iron-stained, fibrous masses (fibrolite) with large clear to milky, striated grains occurring in places. Micaceous aggregates in some samples appear to be retrogressed sillimanite.

Figure 8 shows the distribution of these minerals within the Forsayth 1:100 000 Sheet area and the metamorphic zones that can be inferred from them. Andalusite and staurolite are confined to streams draining Robertson River Formation rocks, but sillimanite is more general in its distribution. The onset of amphibolite facies conditions is marked by the formation of andalusite and staurolite. At higher pressures, andalusite disappears and staurolite coexists with sillimanite. At still higher pressures staurolite disappears and sillimanite is the only one of these metamorphic indicators preserved in the heavy-mineral assemblages. In a similar application, Stendal (1978) mapped metamorphic facies boundaries in Norway by noting the distribution of hornblende and hypersthene in heavy-mineral samples.

The heavy-mineral technique may have exploration significance in an area where syngenetic mineralisation has reached economic grade (or economic grain size) only when the host rocks were subjected to certain metamorphic conditions. In addition, heavy-mineral reconnaissance in unmapped areas could indicate whether metamorphism has been severe enough to cause the reduction of pyrite to pyrrhotite and enable the usefulness of magnetic surveys to be assessed.

## Other minerals

Garnet, hornblende, and iron oxides and hydroxides are, with epidote, the most abundant minerals in the Forsayth concentrates, and seem to be associated with most of the rock units. Almandine is the most common garnet variety: it occurs as largish, rounded, equidimensional, pink to reddish grains, commonly with pitted surfaces. In streams draining the

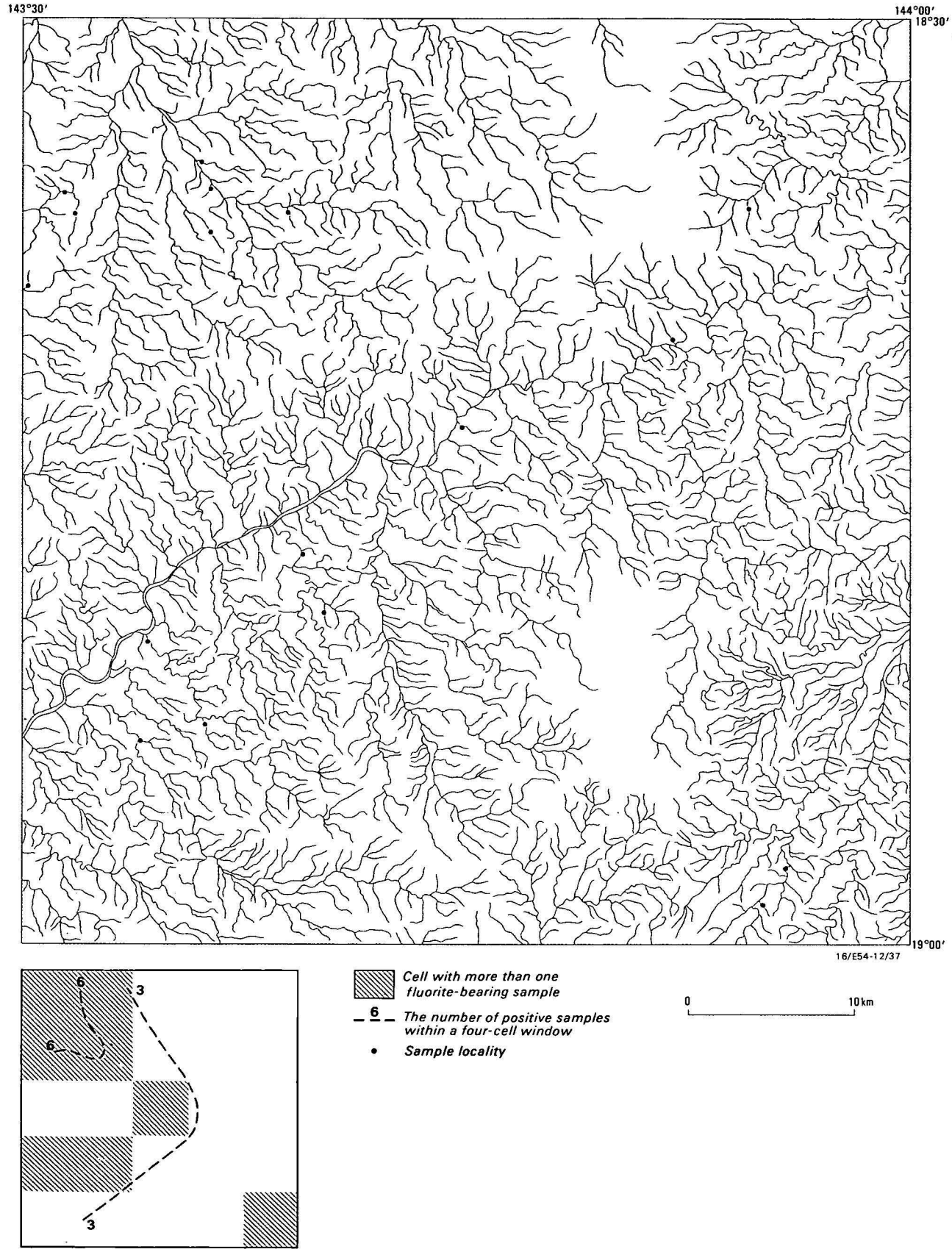


**Figure 5. Distribution of fluorite-bearing heavy-mineral samples.**

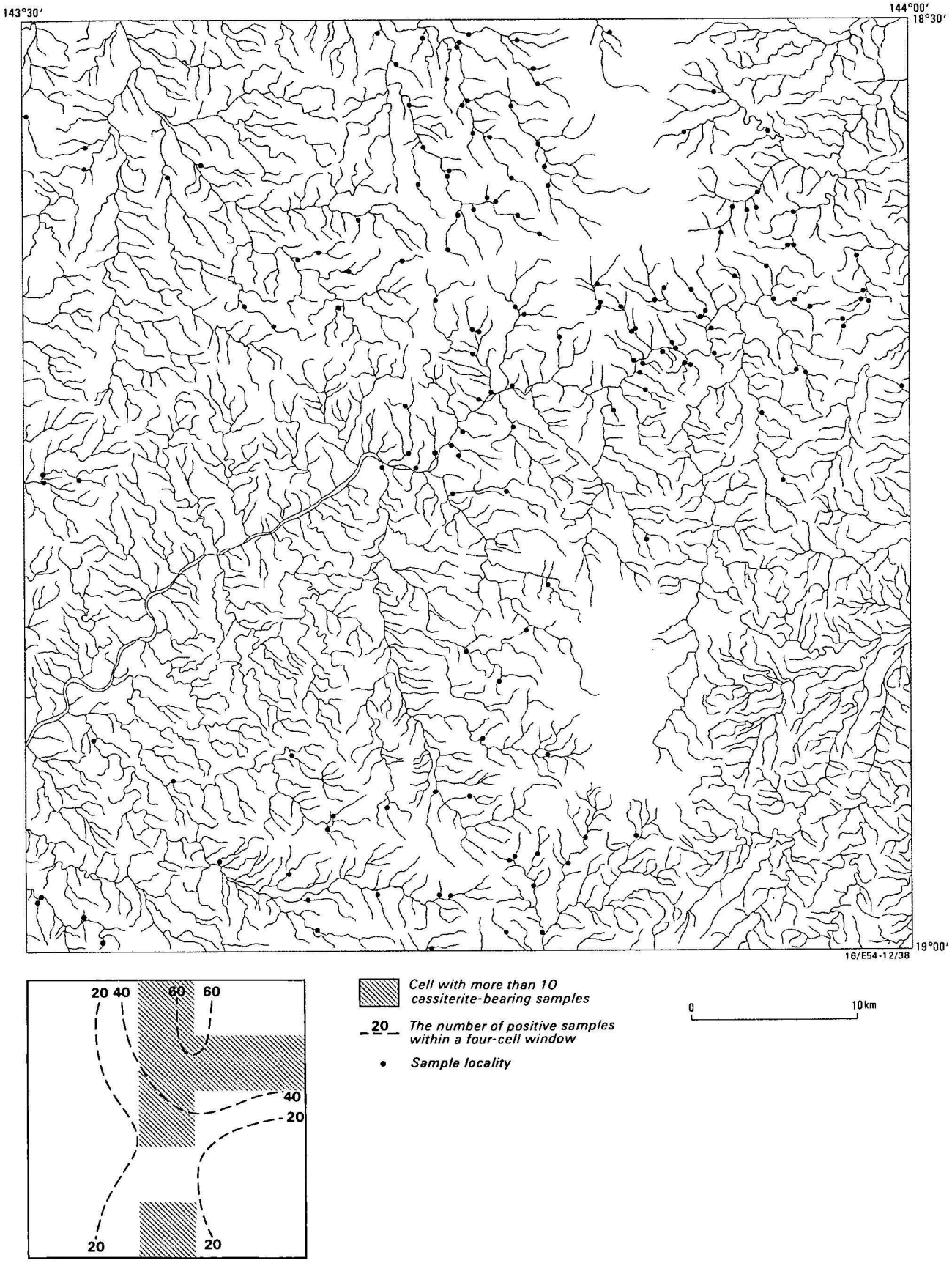


**Figure 6. Distribution of cassiterite-bearing heavy-mineral samples.**

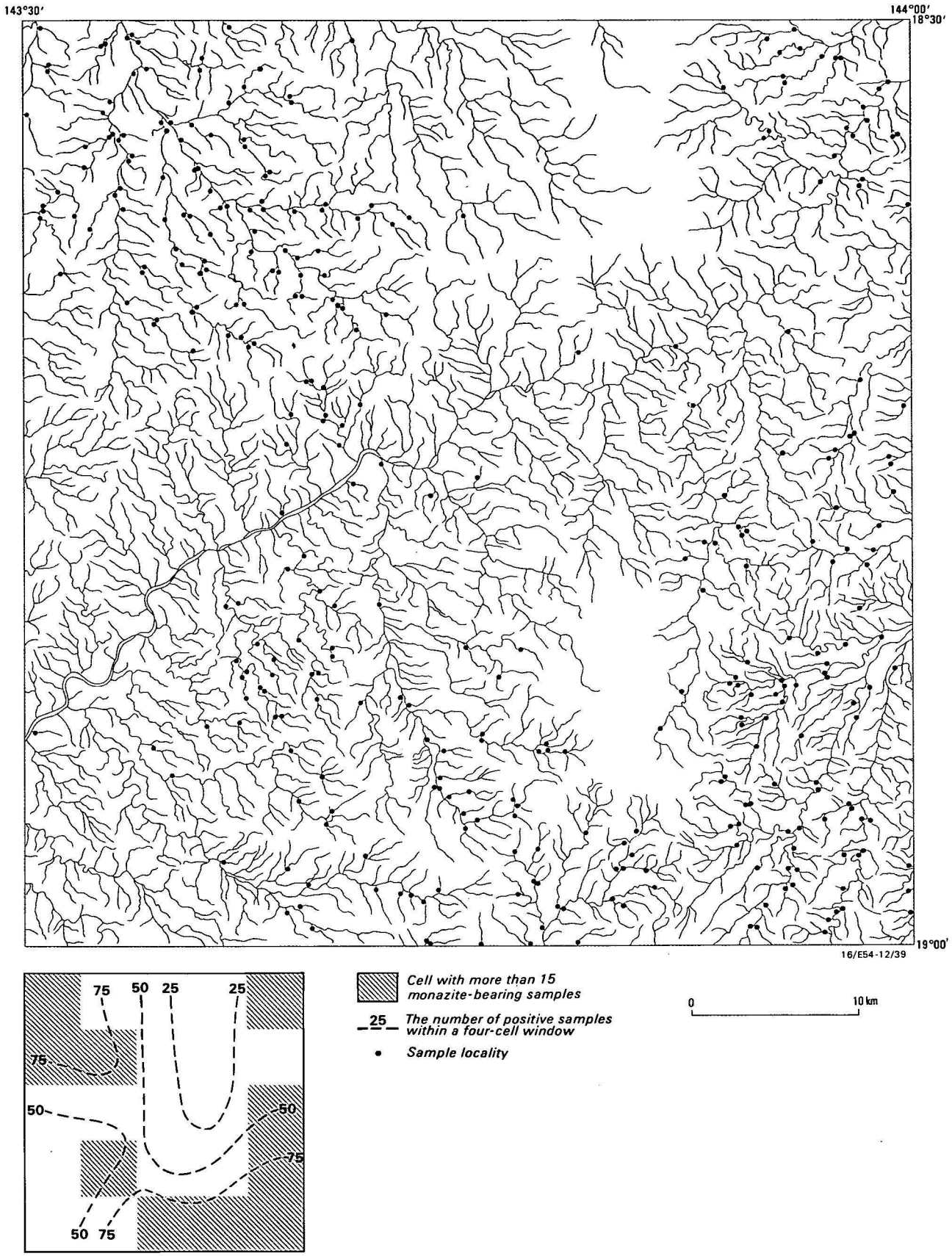


**Figure 7. Distribution of monazite-bearing heavy-mineral samples.**

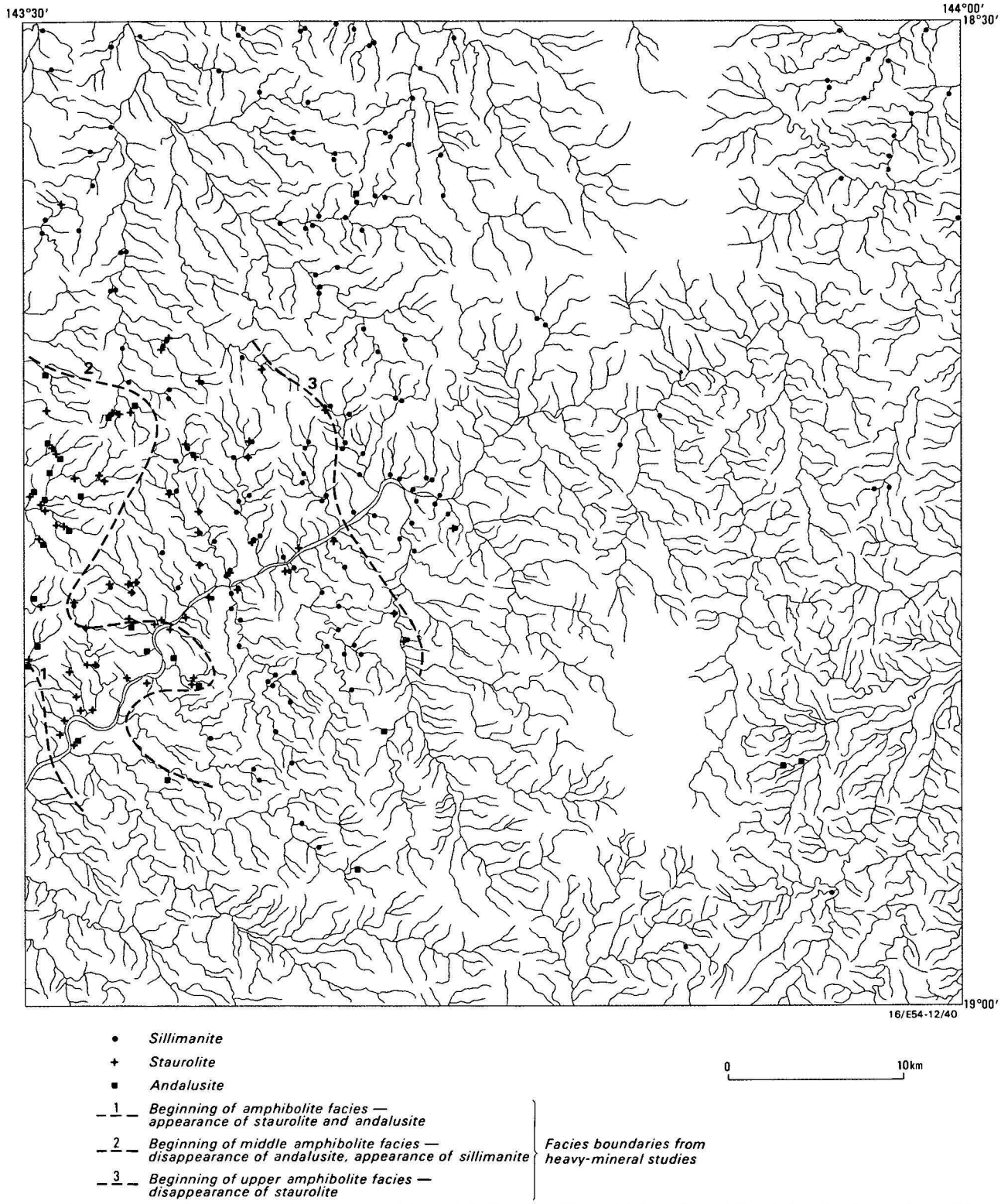


**Figure 8. Distribution of heavy-mineral samples containing andalusite, staurolite, and sillimanite, and their inferred metamorphic zones.**

Copperfield Batholith, small, euhedral, brown spessartine grains are conspicuous. Hornblende is generally dark green, but brown grains are prominent in some areas. The grains are mostly irregular and ragged: striated faces and fractures filled with light green chlorite are prominent features. Iron minerals are represented in every sample. These minerals were not studied in detail, but all concentrates were checked for anomalous chromium. Ilmenite is the most abundant, but hematite and limonite (sometimes forming cubic pseudomorphs after pyrite) are also present. The spectrographic analyses suggest that chromite occurs only in small amounts. The common accessory minerals in the concentrates are brown prismatic-rounded tourmaline, bladed-prismatic red to black rutile, colourless, white, yellow, and brown zircon, showing a variety of habits, and colourless to white apatite grains of diverse form. Of less common occurrence are topaz, sphene, anatase, and spinel; kyanite, grossular, xenotime, barite, andradite, and diopside are rarely present.

## Conclusions and recommendations

As expected, gold emerged as the most important indicator of mineralisation during the Forsayth heavy-mineral survey. It

was found in many streams remote from known mine workings and perhaps there are deposits awaiting discovery within the area. The heavy-mineral survey also proved capable of detecting tin and, probably, uranium concentrations, but produced few data for examples of such mineralisation additional to those provided by the sieved-sample work.

The examination of every concentrate during a program like the Forsayth survey involves an enormous amount of work, and future surveys of this kind could probably be justified only in areas where there is very good reason to suspect potentially economic deposits of gold, platinum-group metals, or diamonds, which would not normally be detected by conventional sieved-sample surveys. It is a fairly simple matter, however, to collect a heavy-mineral separate while carrying out a routine stream-sediment survey, and there is no doubt that examination of the corresponding concentrate can be of great assistance in the interpretation of an ambiguous sieved-sample value. In the Forsayth region such an approach is valuable in the processing of analytical data for copper and uranium. Brown epidote in a heavy-mineral sample can indicate that a copper anomaly in the associated sieved fraction is probably due to mafic igneous rocks. Similarly, monazite can be used to distinguish which uranium anomalies are likely to be associated with mineralisation. In an area of more complex metallogeny the technique could prove even more useful.

This study has established that heavy-mineral work can provide valuable input to geological and metamorphic mapping programs. Indeed, in a particularly inaccessible and densely vegetated area, the technique might prove almost indispensable. The presence in a catchment area of several rock units of the Forsayth 1:100 000 Sheet area is immediately recognisable from the heavy-mineral assemblage. For example, long, doubly terminated, clear zircon prisms with characteristic iron-staining are present in areas occupied by Newcastle Range Volcanics, while apatite prisms with colourless rims and dark cores indicate Forsayth Batholith rocks. Staurolite and andalusite are confined to the Robertson River Formation, spessartine occurs only in Copperfield Batholith rocks, and brown epidote typifies concentrates from streams draining mafic igneous rocks within the Robertson River Formation.

The survey has also shown that checking of heavy-mineral concentrates for andalusite, staurolite, and sillimanite can be used to map metamorphic zones within amphibolite facies terrains. Such work might be applicable to exploration programs in areas where syngenetic mineralisation has reached economic grade (or economic grain size) only when the host rocks were subjected to certain metamorphic conditions. In addition, heavy-mineral reconnaissance in unmapped areas could indicate whether metamorphism has been severe enough to cause the reduction of pyrite to pyrrhotite and enable the usefulness of magnetic surveys to be assessed.

## Acknowledgements

I wish to thank M. Shackleton, K. Armstrong, T. Fletcher, A. Hoey, and F. Stevenson for their assistance with the fieldwork. K. Armstrong painstakingly separated the magnetite from the concentrates with a hand magnet and checked the samples on a gamma-ray spectrometer. T. Slezak and the late J. Weekes carried out emission spectrographic analysis of the concentrates, while D. Barnes assisted with X-ray diffraction identification of problem grains. W. Dallwitz, J. Bain, B. Cruikshank, and J. Ferguson suggested improvements to the manuscript, and P. Griffiths drafted the figures.

## References

Bain, J.H.C., 1977 — Uranium mineralisation associated with late Palaeozoic acid magmatism in northeast Queensland. *BMR Journal of Australian Geology & Geophysics*, 2, 137–147.

Bain, J.H.C., & Withnall, J.W., 1980 — Mineral deposits of the Georgetown region, northeast Queensland. *In* Henderson, R.A., & Stephenson, P.J. (editors), The geology and geophysics of northeastern Australia. *Geological Society of Australia, Queensland Division, Brisbane*, 129–148.

Bain, J.H.C., Withnall, I.W., & Oversby, B.S., 1976 — Geology of the Forsayth 1:100 000 Sheet area (7660) north Queensland. *Bureau of Mineral Resources, Australia, Record* 1976/4.

Hamaguchi, H., & Kuroda, R., 1969 — Tin. Abundance in rock-forming minerals. *In* Wedepohl, K.H. (editor), Handbook of geochemistry, Vol II/4, 50-D-1–50-D-4. *Springer-Verlag, Berlin.*

O'Rourke, P.J., 1975 — Maureen uranium, fluorine, molybdenum prospect, Georgetown. *In* Knight, C.L. (editor), Economic geology of Australia and Papua New Guinea, Volume 1 — Metals. *Australasian Institute of Mining and Metallurgy, Monograph* 7, 764–765.

Rossiter, A.G., 1975 — An orientation geochemical survey in the Georgetown area, north Queensland. *Bureau of Mineral Resources, Australia, Record* 1975/164.

Rossiter, A.G., & Scott, P.A., 1978 — Stream-sediment geochemistry of the Forsayth 1:100 000 Sheet area, north Queensland. *Bureau of Mineral Resources, Australia, Record* 1978/17.

Stendal, H., 1978 — Heavy minerals in stream sediments, southwest Norway. *Journal of Geochemical Exploration*, 10, 91–102.

White, D.A., 1962 — Georgetown, Qld. 1:250 000 geological series. *Bureau of Mineral Resources, Australia, Explanatory Notes* E/54-12.

White, D.A., 1965 — The geology of the Georgetown/Clark River area, Queensland. *Bureau of Mineral Resources, Australia, Bulletin* 71.

Withnall, I.W., 1976 — Mines and mineral deposits of the Forsayth 1:100 000 Sheet area, Queensland. *Geological Survey of Queensland, Report* 91.

Withnall, I.W., Bain, J.H.C., & Rubenach, M.J., 1980 — The Precambrian geology of northeastern Queensland. *In* Henderson, R.A., & Stephenson, P.J. (editors), The geology and geophysics of northeastern Australia. *Geological Society of Australia, Queensland Division, Brisbane*, 109–127.

BMR Journal of Australian Geology & Geophysics, 8, 351–356 

# MIDDLE PROTEROZOIC LANDFORMS PRESERVED AT A DISCONFORMITY IN THE CARRARA RANGE REGION, NORTHERN TERRITORY

I.P. Sweet

The contact between the middle Proterozoic Mitchiebo Volcanics and Top Rocky Rhyolite, in the Carrara Range Region of the Northern Territory, is highly irregular and is interpreted as a disconformity. Sandstones in the Mitchiebo Volcanics were lithified and then eroded into a series of narrow ravines up to 120 m deep. Rhyolitic ignimbrite and lava blanketed and preserved the irregular surface. The preservation of the surface provides us with a rare glimpse of middle Proterozoic landforms.

## Introduction

Our knowledge of the shape of physical features on the Earth's surface during the geologic past relies on evidence preserved in rocks. Most landforms are transient, as they are eroded and destroyed forever, but in rare instances they are preserved — as unconformities. Not all unconformities reflect palaeotopography; most are diachronous, reflecting the cumulative shape of, say, a wave-cut platform or river valley as a transgression or sedimentation proceeded. Some unconformities at the base of non-marine sequences do reflect palaeotopography, but even these are the result of complex processes. An unconformity displaying up to 600 m relief forms the base of the Torridonian in northwestern Scotland (Phemister, 1960), but even this must be, to some degree, a diachronous surface, subjected to progressive modification as the lower parts of it were buried and the upper parts were continually eroded. Nevertheless valuable information is preserved adjacent to parts of the surface. For instance, Williams (1966) described a 3 m-thick zone of decomposed bedrock beneath the surface at one locality and interpreted this as a weathering profile. Such material may be invaluable in studies of the manner in which rocks weathered in the past, and in determining climates prevailing at the time.

The process most likely to preserve a land surface *intact* is volcanism. Ash or lava can completely blanket a region, preserving the existing physical features of the landscape in considerable detail. Examples from relatively young rock sequences are not uncommon, especially in areas where ignimbrite eruptions have blanketed vast areas. Examples from old sequences, particularly Precambrian rocks, are rare. An unusually good example of such a surface was mapped during studies by the Bureau of Mineral Resources in Proterozoic rocks in the Carrara Range region in the eastern Northern Territory, Australia (Fig. 1). The rocks in the region are of middle Proterozoic age (about 1600–1700 Ma), and the disconformity described here is a rare example of the preservation of a cross-section of a highly dissected Proterozoic landscape.

## General geology

The Proterozoic rocks in the Carrara Range region were mapped by BMR in 1977 during a study of the major Proterozoic province in northwestern Queensland and eastern Northern Territory (Sweet & Mond, 1980; Sweet, 1982; Sweet, in press). An Early Proterozoic metasedimentary basement, the Murphy Metamorphics, is overlain by 5000 m of middle Proterozoic volcanic and sedimentary rocks (Fig. 1) assigned to the Carrara Range and McNamara Groups. The disconformable contact described here is between the Mitchiebo Volcanics and the Top Rocky Rhyolite (Fig. 1, 2) in the Carrara Range Group. The best estimate of the age of the

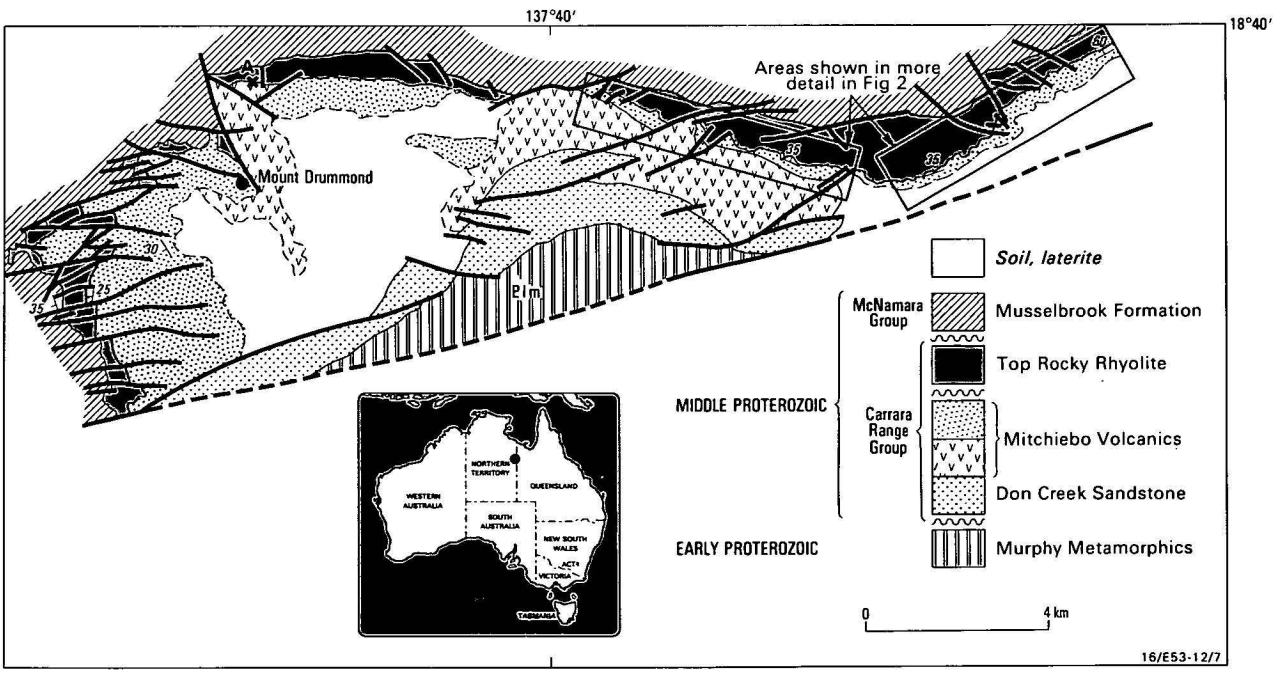


**Figure 1. General geology of part of the Carrara Range Region.**
Locality A is discussed in the text.

rocks is provided by the correlation of the Top Rocky Rhyolite with the Carters Bore Rhyolite, 220 km to the southeast (Hutton & Sweet, 1982), whose U-Pb zircon age is 1678 Ma (Page, 1978).

The Mitchiebo Volcanics consist of amygdaloidal basalt and possible trachyte flows interbedded with feldspathic sandstone and minor siltstone. Several sandstone beds at the top of the formation form a mappable member, and it is as the result of the partial erosion of this member that the disconformity is so admirably displayed.

The Top Rocky Rhyolite consists of massive feldspar porphyry, lacking features which would allow its unequivocal identification as a lava rather than an ignimbrite. However, the presence of contorted flow banding at one locality gives the impression that at least some of the unit may have been extruded as lava.

## Description of the disconformity

The contact between the Top Rocky Rhyolite and the sandstone member of the Mitchiebo Volcanics is concordant. It is strongly faulted west of Mount Drummond, and to the east (Figs. 1, 2) is highly irregular despite the overall concordance of the units. The irregularity of the upper surface of the sandstone is not reflected at its base, nor in the thin basalt layer within the sandstone (Fig. 2). Faulting is therefore discounted as a cause of the irregularity in the upper surface, and, in fact, most of the faults cutting the contact appear to post-date extrusion of the Top Rocky Rhyolite. Furthermore, rhyolite is present in stratigraphically low parts of the contact zone, such as locality $C_2$, indicating that the irregularity is not simply the result of Cainozoic weathering of a tabular sandstone body. At locality $C_2$ (Fig. 2) the sandstone is overlain by about 1 m of poorly sorted sedimentary breccia in which purple, subangular, well-cemented sandstone clasts up to 20 cm across are set in a sandy and silty matrix.

A profile of the disconformity was generated by first making three assumptions: that the faults cutting the sandstone and Top Rocky Rhyolite did not exist, and therefore had no topographic expression, during development of the disconformity; that the movement on them was strike-slip (The shortening of the profile (Fig. 3a) relative to its original strike length (Fig. 2) shows that this was not the case, but the effect on the shape of the surface is minimal.); and that the base of the sandstone was a horizontal plane. With these assumptions, the profile was generated by restoring the outcrop to its pre-fault shape (Fig. 3a) and then reducing its amplitude, by multiplying by the sine of the angle of dip, to allow for regional dip of the strata (Fig. 3b).

## Interpretation

The irregular nature of the contact, unrelated to faulting, coupled with the presence of rhyolite and sedimentary breccia in depressions, and the lack of angular discordance between the formations concerned, indicates that the contact is a disconformity. The local relief on the disconformity surface can be calculated if the dip of the Top Rocky Rhyolite is known. Unfortunately, the Top Rocky Rhyolite is massive with virtually no internal banding, but both the underlying sandstone and the overlying Musselbrook Formation dip north at about 35°, indicating that the rhyolite probably does likewise. At localities B, C, D, and E (Fig. 2) the local relief was 87, 118, 88, and 110 metres, respectively. The corrected profile of the surface (Fig. 3b) shows that it consisted of a series of narrow ravines and broader valleys and plateaus. The trend of the ravines is not known, since there is no information on the shape of the surface down dip.

At locality E the wall of the ravine must have been overhanging. If the ravine trends straight down dip, then the overhang would have been 50 m. This is most unlikely in a ravine only 100 m deep. If, however, the ravine trends obliquely down dip, the overhang is less — 35 m if it trends at 45° to the strike, and 17 m if it is at 20° to the strike.

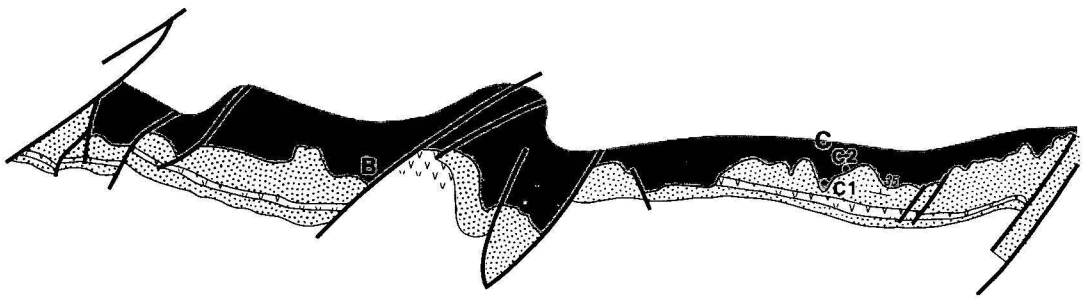


**Figure 2. Detailed map, traced from colour airphotos, of the disconformable contact between the Mitchiebo Volcanics and Top Rocky Rhyolite.**
Symbols as for Fig. 1.

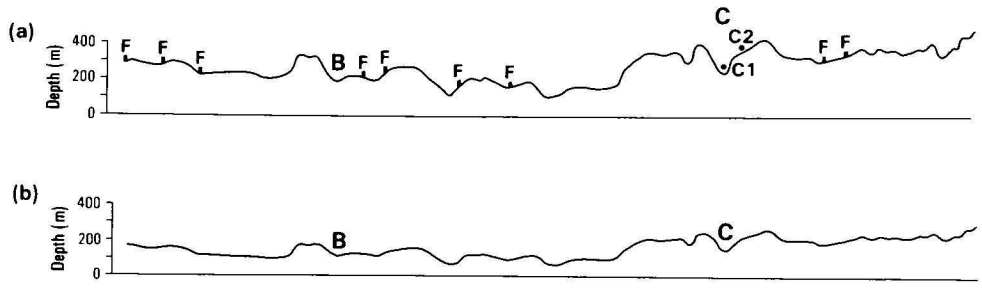


**Figure 3. Profile generated by plotting the distance from the base of the sandstone in the Mitchiebo Volcanics to the disconformity.**
a–Uncorrected for tectonic tilt. b–Corrected for dip; 35° dip assumed for all localities west of G, 60° assumed east of G. The step at the base of the sandstone is not real, but is an artifact of the change in dip used to generate the profile. The dip of the sandstone probably increases gradually, which would alter the overall gradient of the surface between G and H, but not the details of local relief.

## Discussion

The existence of a disconformity within a Proterozoic sequence is, of course, not unusual, but the preservation of such a surface, in which the relief is visible on small-scale aerial photographs, is. The shape of the disconformity surface indicates that the sandstone was partly eroded before extrusion of the Top Rocky Rhyolite, and, furthermore, that the sandstone was well cemented. The amount of erosion cannot be accurately estimated, but the existence of 600 m of sandstone in the west, and as little as 100 m in the east may indicate greater erosion in the east. The Top Rocky Rhyolite is thin in the west (100 m) and thick in the east (250–400 m), suggesting that it may have filled a topographically low area. This must remain speculative, as there is no datum from which to measure elevations.

Were the sandstone not well cemented it is unlikely that steep-sided valleys could have formed. Clean dry sand would have slumped as erosion proceeded, resulting in valley sides sloping at less than about 34° (Bagnold, 1941), but clayey, compacted, or damp (i.e. coherent) sand could form quite steep-sided landforms. However, the height of the steep valley sides (50–100 m), the existence of an apparently overhanging sandstone mass, and the occurrence of well-cemented sandstone clasts in the rubble overlying identical sandstone at locality $C_2$, all indicate considerable cementation. The overhang at locality E would be considered inordinately large, even in a modern landscape, and may imply some movement of large sandstone blocks during or after extrusion of the Top Rocky Rhyolite. However, no evidence of such movement was observed.

The profile of the disconformity gives the impression of a hummocky surface. Its higher points between D and F (Figs. 2, 3b) are regularly spaced, suggesting that erosion may have been controlled by a set of joints or minor faults, or by the uniform lithology of the eroding sandstone. Aggradation on the valley bottoms by sediment was not occurring, as shown by the presence of rhyolite on even the lowest parts of the surface; minor hillwash is present, for example at locality $C_2$. This suggests that the sandstone was an upland area — a dissected plateau. Such sandstone plateaus occur at the present day in many parts of the world. The Dixon Range, in Western Australia, is an Australian example of a highly dissected sandstone plateau.

## Conclusions

The contact between the Mitchiebo Volcanics and the overlying Top Rocky Rhyolite is a disconformity displaying relief of up to 120 m. Because it was preserved largely by blanketing by rhyolitic ignimbrite it represents the topography of a small area as it was 1680 Ma ago. The shape of the surface and the lack of detrital material on it show that it was a mainly bare, probably silicified, undulating sandstone plateau cut by narrow ravines and valleys.

Rhyolite lava is generally very viscous and forms short flows, although Macdonald (1972, p 68) reported an unusually long flow "roughly a mile long and more than 700 feet thick" in the Mono Craters area, California. Outcrops of the Top Rocky Rhyolite extend over a strike length of 25 km, of which most of the eastern half is massive and structureless. The size and uniform composition suggest that most was emplaced as ignimbrite. It may have been deposited during only a few eruptive events, and it is not inconceivable that the entire sandstone surface could have been blanketed during a single eruption. Ross & Smith (1961, p 20) reported that ". . . single units 200 to 300 feet thick are common and units 500 feet thick are probably not rare".

## Acknowledgements

I thank R. Cooper and S. Holliday, of BMR's Computer-assisted Cartography Section, who generated the corrected profile shown in Figure 3. I also thank A.J. Stewart, G.E. Wilford, and C.D. Ollier, who kindly commented on a draft of the manuscript.

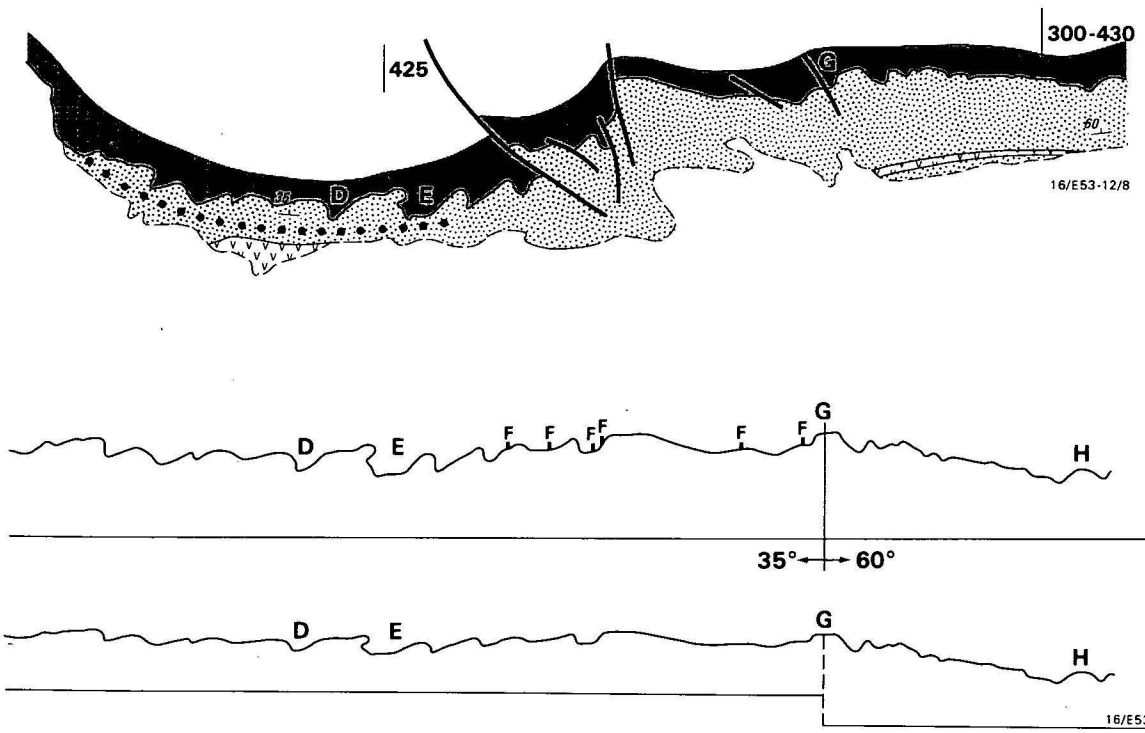

## References

Bagnold, R.A., 1941 — The physics of blown sand and desert dunes. *William Morrow & Co., New York.*

Hutton, L.J., & Sweet, I.P., 1982 — Geological evolution, tectonic style and economic potential of the Lawn Hill Platform Cover — northwest Queensland. *BMR Journal of Australian Geology & Geophysics*, 7, 125–134.

Macdonald, G.A., 1972 — Volcanoes. *Prentice-Hall Inc., Engelwood Cliffs.*

Page, R.W., 1978 — Response of U-Pb zircon and Rb-Sr total-rock and mineral systems to low-grade regional metamorphism in Proterozoic igneous rocks, Mount Isa, Australia. *Journal of the Geological Society of Australia*, 25(3), 141–164.

Phemister, J., 1960 — Scotland : The Northern Highlands. *Geological Survey of Great Britain, Her Majesty's Stationery Office, Edinburgh.*

Ross, C.S., & Smith, R.L., 1961 — Ash flow tuffs : their origin, geologic relations, and identification. *United States Geological Survey, Professional Paper*, 366.

Sweet, I.P., 1982 — Definitions of new stratigraphic units in the Carrara Range region, Northern Territory. *Bureau of Mineral Resources, Australia, Report* 242; BMR *Microform* MF 185.

Sweet, I.P., in press — Carrara Range Region, Northern Territory, 1:100 000 Geological Map Commentary. *Bureau of Mineral Resources, Canberra.*

Sweet, I.P., & Mond, A., 1980 — The geology of the Carrara Range Region, Northern Territory. *Bureau of Mineral Resources, Australia, Record* 1980/76.

Williams, G.E., 1966 — Palaeogeography of the Torridonian Applecross Group. *Nature*, 209, 1303–1306.

BMR Journal of Australian Geology & Geophysics, 8, 355-357


# SULPHIDE MINERALISATION OF MICROBIAL CELLS

B. Bubela[1] & P. Cloud[2].

Microbial cells have been experimentally infiltrated with iron sulphide by counter-diffusion of iron and sulphide ions through an agar medium containing algal cells.

## Introduction

In theory, microbial cells in an aerobic environment could be expected to be mineralised as a result of saturation by a solution of an ion followed by infiltration by another suitable ion, and subsequent precipitation of an insoluble salt. A typical example of such a process would be the saturation of cells by $FeCl_2$, subsequent infiltration by sulfide ions, and precipitation of insoluble iron sulfide. However, if we consider the solubility of the individual components, $FeCl_2$ in particular, and if we assume that the cell is completely filled by the solution of $Fe^{2+}$ and that all the iron precipitates as FeS, a simple calculation will show that the precipitate will occupy only 6 per cent of the cell volume. To completely fill the cell with iron sulfide, the process would have to be repeated 16 times. In nature, this would require an unlikely sequence of diagenetic conditions and, therefore, a more probable mechanism is needed.

We have experimented with the slow continuous counter-diffusion of iron and sulphide ions through a medium containing microbial cells. The feasibility of such counter-diffusion through a variety of geological materials and its possible significance in sulphide formation in sediments have been demonstrated and discussed elsewhere (Bubela & McDonald, 1969; Lambert & Bubela, 1970; Bubela, 1981a, b), and, using agar gel as a diffusion medium comparable to one of fine wet sedimentary particles, we were able to impregnate and infill microbial cells with crystalline iron sulphide.

## Method

A deep plastic Petri dish containing a nutrient agar gel was inoculated under aseptic conditions with an algal culture and incubated under sterile conditions at 20°C until colonies of microbial spheroids were visible. The positions of the colonies were marked and another layer of plain agar gel was poured on top of the colonies. The total thickness of the agar sandwich was approximately 2 cm. The bottom of the Petri dish was then perforated with about 20 holes of 3 mm diameter. The dish was placed on top of a solution of 5N sodium sulphide contained in a larger dish, and the peripheral gap between the dishes was sealed with soft paraffin. The top of the agar sandwich was flooded with fresh 5N $FeSO_4$ and the assembly was placed in a desiccator purged with nitrogen at a temperature of 20°C for 14 days, during which time the iron and sulphide ions counter-diffused and precipitated as iron sulphide. The iron having precipitated, the agar sandwich was removed from the Petri dish, the upper layer of the sandwich was removed, and the marked area was cut out, air dried, and examined by SEM and energy dispersive X-ray analysis. To investigate the inside of the cells, a part of the dried sample was gently crushed by hand in an agate mortar prior to the analysis.

[1]Baas Becking Geobiological Laboratory, GPO Box 378, Canberra, ACT 2601, Australia.
[2]University of California, U.S. Geological Survey, Santa Barbara, California 93103, U.S.A.

## Results

The results obtained by the above procedure are shown in Figures 1–3. We consider they represent both infiltration and filling of the 20–40μm cells of the eucaryotic green alga *Chlorella* sp (Figs. 2, 3) and mineralisation and replacement of the smaller cells of the colonial procaryote *Merismopedia punctata* (Fig. 4).

Spot analysis with the energy dispersion system showed all mineralisation to be iron and sulphur. No spheroidal structures were found apart from the original colonies. The *Chlorella* infilling was identified by X-ray diffraction as pyrite. The *Merismopedia* mineralisation, however, did not produce a characteristic X-ray diffraction pattern, and thus appears to be a crypto-crystalline form of iron sulphide, as would be predicted from the work of Lepp (1957) or Berner (1964).

As summarised by Berner (1964), recognisable pyrite is not usually the primary product of the reducing environments in which it forms as a diagenetic mineral, often aided by bacterial sulphate reduction. This is usually a black, X-ray-opaque mineral, which has been called hydrotroilite, kansite, and melnikovite — cryptocrystalline forms that, with aging, become pyrite, marcasite, or other crystalline iron sulphides.

## Conclusions

The algal cells were grown on the surface of the agar gel and then sealed by another layer of agar. It is most probable that

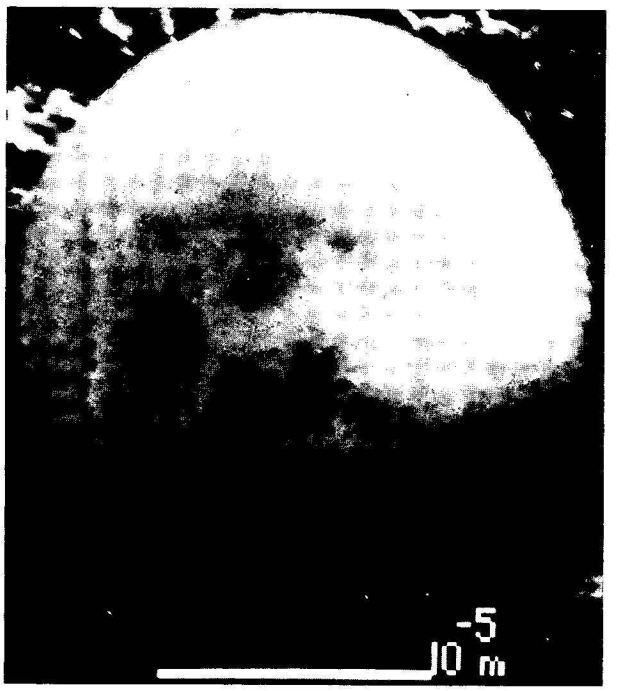


**Figure 1. A non-mineralised *Chlorella* sp.**
The cell surface shows irregularities that may represent areas of weakness in the cell wall, and which may be perforated during mineralisation.

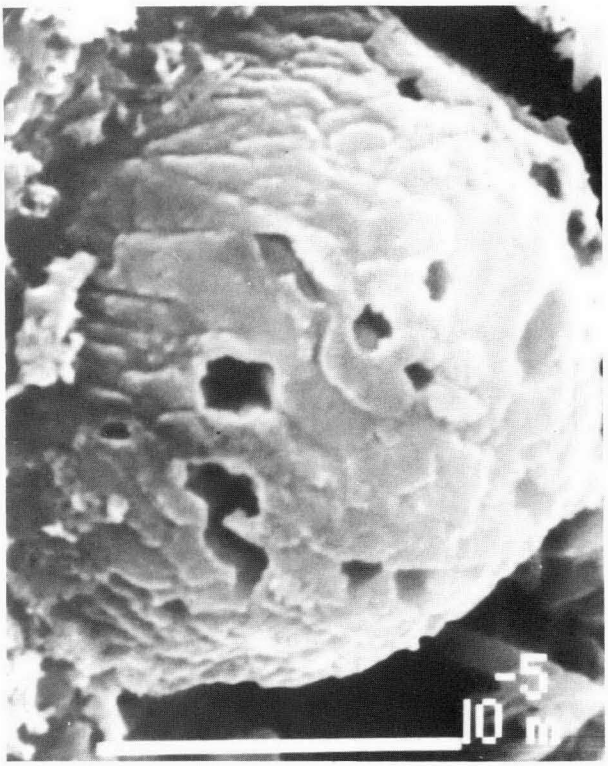


**Figure 2. *Chlorella* sp. cell after mineralisation.**
The cell wall of this specimen shows perforations through which mineralising solutions may have entered, or which may have formed during the mineralisation.

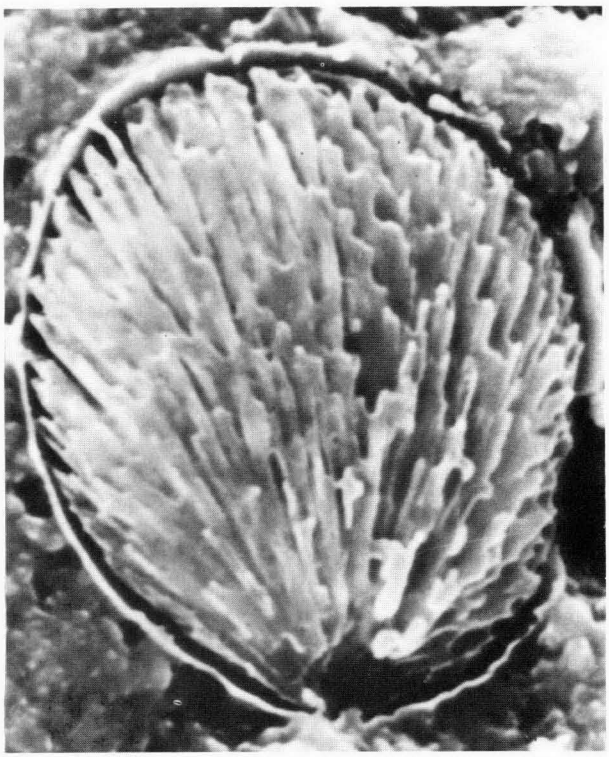

**Figure 3. A mineralised *Chlorella* sp. cell with the cell wall partly broken away.**
The mineralising fluids must have entered the cell before the wall was destroyed as crystalline pyrite growth appears to radiate from a single point (at the bottom of the picture). This particular specimen was selected as an illustration, not because of any uniqueness, but because it suggests most clearly where the mineralising solutions entered the cell. It was selected from a population of mineralised cells, gently crushed by hand to expose the cell content.

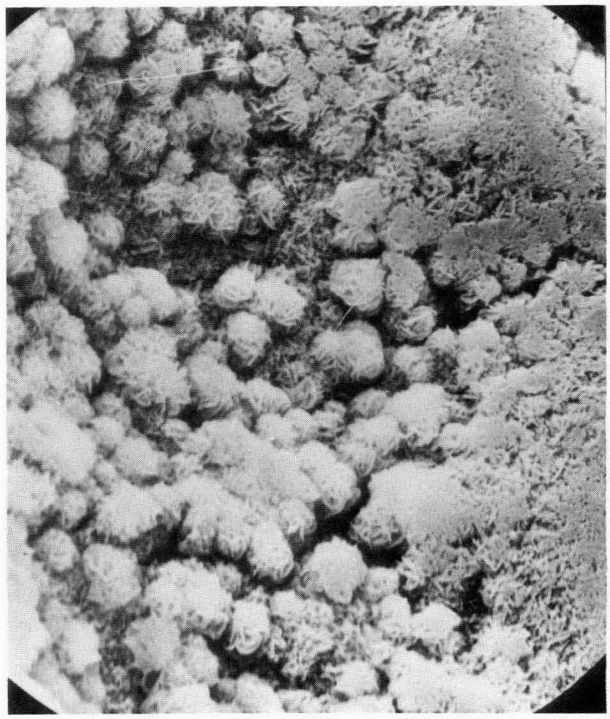

**Figure 4. Mineralised colonies of *Merismopedia punctata*.**
Individual spheroids are 20-40 μm across.

they were dead even before their mineralisation was initiated. It is also highly improbable that in nature the algal cells would be alive after their burial in sediment. This situation does not however affect the mineralisation process, as this is based on diffusion of ions and not biological activity.

Pyrite infiltration and infill of organisms have been suggested as the means of formation of Proterozoic framboids (Allison & Moorman, 1973; Moorman, 1974; Cloud & others, 1975). Our experiments have shown that iron and sulphide ions can, under appropriate conditions, both infiltrate and fill microbial cells with iron sulphide, and we believe that the process we have described could be one possible mechanism for the formation of framboids.

## Acknowledgements

The Baas Becking Laboratory is supported by the Bureau of Mineral Resources, the Commonwealth Scientific and Industrial Research Organization and the Australian Mineral Industries Research Association Limited. Preston Cloud is grateful to the Australian Department of Science & Technology for a Queen Elizabeth II Senior Research Fellowship in 1981.

## References

Allison, C. W., & Moorman, M. A., 1973 — Microbiota from the Late Proterozoic Tindir Group, Alaska. *Geology*, 1(2), 65–68.

Berner, R. A., 1964 — Stability fields of iron minerals in anaerobic marine sediments. *Journal of Geology*, 72, 826–834.

Bubela, B., 1981a — Banded sulfide ores: the experimental formation of sulfide bands in sediments from flowing liquids. *Economic Geology*, 76, 171–172.

Bubela, B., 1981b — A model for sulfide band formation under epigenetic conditions — a study based on simulated sedimentary systems. *BMR Journal of Australian Geology & Geophysics*, 6, 117–122.

Bubela, B., & McDonald, J., 1969 — Formation of banded sulphides: metal ion separation and precipitation by inorganic and microbial sulphide sources. *Nature*, 221, 465–466.

Cloud, P., Moorman, M. A., & Pierce, D., 1975 — *Quarterly Review of Geology*, 50(2), 131–150.

Lambert, I. B., & Bubela, B., 1970 — Banded sulphide ores: the experimental production of monomineralic sulphide bands in sediments. *Mineralium Deposita*, 5, 97–100.

Lepp, H., 1957 — The synthesis and probable geologic significance of melnikovite. *Economic Geology*, 52, 528–535.

Moorman, M. A., 1974 — Microbiota of the Late Proterozoic Hector Formation, southwestern Alberta, Canada. *Journal of Paleontology*, 48(3), 524–539.

 

# A RE-ASSESSMENT OF STROMATOLITE EVIDENCE FOR THE CORRELATION OF THE LATE PROTEROZOIC NEALE AND ILMA BEDS, OFFICER BASIN, WESTERN AUSTRALIA

K. Grey* & M.J. Jackson

The identification of a stromatolite sample as *Baicalia* cf. *B. burra* has been used as evidence for the correlation of the Late Proterozoic Neale beds and Ilma beds in the Officer Basin, Western Australia. However, recent re-examination of field documents has shown that the sample was collected not from an outcrop of Ilma beds, but from a Permian glacial deposit.

The Late Proterozoic Ilma beds were defined by Lowry (1970), who described them as forming part of the basement beneath the northern margin of the Eucla Basin in Western Australia. They are known only from the type locality, in the Mason 1:250 000 Sheet area, and the adjoining area. On geophysical evidence, Lowry thought it likely that the Ilma beds formed part of a sequence, 5000–10 000 m thick, detected about 200 km to the northwest, around Neale Junction.

Three stromatolite specimens (collected by Lowry from the Officer Basin) described as from the Ilma beds were identified by A.E. Cockbain (Geological Survey of Western Australia) as *Cryptozoon australicum* Howchin 1914, a form first recorded from the Late Proterozoic of the Amadeus Basin, and later renamed by Walter (1972) as *Acaciella australica* (Howchin).

The Neale beds (Jackson & van de Graaff, 1981) crop out poorly in the Officer Basin around 28°15'S, 125°15'E, west of Neale Junction in central Neale 1:250 000 Sheet area. They too contain stromatolites, and specimens collected from here by M.J. Jackson were identified by Preiss (1976) as *Baicalia* cf *B. burra*.

Since it was thought likely that the Ilma beds and Neale beds belong to the same sequence, Preiss re-examined one of the specimens that Cockbain had identified as *Cryptozoon australicum* Howchin. He concluded (Preiss, 1976) that this specimen was not *Cryptozoon australicum* Howchin, but was very similar to *Baicalia* cf *B. burra* from the Neale beds. Preiss took this as evidence for correlation of the Ilma beds and Neale beds, and this correlation has since been widely accepted (Jackson & van de Graaff, 1981; Preiss & Forbes, 1981; Grey, 1982a).

One of us recently re-examined two of the specimens collected by Lowry (Grey, 1982b), and concluded that one specimen was *Baicalia* cf *B. burra* and the second was *Acaciella australica* (Howchin). However, it was noticed that the locality data were in error, and that one of the three specimens identified by Cockbain as *Cryptozoon australicum* Howchin, and described as from the Ilma beds in the Mason 1:250 000 Sheet area, was in fact one of the two specimens mentioned above, which occur as glacial erratics in the Permian Wilkinson Range beds, in the Jubilee 1:250 000 Sheet area. Although these probably originated from rocks of Proterozoic age, it is not known whether they were derived from the Neale beds, the Ilma beds, or some other unit. Correlation of the Ilma beds and Neale beds is, however, thought still to be valid on lithological grounds, even though the stromatolite evidence no longer supports it.

The third sample was the only sample collected from the Ilma beds and consisted of a "broken fragment of a colony" (Cockbain, 1967, unpubl.). It is not now possible to verify the identity of this stromatolite, but Cockbain's remarks suggest that columnar stromatolites are present in the Ilma beds and these could be of significance for biostratigraphic correlation.

*Acaciella australica* also occurs in the Bitter Springs Formation of the Amadeus Basin (Walter, 1972) and in the Yackah beds of the Georgina Basin (Walter & others, 1979). Differences in lithology suggest that the provenance of the glacial erratic in question is unlikely to be either of these units and a source within the Officer Basin is more likely. *A. australica* has not so far been unequivocally recorded from any Late Proterozoic outcrops in the Officer Basin, but determination of the provenance of the erratic in the Wilkinson Range beds would be of considerable importance for future stratigraphic correlation.

*Geological Survey of Western Australia, 66 Adelaide Terrace, Perth 6000.
Published with the permission of the Director.

## References

Cockbain, A.E., 1967 — Stromatolites from the Jubilee Sheet. *Geological Survey of Western Australia, Palaeontology Report* 22/1967 (unpublished).

Grey, K., 1982a — Aspects of Proterozoic stromatolite biostratigraphy in Western Australia. *Precambrian Research*, 18, 347–365.

Grey, K., 1982b — A review of Late Proterozoic stromatolite occurrences in the Officer Basin (Neale, Jubilee and Mason 1:250 000 sheets). *Geological Survey of Western Australia, Palaeontology Report* 23/1982 (unpublished).

Jackson, M.J., & van de Graaff, W.J.E., 1981 — Geology of the Officer Basin. *Bureau of Mineral Resources, Australia, Bulletin* 206.

Lowry, D.C., 1970 — Geology of the Western Australian part of the Eucla Basin, *Geological Survey of Western Australia, Bulletin* 122.

Preiss, W.V., 1976 — Proterozoic stromatolites from the Nabberu and Officer Basin, Western Australia and their biostratigraphic significance. *Geological Survey of South Australia Report of Investigations* 47.

Preiss, W.V., & Forbes, B.G., 1981 — Stratigraphy, correlation and sedimentary history of Adelaidean (late Proterozoic) basins in Australia. *Precambrian Research*, 15, 255–304.

Walter, M.R., 1972 — Stromatolites and the biostratigraphy of the Australian Precambrian and Cambrian. *Palaeontology, Special Papers* 2.

Walter, M.R., Krylov, I.N., & Preiss, W.V., 1979 — Stromatolites from Adelaidean (late Proterozoic) sequences in central and South Australia. *Alcheringa*, 3, 287–305.

BMR Journal of Australian Geology & Geophysics, 8, 361-362 

# DISCUSSION: Spectral representation of isostatic models

V. Anfiloff

The main issue arising from Karner (1982) is whether the admittance method is capable of auto-analysis, that is, diagnosing structures. My analysis of ambiguity in marine gravimetry (Anfiloff, 1979) shows that the lack of proximity to the first interface, the sea bottom, makes marine observations inherently more ambiguous than observations on land. One of the findings is that the density profiling method should be applied routinely to assess the degree of ambiguity arising from the water/rock interface, because of its large density contrast, and the large range of possible density contrasts. It is axiomatic that if the density of marine topography cannot be deduced from the data itself, then a major source of ambiguity will pervade the entire analysis.

Karner also claims that the admittance method is applicable to the land situation, and suggests it should render the line-integration method obsolete for the purpose of general forward modelling. However, non-coplanar observations on land pose substantial problems. The equivalent layer method, on which the spectral method is based, is severely restricted by the requirement that observations be coplanar. Yet, isostasy is best studied over steep mountains, where the density of topography can be deduced from the gravity observations themselves, making interpretation less ambiguous than in other situations. For the two-dimensional case, line integration allows the problems of vertical continuation, topography density, and terrain corrections to be tackled in a unified process, (Anfiloff, 1976), resulting in Formal Interpretations (Anfiloff & Flavelle, 1979). Using this approach, the computation of synthetic free-air gravity (or topographic anomaly) has been demonstrated for real traverses across a 35-metre ridge (Anfiloff, 1981), an 800-metre ridge (Anfiloff & Flavelle, 1982), and across the Australian Alps (Anfiloff, 1982).

For forward modelling in the marine environment generally, the spectral method does not have any inherent advantages over line integration, and has the disadvantage of inaccuracies of varying degree. In the marine situation generally, the admittance method has the potential to differentiate between classes of structures, without being able to describe the structures themselves, as it is still subject to ambiguity. Like all auto-analysis methods, it must rely on a hypothetical relationship between a limited number of parameters, and, because of over-simplification, is capable of producing internally consistent but false models of structure with a minimum amount of input. Whereas marine crust may at times provide the simplicity and uniformity necessary for the admittance method, widespread and indiscriminate application could lead to major fallacies. Marine gravimetry has its own suite of problems arising from concealed sedimentary wedges, ambiguous effects of broad topography, lack of proximity to the nearest geological bodies, and a lack of good quality constraints generally. These factors should serve to decrease our expectations of marine gravimetry generally, and of auto-analysis methods in particular.

## References

Anfiloff, V., 1976 — Automated density profiling over elongate topographic features. *BMR Journal of Australian Geology & Geophysics*, 1, 57–61.

Anfiloff, V., 1979 — The proximity and topography factors in airborne and marine gravimetry. *Bulletin of the Australian Society of Exploration Geophysicists*, 10(2), 164–168.

Anfiloff, V., 1981 — Automated density profiling over a 35 metre ridge. *Bulletin of the Australian Society of Exploration Geophysicists*, 12(3), 40–42.

Anfiloff, V., 1982 — Elevation and gravity profiles across Australia: some implications for tectonism. *BMR Journal of Australian Geology & Geophysics*, 7, 47–54.

Anfiloff, V., & Flavelle, A.J., 1979 — Gravity interpretation over escarpments and in two dimensions generally. The Formal Interpretation Method. *Geophysics*, 44, 371 (abstract).

Anfiloff, V., & Flavelle, A.J., 1982 — Formal gravity interpretation over the 800-m Darai Escarpment in New Guinea. *Geophysics*, 47(7), 1091–1099.

Karner, G.D., 1982 — Spectral representation of isostatic models. *BMR Journal of Australian Geology & Geophysics*, 7, 55–62.

Nettleton, L.L., 1939 — Determination of density for the reduction of gravimeter observations. *Geophysics*, 4, 176–183.

# REPLY

G.D. Karner

Anfiloff's discussion is successful in summarising the problems that exist not only with admittance methods (Karner, 1982) and marine gravity data in particular, but *all* gravity methods (including the so-called Formal Interpretation of Anfiloff & Flavelle, 1979) and gravity data in general. However, his discussion is underlain by a number of misconceptions and prejudices towards various methods of gravity interpretation. Rather than specifically addressing the detailed criticisms made by Anfiloff, I prefer to address the basis of his discussion.

The Fourier expansion of a gravity anomaly is mathematically unique, its prime value being to highlight the spectral content of the anomaly. The fast Fourier transform, in particular, allows the rapid analysis of large quantities of data. Admittance functions use the Fourier representation of both gravity and topography data to construct filters which represent isostatic mechanisms that may operate within the lithosphere. In the paper under discussion, I attempted to summarise and describe how this can be achieved. The main advantage of admittance functions is in their computational efficiency relative to the line-integral method when calculating free-air and isostatic gravity effects for complicated topographies, isostatic schemes, or lithospheric rheologies.

A major problem in gravity modelling arises because of the non-uniqueness of gravity data. The use of gravity data for continental studies in the past has invariably been limited to a consistency check of geological structures obtained by other means, particularly reflection and refraction seismology. It is important to realise the possible contributions of gravity studies. They can place maximum limits on the depth to the top of an anomalous density structure (and are therefore useful in rejecting some hypotheses using deep bodies), and they can also show whether a given isostatic mechanism is or is not consistent with observations. Since an infinity of mass distributions can cause a given gravity anomaly, gravity modelling

cannot support one model to the exclusion of all others *unless* additional information from other sources is available. Generally, the arrangement of modelled density variations, or "bodies", used in the interpretation of gravity has been made independent of the physical and mechanical properties of rocks which comprise the continental crust. This modelling philosophy, therefore, cannot address the geological processes (and hence mechanisms) giving rise either to the existence or distribution of these bodies.

Gravity, bathymetric, and seismic studies over loads emplaced on the oceanic lithosphere have been successful in defining the first-order mechanical properties of the lithosphere and hence a geological mechanism for isostasy. In particular, the lithosphere is capable of flexing in response to applied loads, because of its rheological strength, in an *analogous* manner as an elastic plate overlying a weak fluid (e.g. Barrell, 1914; Gunn, 1948; Walcott, 1976; Watts, 1978; Bodine & others, 1981). This same model, when extended to the continents (e.g. Watts & others, 1982; Karner & others, in press), helps explain a number of tectonostratigraphic features of cratonic and foreland sedimentary basins.

The admittance technique, therefore, is particularly useful in studying the mechanical properties of the lithosphere. The isostatic state (or the degree of compensation) of a geological feature is also dependent on its horizontal extent. For the rigidities which characterise flexure of the continental lithosphere, topographic features with wavelengths less than about 100 km will appear uncompensated regardless of mountain steepness or height. The topographic examples presented by Anfiloff suggest a fundamental difference in the wavelengths of interest. His examples are less than 100 km in wavelength, representing, therefore, uncompensated density variations (caused by topography or variations in geology), and so are very sensitive to the various factors he refers to. Gravity anomalies with wavelengths between 100 and 1000 km tend to be compensated within the continental crust and, therefore, are most suited for studying isostasy. These anomalies may be modelled using either the more cumbersome empirical forward modelling techniques or admittance functions.

## References


Anfiloff, V., & Flavelle, A.J., 1979 — Gravity interpretation over escarpments and in two dimensions generally. The Formal Interpretation Method. *Geophysics*, 44, 371 (Abstract).

Barrell, J., 1914 — The strength of the Earth's crust, VIIIA. Physical conditions controlling the nature of the lithosphere and asthenosphere. *Journal of Geology*, 23, 425–443.

Bodine, J.H., Steckler, M.S., & Watts, A.B., 1981 — Observations of flexure and the rheology of the oceanic lithosphere. *Journal of Geophysical Research*, 86, 3695–3707.

Gunn, R., 1948 — Isostasy — extended. *Journal of Geology*, 57, 263–279.

Karner, G.D., 1982 — Spectral representation of isostatic models. *BMR Journal of Australian Geology & Geophysics*, 7, 55–62.

Karner, G.D., Steckler, M.S., & Thorne, J.A., in press — Long-term thermomechanical properties of continental lithosphere. *Nature*.

Walcott, R.I., 1976 — Lithospheric flexure, analysis of gravity anomalies, and the propagation of seamount chains. *In* Sutton, G.H., Manghnani, M.H., & Moberly, R. (editors), *American Geophysical Union, Geophysical Monograph* 19, 431–438.

Watts, A.B., 1978 — An analysis of isostasy in the world's oceans: 1. Hawaiian-Emporor seamount chain. *Journal of Geophysical Research*, 83, 5989–6004.

Watts, A.B., Karner, G.D., & Steckler, M.S., 1982 — Lithospheric flexure and the evolution of sedimentary basins. *Philosophical Transactions of the Royal Society of London*, A304, 249–281.

BMR Journal of Australian Geology & Geophysics, 8, 363 

# CORRECTION

## S. Shafik—Calcareous nannofossil biostratigraphy: an assessment of foraminiferal and sedimentation events in the Eocene of the Otway Basin, southeastern Australia.

Volume 8, number 1, 1-17.

The individual photographs in Figure 3 are mislabelled. To correlate correctly with the figure caption, they should be labelled as shown here.

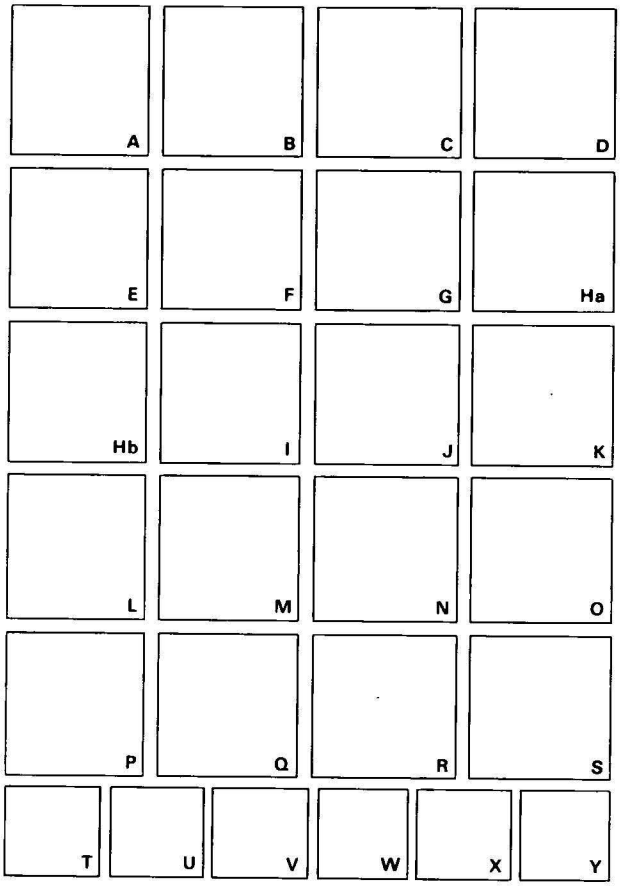

# BMR JOURNAL
## OF AUSTRALIAN GEOLOGY & GEOPHYSICS

VOLUME 8

1983

CONTENTS

VOLUME 8 NUMBER 1 MARCH 1983

## CONTENTS



VOLUME 8 NUMBER 2 JUNE 1983

## CONTENTS

VOLUME 8 NUMBER 3 SEPTEMBER 1983

## CONTENTS



VOLUME 8 NUMBER 4 DECEMBER 1983

## CONTENTS

## CONTENTS



Front cover: Viper Reef—part of a map published by BMR, showing surficial facies of part of the central Great Barrier Reef, mapped using the concept of entropy ratio. A paper by B. M. Radke in this issue explains the concept and describes its application.

R81/103(8) Cat. No. 83 1361 2